DEVELOPMENT AND CHARACTERIZATION OF NEW MAGNESIUM BASED NANOCOMPOSITES

KHIN SANDAR TUN

NATIONAL UNIVERSITY OF SINGAPORE

2009

DEVELOPMENT AND CHARACTERIZATION OF NEW MAGNESIUM BASED NANOCOMPOSITES

KHIN SANDAR TUN
(B. Eng., YTU, M. Sc., NUS)

A THESIS SUBMITTED
FOR THE DEGREE OF DOCTOR OF PHILOSOPHY
DEPARTMENT OF MECHANICAL ENGINEERING
NATIONAL UNIVERSITY OF SINGAPORE
2009

PREFACE

This thesis is submitted for the degree of Doctor of Philosophy in the Department of Mechanical Engineering at the National University of Singapore. The research herein was carried out under the supervision of Associate Professor Manoj Gupta from the Materials Science Division. To the best of my knowledge, this work is original except references which are made to previous work. Neither similar thesis nor any part of this thesis has been or is being submitted for any degrees or other qualification at any other university or Institution. Part of this thesis has been published in international journals. This thesis contains no more than 40,000 words.

ACKNOWLEDGEMENTS

First and foremost, I wish to express my sincere gratitude to my supervisor, Associate Professor Manoj Gupta for his encouragement, support and valuable guidance. This work could not have been completed without his understanding, patience, motivation, enthusiasm, immense knowledge and especially his continuous support. I could not have imagined having a better advisor for my Ph.D study. I am proud to have an opportunity to carry out my research study under his supervision.

I would also like to express my warm thanks to Mr. Thomas Tan Bah Chee, Mr. Abdul Khalim Bin Abdul, Mr. Juraimi Bin Madon, Mr. Ng Hong Wei, Mr. Maung Aye Thein and Mrs. Zhong Xiang Li from the Materials Science Laboratory for their assistance throughout my study in NUS. Special thanks to Mr. Lam Kim Song from Fabrication Support Center (FSC), NUS for his cordial help in preparation of materials using CNC Lathe machine.

My most sincere thanks also go to my colleagues, my fellow labmates and my seniors, especially Dr. Wong Wei Leong, Eugene for their guidance, understanding and kind support. My deep sense of gratitude also goes to my close friend and labmate, Mr. Myo Minn who always offers me encouragement and full-hearted help during the entire length of my study.

My heartfelt thanks go to my family, especially my parents for supporting me with earnest love throughout my life. I owe my warmest gratitude to my elder brother, Mr. Tun Mon Oo for his valuable assistance to make this study possible.

TABLE OF CONTENTS

SUMMARY

In the present work, Mg/Ceramic nanocomposites and Mg/(Ceramic+Metal) hybrid nanocomposites were developed using microwave assisted powder metallurgy route. The current research project can be divided into three sections: (1) development of Mg/Y_2O_3 nanocomposites via powder metallurgy route involving innovative hybrid microwave sintering approach followed by hot extrusion, (2) optimization of primary processing parameter (heating rate during hybrid microwave sintering) and secondary processing parameter (extrusion ratio during hot extrusion) and (3) development of magnesium based hybrid nanocomposites containing ceramic and metal nanoparticulate reinforcements.

Mg/Y_2O_3 nanocomposites were developed using microwave assisted powder metallurgy route. Two different compositions of Mg/Y_2O_3 nanocomposites, $Mg/0.17vol.\%Y_2O_3$ and $Mg/0.7vol.\%Y_2O_3$, were critically investigated. Between two compositions, $Mg/0.7vol.\%Y_2O_3$ exhibited the best strength and ductility combination.

Since microwave sintering is a newly developed method for synthesis of metallic composites, an investigation into the effect of heating rate on pure Mg and optimized nanocomposite composition of $Mg/0.7vol.\%Y_2O_3$ during hybrid microwave sintering was carried out. Two different heating rates, 49°C/min and 20°C/min, were used for the synthesis of materials. Best combination of overall mechanical properties was attained from the nanocomposite synthesized using high heating rate (49°C/min). High heating rate was thus chosen for synthesis of further composite systems. To find the effective extrusion ratio, microwave sintered Mg and $Mg/0.7vol.\%Y_2O_3$ nanocomposite with high heating rate were extruded using three different extrusion

ratios (12:1, 19:1 and 25:1). 25:1 was seen as the best extrusion ratio as it provides the best combination of mechanical properties.

Aiming to further enhance the properties of Mg/0.7vol.%Y_2O_3 and to establish the effectiveness of hybrid microwave sintering approach, two hybrid nanocomposite systems, Mg/(Y_2O_3+Cu) and Mg/(Y_2O_3+Ni) were developed.

For synthesis of Mg/(Y_2O_3+Cu) hybrid nanocomposites, three different volume percentages of Cu (0.3, 0.6 and 1.0) were added as hybrid reinforcements into Mg/0.7vol.%Y_2O_3 composition. As compared to Mg/0.7Y_2O_3 nanocomposite, a significant reduction in grain size was observed in Mg/(Y_2O_3+Cu) hybrid nanocomposites realizing the efficient use of metal nanoparticulates as hybrid reinforcement. The resultant grain refinement and good distribution of secondary phases led to an achievement in higher tensile strengths (0.2%YS and UTS) and ductility in Mg/(0.7Y_2O_3+0.3Cu) hybrid nanocomposite composition over Mg/0.7Y_2O_3 nanocomposite. From microhardness and compression tests, the best microhardness and significant improvement in 0.2%CYS and UCS with a compromise in ductility was observed in Mg/(0.7Y_2O_3+1.0Cu) hybrid nanocomposite.

The same variation in volume percentages of Ni nanoparticulate reinforcements as in Mg/(Y_2O_3+Cu) hybrid nanocomposites was chosen for the preparation of Mg/(Y_2O_3+Ni) hybrid nanocomposite systems to investigate the effect of type of metal reinforcements on microstructure and mechanical properties. Similar trend of grain refinement and good distribution of secondary phases was observed in Mg/(Y_2O_3+Ni) hybrid nanocomposite system as that in Mg/(Y_2O_3+Cu) hybrid nanocomposite system. The best microhardness was exhibited by Mg/(0.7Y_2O_3+1.0Ni) hybrid nanocomposite. Best combination of tensile strengths and ductility was exhibited by

Mg/(0.7Y_2O_3+0.6Ni) hybrid nanocomposite. Compression testing results revealed a significant improvement in both 0.2%CYS and UCS in the case of Mg/(Y_2O_3+Ni) hybrid nanocomposites over pure magnesium while the ductility was adversely affected.

LIST OF TABLES

LIST OF FIGURES

PUBLICATIONS

Journal Papers

1. K.S. Tun and M. Gupta, "Improving Mechanical Properties of Magnesium Using Nano-Yttria Reinforcement and Microwave Assisted Powder Metallurgy Method", ***Composite Science and Technology*, *67 (2007) 2657-2664*.**
2. K.S. Tun and M. Gupta, "Effect of Heating Rate during Microwave Sintering on the Tensile Properties of Magnesium and Mg/Y_2O_3 Nanocomposites", ***Journal of Alloys and Compounds*, *466 (2008) 140-145*.**
3. K.S. Tun and M. Gupta, "Effect of Extrusion Ratio on Microstructure and Mechanical Properties of Microwave-sintered Magnesium and Mg/Y_2O_3 Nanocomposites", ***Journal of Materials Science*, *43 (2008) 4503-4511*.**
4. K.S. Tun, M. Gupta and T.S. Srivatsan, "Investigating Microstructure and Tensile Properties of Mg Containing Hybrid (Yttria+Copper) Nanoparticulate Reinforcements", ***Materials Science and Technology*, *26 (2010) 87-94*.**
5. K.S. Tun and M. Gupta, "Development of Magnesium (Yttria+Nickel) Hybrid Nanocomposites Using Hybrid Microwave Sintering: Microstructure and Tensile Properties", ***Journal of Alloys and Compounds*, *487 (2009) 76-82*.**
6. A. Mallick, K. S. Tun, S. Vedantam and M. Gupta, "Mechanical Characteristics of Pure Mg and a Mg/Y_2O_3 Nanocomposite in the 25 – 250°C Temperature Range", ***Journal of Materials Science, Accepted on 9 Feb 2010.***
7. K.S. Tun and M. Gupta, "Role of Microstructure and Texture on Compressive Strength Improvement of Mg/(Y_2O_3+Cu) Hybrid Nanocomposites", ***Journal of Composites Materials, Accepted on 12 Feb 2010.***

Conference Papers

1. K.S. Tun and M. Gupta, "Development and Characterization of High Performance Mg-Y_2O_3 Composite", ***MP^3 2006, Singapore. (Presented and published in the conference proceedings)***
2. K.S. Tun and M. Gupta, "Effect of Extrusion Ratio on Tensile Behavior of Mg and Mg/Y_2O_3 Nanocomposite Synthesized Using Microwave Assisted Powder Metallurgy Route", ***PFAM XVI 2007, Singapore. (Presented and published in the conference proceedings)***
3. W.L.E. Wong, K.S. Tun and M. Gupta, "Tailoring the Properties of Pure Magnesium Using Different Microwave Heating Rates", ***PFAM XVI 2007, Singapore. (Presented and published in the conference proceedings)***
4. K.S. Tun, M. Gupta and T.S. Srivatsan, "The Intrinsic Influence of Nano-length Scale Metal and Ceramic Particulate Reinforcements on Strength, Ductility and Work of Fracture of Magnesium", ***PFAM XVII 2008, India. (Published in the conference proceedings).***
5. M. Paramsothy, Q.B. Nguyen, K.S. Tun and M. Gupta, "Enhancing Ductility of Magnesium Using Composite Technology", ***PFAM XVIII 2009, Tohoku University, Sendai, Japan. (Presented and published in the conference proceedings)***
6. Q.B. Nguyen, M. Shanthi, M. Paramsothy, K.S. Tun and M. Gupta, "Light Weight Magnesium Nanocomposites for Aerospace", ***NCATMC 2010, Singapore.***

Poster Exhibition

1. K.S. Tun and M. Gupta, "ynthesis of High Performance Magnesium Nanocomposites Using Powder Metallurgy Technique Incorporating Hybrid Microwave Sintering", ***ICMAT 2009, Industrial Symposium II: Microwave Processing of Materials, Singapore.***

Development and Characterization of New Magnesium Based Nanocomposites

CHAPTER 1

INTRODUCTION

CHAPTER 1

INTRODUCTION

1.1 Overview

The development of metal matrix composites (MMCs) has been one of the major innovations in materials community over past three decades. These innovative materials allow unlimited possibilities for research and development in the area of materials science. Metal matrix composites offer several attractive advantages over traditional engineering materials due to their improved properties [1, 2]. MMCs can be classified into three main categories with respect to the shape of their reinforcements, namely long fiber reinforced composites, short fiber reinforced composites and particulate reinforced composites. Among these three types of MMCs, particulate reinforced metal matrix composites are of great interest due to their isotropic properties and lower production cost. For many researchers, the term metal matrix composites is often equated with the term light metal matrix composites (MMCs) [3]. In light metal matrix composites, Al, Mg and Ti are mostly used as base metal matrix and ceramic particles (oxides, carbides and nitrides) are commonly used as reinforcing phase. Generally, micron length scale particles are used as reinforcing phase in base matrix.

Recently, there is considerable interest in production of metal matrix nanocomposite in which nanoparticulates are incorporated into base matrix. The production of nanocomposites is currently under exploration and experimental research stage. When compared to composites with micron-sized reinforcements,

nanocomposites exhibit comparable or better mechanical properties with the use of lesser amount of nanoparticulate reinforcements [4-9]. Both liquid metallurgy methods and powder metallurgy (PM) methods can be used to fabricate metal matrix nanocomposites. Historically, PM methods have been developed successfully and commercially by different manufactures and have also been applied in the production of MMCs for aerospace applications [10]. As compared to liquid metallurgy, PM approach has shown its advantage by producing higher strength composite materials with better microstructural uniformity [2, 11, 12]. PM methods usually involve mixing of powders, compaction and solid state sintering followed by secondary consolidation process such as extrusion. Among these steps, sintering is a very important step due to its ability to evolve microstructural features that govern the end properties. Sintering can be done using a number of ways involving radiant, plasma, induction and microwave heating sources [13]. Among various sintering techniques, microwave sintering is emerging as a rapid, energy efficient and environment friendly technique [14-17].

Most of the work on microwave heating and sintering was applied extensively for the processing of ceramic materials till 1990's [17-20]. Only limited research was conducted on investigating interaction between microwave and metal based materials [21-25]. Microwave heating has many advantages over conventional heating including cost and energy savings, and considerable reduction in processing time. By using microwave energy as heating source, short sintering time at desired temperature offers an opportunity to control especially the microstructure coarsening during sintering leading to excellent mechanical properties [22]. Instead of using only microwaves as a heating source, hybrid heating system through combination of conventional

conduction heating and energy conversion heating using microwave is found to be more advantageous for heating or sintering of materials [14, 26-30].

At present, the development of metal matrix composites with light metal matrices are increasingly paid attention due to their high performance and tailorable properties coupled with weight savings which is a primary requirement in many applications such as automotive and aircraft industries in which weight reduction is the critical factor. So far extensive research has been done for production of aluminum matrix composites and they are manufactured commercially for numerous industrial applications [31]. Magnesium based composites also exhibit comparable mechanical properties when compared to aluminum based composites [2]. However, relatively limited research has been done on magnesium based composites. One of the issues in production of magnesium matrix composites for industrial applications is its high production cost [32]. The demand of reducing production cost favors the development of high performance magnesium matrix composite using cost effective manufacturing route. In addition, the need for high performance and light weight innovative materials has triggered the widespread R&D efforts in the development of magnesium based nanocomposites which are about 33% lighter than aluminum based composites. The development of potential magnesium nanocomposites using cost effective fabrication techniques will serve the requirement for light weight structural materials suitable for the commercial applications at a reasonable cost. By making good use of microwaves as energy efficient heating tool, new magnesium based nanocomposites are synthesized in the current research project. The main objective was to fabricate high performance magnesium nanocomposites via cost effective processing technique based on PM route incorporating hybrid microwave sintering method.

In this study, Mg/Y_2O_3 nanocomposites containing yttria nanoparticulates were developed via energy/cost effective microwave sintering route. By using microwaves as heating source, it takes only 13 minutes to sinter the materials. The microwave sintered materials were hot extruded for secondary consolidation and the extruded rods were used for further characterization studies. Studies were carried out to evaluate the physical, microstructural and mechanical properties of synthesized materials. Focus was placed on investigating the effects of the addition of nano yttria particulates on mechanical properties of resultant nanocomposites. A successful development of new magnesium nanocomposites with comparable or enhanced mechanical properties using cost effective processing route will assist in the economical production of high performance magnesium nanocomposites for a variety of structural and non structural applications. Nowadays, the demand of reducing energy consumption especially in automotive industries to save the environment is becoming a critical issue. Development of light weight magnesium based composites can be seen as one of the solutions to address this issue.

Since hybrid microwave sintering is a relatively new method, optimization of sintering parameters is beneficial in obtaining the best properties of sintered materials. Consequently, the effect of heating rate during microwave sintering on the properties of sintered materials has not been done before. The heating rate effect was thus studied on the selected nanocomposite formulation and pure Mg which was used for benchmarking. To see the extent of secondary consolidation on the properties of microwave sintered materials, investigation was also made to optimize the extrusion ratio for achieving best performance materials.

In order to further develop new magnesium nanocomposites, hybrid magnesium nanocomposites containing ceramic and metal nanoparticulates were synthesized. Characterization studies were carried out and the focus was placed on the correlation between microstructure evolution due to co-presence of ceramic and metal nanoparticulates in Mg matrix and mechanical properties of hybrid nanocomposites.

Based on the existing literature, most of the studies on magnesium composites are focused on the tensile properties and tensile/compression asymmetry. There are very few reports on compressive properties of magnesium based composites where reinforcements are not in nano length scale [33-38]. Compressive properties and deformation behavior of especially hybrid magnesium nanocomposites have not yet been researched systematically. To further gain the understanding of mechanical properties under both tension and compression, and to enhance the reliability of the synthesized materials, investigations were made on two types of hybrid nanocomposites in the current research project.

1.2 Organization of Thesis

The forthcoming chapters of the thesis are organized as follows:

Chapter 2 introduces the literature survey related to the current research project. It includes background of composite materials, different types of metal matrix composites, details of various liquid metallurgy and solid metallurgy methods for fabrication of magnesium based composites and microwave processing/heating

technology which is relatively new and promising processing technique for fabrication of metallic materials.

Chapter 3 describes the materials, details of processing methods and characterizations techniques used for the synthesis of magnesium matrix nanocomposites. Characterization studies were conducted to assess the densification response, evolution of microstructure, identification of phases, hardness, tensile properties and compressive properties of synthesized materials.

Chapter 4 presents the development of magnesium nanocomposites containing yttria (Y_2O_3) nanoparticulates of two different compositions, 0.17 vol.% (0.5 wt.%) and 0.7 vol.% (2wt.%). Nanocomposites were synthesized using powder metallurgy route incorporating hybrid microwave sintering followed by hot extrusion. Between two Mg/Y_2O_3 nanocomposite compositions, Mg/0.7vol.%Y_2O_3 composition showed the best overall mechanical properties (microhardness and tensile properties).

Chapter 5 presents the effect of heating rate on the tensile properties of Mg and Mg/0.7vol.%Y_2O_3 nanocomposite which was chosen due to its best mechanical properties as mentioned in Chapter 4. Heating rates of 49°C/min and 20°C/min were applied to sinter the materials using microwave heating. Based on the results obtained, high heating rate was selected for further synthesis of nanocomposites.

Chapter 6 provides the optimization of secondary processing parameter i.e. extrusion ratio. Based on the results from first part of investigation, Mg and

Mg/0.7vol.%Y_2O_3 nanocomposite sintered at high heating rate were extruded at 12:1, 19:1 and 25:1 extrusion ratios. The characterization results showed an extrusion ratio of 25:1 to be the most effective extrusion ratio.

Chapter 7 presents the development of magnesium based hybrid nanocomposites containing yttria and copper particulates at nano length scale. Three different compositions of hybrid nanocomposites were synthesized by adding increasing amount of copper particulates in to a fixed composition of Mg/0.7vol.%Y_2O_3. High heating rate (49°C/min) during microwave sintering and an optimum extrusion ratio (25:1) were used for the synthesis of hybrid nanocomposites. Discussion is made focusing on the interrelation between microstructure and tensile properties of Mg/(Y_2O_3+Cu) nanocomposites.

Chapter 8 presents the use of nickel nanoparticulates as hybrid reinforcement in Mg/0.7vol.%Y_2O_3 composition. High heating rate (49°C/min) during microwave sintering and an optimum extrusion ratio (25:1) were once again used for the synthesis of hybrid nanocomposites. Discussion is made focusing on the effect of increasing amount of nickel nanoparticulates on microstructure, hardness and tensile properties of resultant hybrid nanocomposites.

Chapter 9 discusses the deformation behavior of hybrid nanoparticulates (ceramic+metal) reinforced Mg composites under compressive loading. Compressive properties of Mg, Mg/(Y_2O_3+Cu) and Mg/(Y_2O_3+Ni) nanocomposites were evaluated and characterization studies were conducted. The compressive responses of Mg and

Mg hybrid nanocomposites were correlated with microstructural evolution like twinning and texture evolution (orientation changes of basal planes).

Chapter 10 summarizes the key findings based on the synthesis of new magnesium based nanocomposites from current investigations.

Chapter 11 provides suggestions for the future work in this research area.

1.3 References

[1] I.A. Ibrahim, F.A. Mohamed and E.J. Lavernia, J. Mater. Sci., 26 (1991) 1137-1156.

[2] D.J. Lloyd, Int. Mater. Rev., 39 (1994) 1-23.

[3] K.U. Kainer, *Basic of Metal Matrix Composites*. In Metal matrix composites: custom-made materials for automotive and aerospace engineering, edited by K.U. Kainer, Weinheim, Chicheste, Wiley-VCH, 2006.

[4] Z.Y. Ma, Y.L. Li, Y. Liang, F. Zheng, J. Bi and S.C. Tjong, Mater. Sci. Eng. A, 219 (1996) 229-231.

[5] Y.C. Kang and S.L. Chan, Mater. Chem. Phy., 85 (2004) 438-443.

[6] S.F. Hassan and M. Gupta, Comp. Struct., 72 (2006) 19-26.

[7] S.F. Hassan and M. Gupta, J. Alloys Compd., 429 (2007) 176-183.

[8] W.L.E. Wong and M. Gupta, Adv. Eng. Mater., 8 (2006) 735-740.

[9] H. Ferkel and B.L. Mordike, Mater. Sci. Eng. A, 298 (2001) 193-199.

[10] Website: http://mmc-assess.tuwien.ac.at/public/mmc_in_ind.pdf.

[11] M.M. Schwartz, *Composite Materials: Properties, Fabrication and Applications*, N.J., Prentice Hall, 1997, pp.149, 150.

[12] S.C. Tjong, Adv. Eng. Mater., 9 (2007) 639-652.

[13] R.A. German, *Sintering Theory and Practice*, New York, John Wiley & Sons Inc., 1996.

[14] D.E. Clark and W.H. Sutton, Annu. Rev. Mater. Sci., 26 (1996) 299-331.

[15] D. Agrawal, J. Cheng and R. Roy, Innovative Processing/Synthesis: Glasses, Composites IV, Am. Ceramic Soc. Publ. (2000) 273-284.

[16] A. Upadhyaya, G. Sethi and D. Agrawal, Microwave Sintering of Cu-12Sn alloy in Sintering 2003 Conference, 15-17 September 2003, Penn State University, Pennsylvania, USA.

[17] A. Chatterjee, T. Basak and K.G. Ayappa, AIChE Journal, 44 (1998) 2302-2311.

[18] Z. Xie, C. Wang, X. Fan and Y. Huang, Mater. Letters, 38 (1999) 190-196.

[19] A.W. Fliflet, R.W. Bruce, A.K. Kinkead, R.P. Fischer, D. Lewis, R. Rayne, B. Bender, L.K. Kurihara, G.M. Chow and P.E. Schoen, IEEE Trans. plasma Sci., 24 (1996) 1041-1049.

[20] D.K. Agrawal, Current Opinion in Solid State & Mater. Sci., 3 (1998) 480-486.

[21] S. Leparoux, S. Vaucher and O. Beffort, Adv. Eng. Mater., 5 (2003) 449-453.

[22] R. Roy, D. Agrawal, J. Cheng and S. Gedevanishvili, Nature, 399 (1999) 668-670.

[23] R.M. Anklekar, D.K. Agrawal and R. Roy, Powder Metall., 44 (2001) 355-362.

[24] E. Breval, J.P. Cheng, D.K. Agrawal, P. Gigl, M. Dennis, R. Roy and A.J. Papworth, Mater. Sci. Eng. A, 391 (2005) 285-295.

[25] K. Saitou, Scripta Mater., 54 (2006) 875-879.

[26] D.F. Stein (Chairman), *Microwave Processing of Materials*, Committee on Microwave Processing of Materials, National Materials Advisory Board, 1994.

[27] E.T. Thostenson and T.W. Chou, Comp. Part A: Appl. Sci. Manuf., 30 (1999) 1055-1071.

[28] Y.V. Bykov, K.I. Rybakov and V.E. Semenov, J. Phys. D: Appl. Phys., 34 (2001) R55-R75.

[29] M. Gupta and W.L.E Wong, Scripta Mater., 52 (2005) 479-483.

[30] W.L.E. Wong and M. Gupta, Comp. Sci. Tech., 67 (2007) 1541-1552.

[31] R. Buschmann, *Preforms for the Reinforcement of Light Metals-Manufacture, Applications and Potential*. In Metal matrix composites: custom-made materials for automotive and aerospace engineering, edited by K.U. Kainer, Weinheim, Chicheste, Wiley-VCH, 2006.

[32] V.K. Lindroos and M.J. Talvitie, J. Mater. Process. Tech., 53 (1995) 273-284.

[33] D.J. Towle and C.M. Friend, Mater. Sci. Tech., 9 (1993) 35-41.

[34] G. Garces, M. Rodrıguez, P. Perez and P. Adeva, Mater. Sci. Eng. A, 419 (2006) 357-364.

[35] M. Guden, O. Akil, A. Tasdemirci, M. Ciftcioglu and I.W. Hall, Mater. Sci. Eng. A, 425 (2006) 145-155.

[36] B.Q. Han and D.C. Dunand, Mater. Sci. Eng. A, 277 (2000) 297-304.

[37] J.Q. Li, L. Wang, H.W. Cheng, H.F. Zhang, Z.Q. Hu and H.N. Cai, Mater. Sci. Eng. A, 474 (2008) 24-29.

[38] Z. Szaraz, Z. Trojanova, M. Cabbibo and E. Evangelista, Mater. Sci. Eng. A, 462 (2007) 225-229.

CHAPTER 2

LITERATURE REVIEW

CHAPTER 2

LITERATURE REVIEW

2.1 Introduction

In the search of potential candidates for light weight structural and non structural applications, a wide variety of materials is currently available for the creative product designers. Although the utilization of various engineering plastics and polymer matrix composites in many applications including aircraft structures has grown considerably, the use of light metals and metallic alloys have defended their end applications due to their superior resistance to mechanical damages, high through-thickness strength and low production cost which are necessary for high performance and loaded structures [1]. The use of materials as structural components in aircraft industries is determined based on the factors related to materials' properties, availability, price, innovative and cost effective processing methods, compliance with the environmental regulations etc [2]. The rapid growth of polymer matrix composites experienced during the last 20 years will probably stabilize or may go down [1]. The increasing demand for the production of light weight structural components and systems is expected to be fulfilled by the development of innovative metallic materials such as alloys and composites particularly based on aluminum and magnesium.

Composites have been recognized as superior alternative to other traditional materials. With innovative technologies and development of various processing techniques, composites with improved properties have emerged as attractive candidates to materials community. The use of composite materials has also become

increasingly important in engineering design. A composite material is a mixture of two or more materials, which have been unified together at a scale that is sufficiently fine so that the result can be considered as a material with unique properties [3]. Generally, composite consists of reinforcing materials intimately bonded to another material called a matrix. Depending on the base matrix materials, there are three types of composite materials namely, metal matrix composites (MMCs), ceramic matrix composites (CMCs) and polymer matrix composites (PMCs). Research on metal matrix composites was initiated in the 1960's and progressed through 1970's. Significant development of MMC technology was reached in the 1980s [3]. Research on MMCs was primarily introduced with continuous fiber reinforced metal matrix composites. The greatest improvements in mechanical properties were obtained from these composites and they were commercially manufactured for a few applications, especially in the aerospace industry. In weight critical structural applications, MMCs based on light metals (aluminum, magnesium and titanium) and most of the PMCs are usually considered as the most suitable materials. Comparison between fiber MMCs and PMCs are shown in Table 2.1. As seen from the table, fiber MMCs showed advantages in terms of materials properties although there still have some disadvantages to compete with PMCs [1]. To fabricate better performance MMCs and to address the weakness of fiber MMCs, particulate reinforced metal matrix composites (PMMCs) have emerged as viable replacements [4, 5]. The advantages of particulate reinforced metal matrix composites over continuous fiber reinforced metal matrix composites include low cost of reinforcing particulates, simple and low cost production process, and isotropic properties [6-8].

Table 2.1. Advantages and disadvantages of fiber MMCs compared to PMCs [1].

- **MMC Systems**
  - Aluminum alloy/Boron; Aluminum/ Silicon carbide; Aluminum/Alumina
  - Titanium/Silicon carbide
  - Aluminum/Carbon; Magnesium/Carbon

- **Advantages**
  - High temperature capability, particularly Titanium
  - High through-thickness strength
  - High compressive strength
  - Impact damage resistance
  - High electrical and thermal conductivity

- **Disadvantages**
  - Limited and high cost fabrication technology
  - Difficult and inefficient joining technology
  - Matrix/fiber chemical incompatibility
  - Mismatch in matrix/fiber expansion, low resistant to thermal fatigue
  - Susceptible to corrosion, particularly with conducting fibers

After understanding metal based composite materials over 40 years, researchers are emphasizing intensively on the development of light metal composites such as aluminum and magnesium matrix composites [7-9]. Most of the studies in last 20 years were focused on the development of aluminum matrix composites [10]. Interest was less on the magnesium based composites mainly due to its intrinsic properties of low deformability at room temperature and low corrosion resistance although they can offer similar or higher property improvement when compared to aluminum based composites [7]. Previous works on magnesium based composites

were focused on the development of micron sized particulate reinforced magnesium composites (PMMCs). PMMCs can involve particulate size ranging from around 10nm to 1500nm and above, and the use of particulates smaller than 100 nm in matrix was expected to give excellent properties of PMMCs [11]. Recent investigations [12-16] have reported that superior mechanical properties can be obtained by using nanoparticulate reinforcements. Conventional liquid metallurgy and solid metallurgy are the techniques generally used to manufacture PMMCs [3].

2.2 Different Types of Metal Matrix Composites (MMCs)

There are different types of metal matrix composites based on type of metallic matrix. Among these composites, light metal matrix composites such as aluminum, magnesium and titanium based composites are described here.

2.2.1 Aluminum Matrix Composites (Al-MMCs)

These are most common type of MMCs existing currently. In these MMCs, aluminum and aluminum alloys are used as matrices. Aluminum and alloys are chosen as matrices due to their low density which is an important requirement for weight critical applications. Furthermore, aluminum is inexpensive when compared to other light metals such as magnesium and titanium. Aluminum matrix composites (Al-MMCs) can be fabricated traditionally using either liquid state processes (casting methods) or solid state processes [5, 17]. The most commonly used particulate reinforcements in aluminum matrix are Silicon Carbide (SiC) and Alumina (Al_2O_3) [5, 10, 17]. The densities of these reinforcements are higher than that of aluminum. They

are readily available and relatively cheap and the addition of these particulates can enhance the elastic modulus and strength of composites. Other ceramic particulates such as TiB_2, B_4C and ZrO_2 have also been used as reinforcements in aluminum matrix composites [5]. Currently, aluminum based metal matrix composites are manufactured for potential industrial applications [18]. Research efforts on aluminum based composites are still growing to fulfill the special requirements for space applications [3].

2.2.2 Titanium Matrix Composites (Ti-MMCs)

Titanium has considerably higher density than magnesium and aluminum. However, it shows excellent strength to weight and stiffness to weight ratios when compared to other metals such as steel. The major advantage of Ti-MMCs over Al-MMCs and Mg-MMCs is the weight saving in elevated temperature applications. Ti-MMCs were introduced to be used initially in turbine engine components and subsequently their use extended to a variety of aerospace applications [19]. For aerospace applications, weight saving, good stiffness and strength at high temperatures are the most essential and desired properties. In that respect, titanium is the suitable light structural metal besides aluminum. Various processing routes have been investigated to fabricate Ti-MMCs, including powder metallurgy and in situ reactions. However, the difficulty in processing and production of Ti-MMCs is related to the high reactivity of the matrix. During application at higher temperature, the reactions between matrix and reinforcement cannot be avoided and it led to the use of coated fiber reinforcements to minimize the interfacial reactions. This is also the limitation for the use of discontinuous reinforcements in titanium matrix. Apart from this, the cost of

titanium is rather expansive. The coating cost coupled with the matrix cost results in additional production costs during processing. Because of the complex processing route and high production cost, the use of Ti-MMCs in common engineering applications is limited. More research efforts to establish the suitable processing methods to reduce the matrix/reinforcement interface reactions are needed for the development of Ti-MMCs for a wide range of applications [5, 10].

2.2.3 Magnesium Matrix Composites (Mg-MMCs)

Magnesium was discovered in 1774 and the metal was first isolated by French scientist Antoine Alexander Bussy in 1828. Commercial production of magnesium commenced in the middle of nineteenth century and subsequently many countries started producing it by 1900 [20]. Magnesium is available abundantly (2.7% of earth's crust) and magnesium ores which are enough for commercial production can be found in most of the countries. Magnesium, the lightest structural metal, which is approximately 35% lighter than aluminum is attractive in various applications. Increasing the drive of light structural materials in aircrafts and automotive vehicles leads to reduction in energy consumption and environmental impact [20, 21]. Especially due to its high specific strength, magnesium alloys play an important role among non-ferrous engineering alloys. The application of magnesium alloys in automotive industries is growing considerably and expected to be increased in the near future [20]. Although magnesium alloys are successfully applied in many industrial applications, their usage was relatively less when compared to aluminum alloys. This is due to some disadvantages of magnesium alloys which include limited workability and toughness at room temperature, poor corrosion properties and limited high

temperature properties. Efforts have been made to develop new magnesium alloy systems for high temperature applications. However, these alloys could not penetrate into automobile market significantly because of either not enough high temperature strength or high cost [22]. In the meantime, composite technology was established to create advanced and innovative composite materials which can offer unique and superior mechanical properties. As an alternative to magnesium alloys, researchers studied on the development of magnesium composite materials, intending to develop high performance and light weight materials for various demanding applications as well as to overcome some issues experienced by magnesium alloys [22]. At the beginning of composite age, continuous and discontinuous ceramic reinforcements were added to magnesium alloy matrix. Particularly due to isotropic mechanical properties and low cost of ceramic particulates, much attention was paid on the development of particulate reinforced magnesium composites. Ceramic particulates such as SiC, Al_2O_3 and B_4C are mostly used reinforcement types in magnesium matrix whereas metal particulates are rarely used as reinforcements. In general, the size of the particulates used in magnesium matrix is in micron and submicron length scale. The properties of some magnesium micro-composites can be seen in Table 2.2 [23].

Although the strength level can be increased, the main issue experienced with micron size particulate reinforcement is the reduction in ductility of magnesium except for metal particulate reinforcement like titanium. Recently, researchers found out that the use of nano particulates as reinforcement has the ability to enhance both strength and ductility of magnesium [14-16]. However, investigation on the development of magnesium matrix nanocomposites (Mg-MMNCs) is relatively limited at global scale. Detailed research works are still needed to improve the performance and reduce the

cost of these materials for wide spread applicability in engineering applications. With a proper selection of material compositions and fabrication methods, high performance Mg-MMCs can be realized as possible replacements for Al-MMCs [5, 10, 22].

Table 2.2. Mechanical properties of various Mg based materials [23].

Materials	0.2%YS (MPa)	UTS (MPa)	Ductility (%)	Specific YS	Specific UTS
Mg	100	258	7.7	58	148
Mg/2%Cu	281	335	2.5	148	177
Mg/4%Cu	355	386	1.5	170	184
Mg/7%Cu	–	433	1.0	–	195
Mg/2%Ni	337	370	4.8	177	194
Mg/3%Ni	420	463	1.4	203	224
Mg/6%Ni	–	313	0.7	–	131
Mg/2%Ti	163	248	11.1	90	137
Mg/4%Ti	154	239	9.5	81	126
AZ91	263	358	7.2	145	197
AZ91/4%Cu	299	382	6.2	142	181
Mg/30%SiCp	229	258	2	105	118
AZ91D/10%SiC_p	135	152	0.8	69	77
AZ91D/15%SiC_p	257	289	0.7	126	142

2.3 Production Methods for Mg-MMCs

Magnesium matrix composites can be produced by conventional processing techniques similar to aluminum matrix composites due to their comparable melting temperature. One of the challenges in processing of composites is to produce materials with homogeneously distributed reinforced phases essential for achieving good mechanical properties. Depending on the processing route and the different matrix-reinforcement combination, the performance of composites can be anticipated. Both liquid metallurgy and powder metallurgy based methods can be used to synthesize magnesium composites [7, 8, 10].

2.3.1 Liquid Phase Processes

In liquid phase processing, reinforcement particulates are incorporated into a molten matrix followed by mixing and casting or solidification of resultant molten metal matrix composites. Liquid phase processes are not only economical but also have many advantages which include the ability of producing composite materials with various shapes. However, the problem often encountered with these processes is the wettability of reinforcements, the formation of undesired reaction products between matrix and reinforcements and high viscosity of the melt, especially when fine reinforcement particulates are used.

2.3.1.1 Stir Casting

In general, stir casting of MMCs involves mechanical mixing of reinforcements into molten metal or metal alloy followed by casting. Suitable distribution of reinforcing phase is achieved through mechanical stirring [21, 24]. The most important part in this process is mechanical stirring in the furnace. The resultant metal matrix composite containing reinforcement particulates can then be solidified by various methods of die casting, permanent mold casting, or sand casting. The addition of reinforcements to the molten metal can cause the increase in viscosity of the melt and this is a common problem in stir casting processes. This can lead to undesirable inhomogeneous reinforcement distribution and agglomeration. The particulate size and stirring speed have also significant influence on the distribution and porosity level in resultant composites [24]. Another problem is the significant interfacial reaction which comes from prolonged liquid-reinforcement contact during casting. However, stir casting can produce composites containing high volume fraction of reinforcements

ranging from 10% to 40% [21, 23]. The cast composites are sometimes further processed via secondary consolidation processes such as extrusion to reduce porosity. This method is applied to fabricate magnesium composites with various magnesium alloy matrices such as AZ31, CP-Mg (chemically pure magnesium), ZC63, ZC71, and AZ91 [23]. Stir casting is economical and it has the ability of large-scale production of particulate reinforced metal matrix composites [3, 23, 25].

2.3.1.2 Squeeze Casting

Squeeze casting is a combination of casting and forging process. In squeeze casting technique, the reinforcements of various shapes (powders or fibers) are usually prepared as a preform and the preform is placed into a casting die or mold. The molten metal is then poured into the die. As soon as the composite material starts solidifying, high pressure is applied during the solidification process. The high pressure and the close contact of molten alloy with the metal die surface results in minimum porosity. In comparison to conventional die casting, squeeze casting can reduce the amount of shrinkage porosity and entrapped gas which can result in the highest mechanical properties attainable in a cast product [24]. In conventional casting, the particle content for making composites is limited to approximately 20 vol.%. For MMCs fabricated with the use of particle preform, higher particle content (more than 40 vol.%) can be incorporated into molten metal [26]. Generally, this technology is more useful for continuous reinforcements such as fibers and whiskers than stir casting method in which damage related to continuous reinforcements is one of the issues in manufacturing fiber reinforced MMCs. The squeeze casting can offer increased casting yield, better castability, near net shaped products with little or no additional

machining. However, the applied pressure for squeeze casting has to be carefully controlled because an extremely high pressure may produce a turbulent flow of magnesium melt, causing entrapment of gas and oxidation of magnesium [27]. The use of very high pressure can also cause the reinforcement damage in the resultant composites and deterioration of related mechanical properties of the materials [28]. The limitations of the squeeze casting process mainly based on the restrictions on the processing imposed by the shape and dimensions of the cast produce, and less availability of mass production [23].

2.3.2 Solid Phase Processes

Solid phase processing methods are relatively complicated. But they have advantages over liquid phase processes including minimizing interfacial reaction between matrix and reinforcement, and ability of using reactive materials such as titanium as matrix. Among numerous solid phase processing methods, mechanical alloying and powder metallurgy techniques are mostly used for the fabrication of magnesium matrix composites.

2.3.2.1 Mechanical Alloying (MA)

Mechanical alloying is a well established technique for the production of high performance materials. This method is also remarked as a potential method for achieving good dispersion of especially particulate reinforcements in the base metal matrix [29-31]. MA process involves mixing of raw powders with high energy milling balls mostly with additives in an inert atmosphere. During milling stage, the powders experience repeated cold welding and fracturing until fine mixed powder which are

finer than the starting constituents are obtained. After high energy mechanically milled powders are produced, these powders are usually consolidated through a number of consolidation processes such as hot isostatic pressing, cold or hot rolling and extrusion. Different characteristics of the final milled products are affected by several factors such as milling time, miller type, type of ball material, ball to powder weight ratio, milling atmosphere, process control agent or additive in the stage of milling [32]. With the use of prolong milling time and mixing of powders with high energy milling balls, solid state chemical reaction can occur, driven by repeated plastic deformation during milling. At an optimum milling time, welding and fracture mechanism of mixed powders reach equilibrium and equiaxed particles can be obtained. If the milling time is too long, the resultant particles exhibit irregular shape [33] and affect the mechanical properties of consolidated products. Mechanical alloying technique has been extensively used for the manufacturing of magnesium matrix composites [23, 34]. The development of functional magnesium matrix composites to be used as hydrogen storage materials has also been studied using this technique [23].

2.3.2.2 Powder Metallurgy (PM)

Powder metallurgy method is one of the conventional and well established methods used for the production of metal matrix composites, especially particulate reinforced metal matrix composites [7, 8, 24]. Powder metallurgy processed MMCs are manufactured by initially mixing the raw powders of matrix metal and reinforcement usually in dry condition with or without process control agent and/or controlled atmosphere. Various devices such as asymmetric mixers, mills or grinders can be used for mixing. Mixing of powders is followed by consolidation.

Consolidation can be done by a number of techniques such sintering, hot isostatic pressing, cold isostatic pressing, extrusion, forging, rolling, etc. At times, consolidation processes are combined to realize near dense products [7, 24, 27, 35, 36]. The advantages of PM methods include the capability of using almost any type of reinforcement and possibility of using high volume fractions of reinforcement. PM products usually achieve higher overall strength when compared to the products processed by solidification methods although ductility is reduced [7]. A variety of magnesium matrix composites are fabricated using PM method. Numerous magnesium based micro and nano composites have been produced using PM method [37-43]. Although PM process can offer near net shape and high precision samples, its main disadvantage of complex processing steps associated with high processing cost hinders the application of this method in manufacturing of various materials and components commercially. However, PM method is chosen when highly accurate and high performance components are needed in some of the end applications such as in aerospace industry [44].

2.4 Microwave Processing of Materials

2.4.1 Background on Microwave Heating

The development of microwave technology began in 1940 and was used in radar system for military purpose during the Second World War. In 1947, the first commercial microwave oven operating at 2.45 GHz for heating food was introduced by Raytheon [45]. Starting from the late 1950s, the use of microwave energy was expanded for the processing of materials like ceramics and polymer [46]. Around

2000, research work on microwave processing of metal based materials was paid much attention [47-51]. Microwaves occupy the portion of electromagnetic radiation spectrum between 300 MHz and 300 GHz with wavelengths ranging from 1mm to 1m in free space. Although the frequencies available for processing of materials are 915 MHz, 2.45 GHz, 5.8 GHz and 24.124 GHz, two most commonly used frequencies are 915 MHz and 2.45 GHz [52, 53]. Generally, 915 MHz is used in industries and 2.45 GHz is used for common domestic ovens. There are two types of microwave cavities, single-mode resonance cavities and multimode resonance cavities. Single-mode cavities are specially designed and generally used for industrial applications. The domestic microwave ovens are multimode cavities in which multiple plane waves impinges on the load (material to be heated) from different directions [54]. The characteristic of microwave heating is fundamentally different from that of conventional heating. In conventional heating methods, heat is transferred to the materials by different ways such as conduction, convection and radiation. The most common method of conventional heating is resistant heating in which heat is radiated onto the materials being processed. So heat is transferred from the surface of the materials into the interior by thermal conduction, making the surface hotter than the center. In contrast to conventional heating, microwaves exhibit inverse temperature distribution. In microwave heating, electromagnetic radiations are transformed into heat inside the materials and hence the heating is from core of the sample to outside. Heating is very rapid and volumetric due to energy conversion rather than energy transfer as in conventional heating.

2.4.2 Microwave Sintering of Materials

In principle, sintering is one of the consolidation methods to make bulk objects from loose powder compact by heating the material below its melting point. Conventionally, the green body (unsintered powder compact) is sintered using resistant heating. Since the resistant heating is the application of thermal energy, sintering process depends on the diffusion of atoms that cause the adherence of loose particles to each other [55, 56]. Sintering of materials using microwaves is a newly explored method and it has been applied successfully in processing of various materials. For sintering using microwaves, the electric and magnetic field components of the microwaves interact directly with the materials and dielectric and magnetic losses in the materials leads to self heating of materials. In this case, electromagnetic energy in the form of heat is generated volumetrically in the materials primarily through absorption during microwave-matter interaction. Initially, microwave energy was used to sinter various types of ceramic materials [46, 48]. By using microwave sintering, equal or superior performance ceramic products can be produced through shorter sintering time at lower temperature and at low cost when compared to conventionally sintered products. At room temperature, most of the ceramics do not couple well with microwaves particularly at 2.45 GHz microwave frequency and they are not heated appreciably. Their coupling efficiency or absorption can be increased by increasing the temperature, using microwave susceptor/absorber, altering their microstructure and defect structure, and changing the microwave frequency. Researchers normally apply the method of increasing the room temperature coupling by using external susceptor to bring temperature of the materials to its microwave coupling temperature. The microwave sintering technique using microwave susceptors is usually termed as hybrid

sintering which is the combination of pure microwave heating and conventional heating from the susceptor. In most of the hybrid sintering methods, SiC of various forms such as SiC tube [57] SiC rods [58-60], SiC sample holders [61] are preferably used mainly due to its high loss factor. The advantages of hybrid microwave sintering include rapid and more uniform heating, prevention of hot spot formation, more uniform and finer microstructure leading to high performance samples [62].

Most of the investigations were conducted on the microwave sintering of semiconductors, inorganic, ceramics and polymeric materials until 2000. Lack of research on microwave sintering of metals is based on the well known fact that all metals reflect the microwave causing arching during microwave heating and limited penetration of the microwave radiation. Later, researchers have realized that arching phenomenon only applies to bulk metals and all metallic materials in powder or particle form can couple with and absorb microwaves [48, 62-64]. The idea of applying microwave energy to sinter metals and metallic materials is relatively new and limited studies have been done on sintering of metal based materials. From the literature search, most of the studies are reported on the microwave sintering of iron based materials and only a few reports are based on copper, aluminum and magnesium based materials/composites [64].

2.5 Motivation of Current Work

Based on the literature survey, it was found that magnesium based micro-composites containing mostly ceramics reinforcements were fabricated by using common processing methods. Limited studies have been reported on metal particle

reinforced magnesium composites. The use of ceramics as well as metal reinforcements in magnesium showed appreciable improvement in strength and reduction in ductility. The reduction in ductility led to reduced deformability of Mg-MMCs prompting the researchers to use reinforcements at nano length scales. Recent reports on magnesium nanocomposites showed the feasibility of using ceramic nanoparticulates such as alumina and yttria to improve both strength and deformability of magnesium. Both liquid metallurgy and solid metallurgy were attempted for the synthesis of magnesium nanocomposites. In the meantime, microwave processing of metallic materials has been gaining attention due to its ability to reduce significantly the time required for sintering and energy consumption. At the time when this Ph.D project started, no attempt was made to investigate: a) effects of microwave processing step such as heating rate, b) effects of extrusion ratio on end properties of Mg nanocomposites and c) effects of hybrid reinforcements on the microstructure and properties of magnesium based nanocomposites. The present Ph.D research thesis thus provides the insight into these issues. Target materials were Mg/Y_2O_3, Mg/(Y_2O_3+Cu) and Mg/(Y_2O_3+Ni). All these materials were synthesized using powder metallurgy technique incorporating hybrid microwave sintering followed by hot extrusion. It may be noted that materials developed in this study are new and have not been investigated in the past using the methodology described in this thesis.

2.6 References

[1] A.A. Baker, *Introduction and Overview*. In Composite materials for aircraft structures, 2nd ed., edited by A.A. Baker, S. Dutton and D. Kelly, Reston, Virginia, American Institute of Aeronautics and Astronautics, 2004, pp. 1-21.

[2] National Research Council (U.S), "*New materials for next-generation commercial transports*", Washington, D.C, National Academy Press, 1996.

[3] A. Evans, C.S. Marchi and A. Mortensen, *Metal matrix composites in industry: An introduction and a survey*, Dordrecht, Boston, Kluwer Academic, 2003.

[4] A. Luo, Metall. Mater. Trans. A, 26A (1995) 2445-2455.

[5] V.K. Lindroos and M.J. Talvitie, J. Mater. Process. Tech., 53 (1995) 273-284.

[6] D.L. McDanels, Metal. Trans. A, 16A (1985) 1105-1115.

[7] D.J. Lloyd, Int. Mater. Rev., 39 (1994) 1-23.

[8] I.A. Ibrahim, F.A. Mohamed and E.J. Lavernia, J. Mater. Sci., 26 (1991) 1137-1156.

[9] K.U. Kainer, *Basic of Metal Matrix Composites*. In Metal matrix composites: Custom-made materials for automotive and aerospace engineering, edited by K.U. Kainer, Weinheim, Chicheste, Wiley-VCH, 2006.

[10] N. Hort and K.U. Kainer, *Powder Metallurgically Manufactured Metal Matrix Composites*. In Metal matrix composites: Custom-made materials for automotive and aerospace engineering, edited by K.U. Kainer, Weinheim, Chicheste, Wiley-VCH, 2006.

[11] Y.C. Kang and S.L. Chan, Mater. Chem. Phy., 85 (2004) 438-443.

[12] Z.Y. Ma, Y.L. Li, Y. Liang, F. Zheng, J. Bi and S.C. Tjong, Mater. Sci. Eng. A, 219 (1996) 229-231.

[13] S.F. Hassan and M. Gupta, Comp. Struct., 72 (2006) 19-26.

[14] S.F. Hassan and M. Gupta, J. Alloys Compd., 429 (2007) 176-183.

[15] W.L.E. Wong and M. Gupta, Adv. Eng. Mater., 8 (2006) 735-740.

[16] H. Ferkel and B.L. Mordike, Mater. Sci. Eng. A, 298 (2001) 193-199.

[17] J.M. Torralba, C.E. da Costa and F. Velasco, J. Mater. Process. Tech., 133 (2003) 203-206.

[18] J. Hooker and P. Doorbar, *Metal Matrix Composites for Aeroengines*. In Metal and Ceramic Matrix Composites, Bristol, Institute of Physics Pub., 2004.

[19] S. Mall, T. Nicholas (Editors), *Titanium Matrix Composites: Mechanical Behavior*, Lancaster, Technomic Pub. Co. Inc., 1998.

[20] M. Avedesian and H. Baker (Editors), *ASM handbook, Magnesium and Magnesium Alloys*, Materials Park, Ohio, ASM International, 1999.

[21] D.B. Miracle, Comp. Sci. Tech., 65 (2005) 2526–2540.

[22] K.U. Kainer (Editor), *Magnesium Alloys and Technology*, Weinheim, Cambridge, Wiley-VCH, 2002.

[23] H. Z. Ye, X. Y. Liu, J. Mater. Sci., 39 (2004) 6153-6171.

[24] M.M. Schwartz, *Composite Materials: Properties, Fabrication and Applications*, N.J., Prentice Hall, 1997.

[25] P. Rohatgi, AFS Trans., 01-133 (2001) 1-25.

[26] R. Buschmann, *Preforms for the Reinforcement of Light Metals: Manufacture, Applications and Potential*. In Metal matrix composites: Custom-made

materials for automotive and aerospace engineering, edited by K.U. Kainer, Weinheim, Chicheste, Wiley-VCH, 2006.

[27] H. Lianxi and W. Erde, Mater. Sci. Eng. A, 278 (2000) 267-271.

[28] K.S. Sohn, K. Euh, S. Lee and I. Park, Metall. Mater. Trans. A, 29 (1998) 2543-2554.

[29] D.C. Jia, Mater. Sci. Eng. A, 289 (2000) 83-90.

[30] F. Tang, M. Hagiwara and J.M. Schoenung, Scripta Mater., 53 (2005) 619-624.

[31] F.Y. Boey, Z. Yuan and K.A. Khor, Mater. Sci. Eng. A, 252 (1998) 276-287.

[32] C. Suryanarayana, Prog. Mater. Sci., 46 (2001) 1-184.

[33] Z. R. Hesabi, A. Simchi and S.M. Reihani, Mater. Sci. Eng. A, 428 (2006) 159-168.

[34] L. Lu, M.O. Lia and M.L. Hoe, Nanostruct. Mater., 10 (1998) 551-563.

[35] S. Suresh, A. Mortensen and A. Needleman (Editors), *Fundamental of Metal Matrix Composites*, Boston, Butterworth-Heinemann, 1993.

[36] R.M. German, *Powder metallurgy science*, Princeton, N.J., Metal Powder Industries Federation, 1994.

[37] Q.C. Jiang, H.Y. Wang, B.X. Ma, Y. Wang and F. Zhao, J. Alloys Compd., 386 (2005) 177-181.

[38] G. Graces, M. Rodriguez, P. Perez, P. Adeva, Mater. Sci. Eng. A, 419 (2006) 357-364.

[39] C. Badini, F. Marino, M. Montorsi and X. B. Guo, Mater. Sci. Eng. A, 157 (1992) 53-61.

[40] B.W. Chua, L. Lu and M.O. Lai, Comp. Struct., 47 (1999) 595-601.

[41] S. F. Hassan, M. Gupta, Trans. ASME, 129 (2007) 462-467.

[42] C.S. Goh, J. Wei, L.C. Lee and M. Gupta, Acta Mater., 55 (2007) 5115-5121.

[43] C.S. Goh, J Wei, L.C. Lee and M. Gupta. Nanotech., 17 (2006) 7-12.

[44] Website: http://mmc-assess.tuwien.ac.at/public/mmc_in_ind.pdf.

[45] T.V.C.T. Chan and H.C. Reader, *Understanding microwave heating cavities*, Boston, MA, Artech House, 2000.

[46] D.E. Clark and W.H. Sutton, Annu. Rev. Mater. Sci., 26 (1996) 299-331.

[47] S. Leparoux, S. Vaucher and O. Beffort, Adv. Eng. Mater., 5 (2003) 449-453.

[48] R. Roy, D. Agrawal, J. Cheng and S. Gedevanishvili, Nature, 399 (1999) 668-670.

[49] R.M. Anklekar, D.K. Agrawal and R. Roy, Powder Metall., 44 (2001) 355-362.

[50] E. Breval, J.P. Cheng, D.K. Agrawal, P. Gigl, M. Dennis, R. Roy and A.J. Papworth, Mater. Sci. Eng. A, 391 (2005) 285-295.

[51] K. Saitou, Scripta Mater., 54 (2006) 875-879.

[52] D.F. Stein (Chairman), *Microwave Processing of Materials*, Committee on Microwave Processing on Materials, National Materials Advisory Board, 1994.

[53] W.H. Sutton, Am. Ceram. Soc. Bull., 68 (1989) 376-386.

[54] H. Zhang and A.K. Datta, *Electromagnetics of Microwave Heating: Magnitude and Uniformity of Energy Absorption in an Oven*. In Handbook of microwave technology for food applications, edited by A.K. Datta and R.C. Anantheswaran, New York, Marcel Dekker, 2001.

[55] R.M. German, *Sintering Theory and Practice*, New York, Wiley, 1996.

[56] I. Jenkins and J. Wood (Editors), *Powder Metallurgy: An Overview*, London, Institute of Metals, 1991.

[57] C. Zhao, J. Vleugels, C. Groffils, P. J. Luypaert and O. van der biest, Acta Mater., 48 (2000) 3795-3801.

[58] Z. Xie, Y. Huang, R. Zhang, J. Yang and S. Wang, Am. Ceram. Soc. Bull., 76 (1997) 46-50.

[59] G. Xu, H. Zhuang, W. Li and F. Wu, J. Eur. Ceram. Soc., 17 (1997) 977-981.

[60] G. F. Xu, H.R. Zhang, F.Y. Wu, and W.L. Li, J. Eur. Ceram. Soc., 17 (1997) 675-680.

[61] J. Wilson and S.M. Kunz, J. Am. Ceram. Soc., 71 (1988) C40-C41.

[62] M. Gupta and W.L.E. Wong, *Microwaves and Metals*, Singapore, John Wiley & Sons Pte. Ltd., 2007.

[63] J.W. Walkiewicz, G. Kazonich and S.L. McGill, Miner. Metall. Proc., 5 (1988) 39-42.

[64] H. Sheinberg, T.T. Meek and R.D. Blake, US Patent 4942278, *Microwaving of Normally Opaque and Semi-opaque Substances*, 17 July 1990.

CHAPTER 3

MATERIALS AND EXPERIMENTAL METHODOLOGIES

CHAPTER 3

MATERIALS AND EXPERIMENTAL METHODOLOGIES

3.1 Overview

In the current study, matrix material used was pure magnesium. Two different volume percentages, 0.17vol.% and 0.7vol.% (0.5wt.% and 2wt.%), of Y_2O_3 nanoparticulates were used as reinforcements in the first part of the study to develop Mg/Y_2O_3 nanocomposites using hybrid microwave sintering instead of conventional sintering which is part of the powder metallurgy processes. Based on the best Mg nanocomposite composition, $Mg/0.7Y_2O_3$, the heating rate during microwave sintering was optimized. For synthesis of materials, extrusion was used as the secondary processing step after blend-press-sinter powder metallurgy processes used in this study. Three different extrusion ratios were used to extrude Mg and $Mg/0.7Y_2O_3$ to find the effective extrusion ratio for secondary consolidation of microwave sintered materials. The next step of this study was the development of new hybrid magnesium nanocomposites using Cu and Ni metal nanoparticulates as hybrid reinforcements in $Mg/0.7Y_2O_3$ composition. Materials synthesized by microwave assisted powder metallurgy route followed by hot extrusion were characterized in terms of their microstructural, physical and mechanical properties.

3.2 Materials

Magnesium powder of 98.5% purity and with a size range of 60-300 μm, acquired from Merck, Germany was used as the matrix material. Ceramic

reinforcement used was yttria (Y_2O_3) with a particulate size range of 30-50 nm, supplied by Inframat Advanced Materials, USA. Metal reinforcements used were copper (Cu) and nickel (Ni) with an average particulate size of 25 nm and 20 nm respectively and were purchased from Nanostructured & Amorphous Materials Inc., USA.

3.3 Primary Processing

Monolithic magnesium and its nanocomposites were synthesized using the powder metallurgy technique. The synthesis procedure involved blending pure magnesium powder with nano-sized powder in a mechanical alloying machine [Model: RETSCH PM-400] at 200 rpm for 1 hour (60 minutes). The blended powder mixtures were subsequently cold compacted at a pressure of 97 bars (510 MPa) using a 100-ton press to form billets that measured 35-mm in diameter and 40-mm in height. Monolithic magnesium was compacted using the same parameters but without blending of the powder. The compacted billets were coated with colloidal graphite and immediately sintered using an innovative hybrid microwave sintering technique [1] for 13 minutes to reach a temperature (~640°C) near the melting point of magnesium using a 900W, 2.45 GHz SHARP microwave oven (multimode cavity) under the ambient conditions. The schematic diagram of experimental setup is shown in figure 3.1.

To study the effect of hybrid microwave heating rate on Mg and Mg/Y_2O_3 nanocomposite, the billets were heated to 640ºC in a microwave oven using average heating rate of 49˚C/min and 20˚C/min, respectively. The higher heating rate

(49˚C/min) was realized by using maximum possible amount of susceptor (400g) that was possible in the present experimental set-up. The lower heating rate (20˚C/min) was realized by using lower amount of susceptor (300g). Lower heating rate selection in this study was governed by the oxidizing tendency of magnesium under the ambient conditions used in the present study. A further lower heating rate led to significant oxidation and was not attempted.

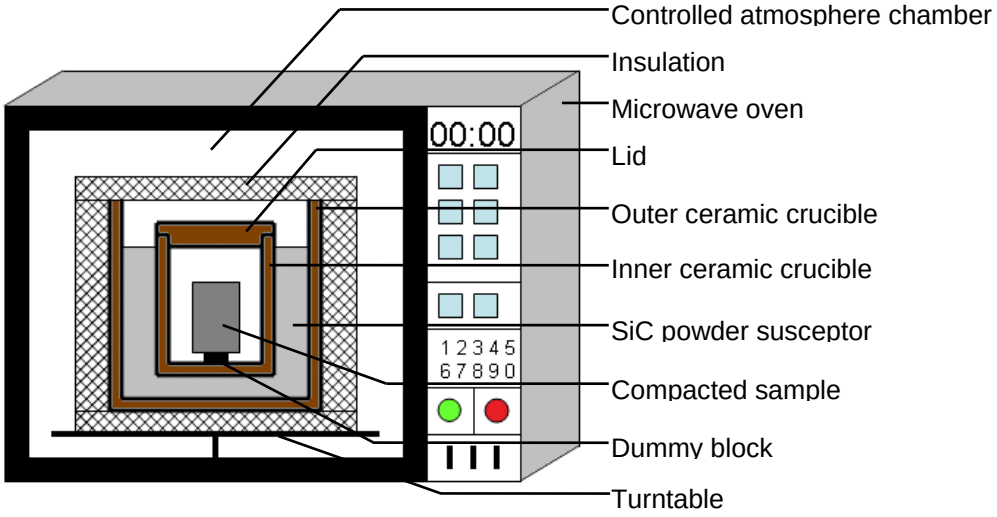

Figure 3.1. Schematic diagram of experimental setup.

3.4 Secondary Processing

3.4.1 Extrusion

Billets of microwave sintered Mg and Mg nanocomposites were extruded at a temperature of 350ºC using an extrusion ratio of 25:1 on a 150-ton hydraulic press. Before extrusion, the billets were soaked at a constant temperature of 400ºC for 1 hr (60 minutes) in resistant furnace. Colloidal graphite was used as lubricant during extrusion and rods of 7 mm diameter were obtained following extrusion.

To study the effect of extrusion ratio on microwave sintered Mg and Mg/Y_2O_3 nanocomposite, three different extrusion ratios (12:1, 19:1 and 25:1) were used. Same soaking time and temperature were used before extrusion and rods of 10 mm, 8 mm and 7 mm were obtained following extrusion accordingly.

3.5 Density Measurements

The density of extruded magnesium and magnesium nanocomposites in the as-polished condition was measured in accordance with Archimedes' principle [2]. Three samples were randomly selected from the extruded rods and were carefully weighed both in air and when fully immersed in distilled water. An electronic balance [Model: AND ER-182A] with an accuracy of 0.0001g was used for recording the weights. The theoretical densities of each of the nanocomposite formulations were calculated using rule-of-mixtures. For computing theoretical densities of composites, density values of 1.74 g/cc for Mg, 5.03 g/cc for Y_2O_3, 8.94 g/cc for Cu and 8.908 g/cc for Ni were used.

3.6 Microstructural Characterization

Microstructural characterization studies were conducted to determine grain size, grain morphology, formation of twinned grains, presence and distribution of reinforcement and intermetallics, and interfacial integrity between matrix and secondary phases. A metallographic optical microscope [Model: OLYMPUS] and a Scion Image Analyzer, and Field Emission Scanning Electron Microscope (FESEM)

[Model: HITACHI S-4300] equipped with Energy Dispersive Spectroscopy (EDS) were used for this purpose.

3.7 X-ray Diffraction Studies

X-ray diffraction analysis was carried out on the polished extruded Mg and Mg nanocomposite samples using automated Shimadzu LAB-X XRD-6000 diffractometer. The samples were exposed to CuK_{α} radiation (λ=1.54056A°) at a scanning speed of 2°C/min. The Bragg angle and the values of the interplanar spacing (d) obtained were subsequently matched with the standard values for Mg, Y_2O_3, Cu, Ni and related phases. With the purpose of analyzing compressive properties of synthesized materials, reorientation of crystal planes before and after compression was also analyzed.

3.8 Coefficient of Thermal Expansion

The coefficients of thermal expansion (CTEs) of extruded magnesium and its composites were determined using thermomechanical analyzer [Model: SETARAM 92-16/18]. Displacement of the samples as a function of temperature (50–400ºC) was measured using an alumina probe under argon atmosphere. SETARAM software was used to determine the CTE values for the samples.

3.9 Mechanical Characterization

3.9.1 Microhardness

Microhardness measurements were performed on the polished samples using an automatic digital microhardness tester [Model: Matsuzawa MXT 50 and Shimadzu-HMV]. The microhardness tests were performed using a Vickers indenter under a test load of 25 gf and a dwell time of 15 s in accordance with the ASTM standard E384–99.

3.9.2 Tensile Testing

The tensile properties of the as-extruded monolithic magnesium and its composite counterparts were determined in accordance with procedures outlined in ASTM standard E8M-01. The tensile tests were conducted on round tension test specimens (5-mm gage diameter and 25-mm gage length) on a fully-automated servo-hydraulic mechanical testing machine [Model: MTS 810] at a crosshead speed set at 0.254 mm/min. The stress versus strain curves obtained following testing were used to compute the work of fractures (area under the engineering stress versus engineering strain curve) using an excel software. Extensometer [Model: MTS 634. 12F-24] was used for strain recording.

3.9.3 Compression Testing

Room temperature uniaxial compressive tests were performed on cylindrical monolithic and composite samples according to ASTM E9-89a using an automated servo hydraulic testing machine [Model: MTS 810]. Extruded rod of 7 mm diameter

was cut into 7 mm length samples for compression tests to provide the aspect ratio (l/d) of unity. Samples were tested at a strain rate of 5×10^{-3} min^{-1} and the compression load was applied parallel to the extrusion direction.

3.10 Fractography

Fracture surface characterization studies were carried out on the tensile and compressive fracture surfaces of Mg and Mg nanocomposites with the objective of establishing the failure mechanisms. Fractography was accomplished using a scanning electron microscope (SEM) [Model: JEOL JSM-5600 LV] and a Field Emission Scanning Electron Microscope (FESEM) [Model: HITACHI S-4300].

3.11 References

[1] M. Gupta and W.L.E. Wong, Scripta Mater., 52 (2005) 479-483.

[2] M. Gupta, M.O. Lai and D. Saravanaranganathan, J. Mater. Sci., 35 (2000) 2155-2165.

CHAPTER 4

DEVELOPMENT OF Mg/Y_2O_3 NANOCOMPOSITES

The work presented in this chapter is published. The citation is as follows:

K.S. Tun and M. Gupta, "Improving mechanical properties of magnesium using nano-yttria reinforcement and microwave assisted powder metallurgy method", Comp. Sci. Tech., 67 (2007) 2657-2664.

CHAPTER 4

DEVELOPMENT OF Mg/Y_2O_3 NANOCOMPOSITES

Summary

The main aim of this part of study was to determine the amount of Y_2O_3 reinforcement that results into best combination of strength and ductility. Magnesium nanocomposites containing 0.17 and 0.7 volume percentage of Y_2O_3 were synthesized through powder metallurgy route incorporating microwave assisted rapid sintering technique (heating rate: 49°C/min) followed by hot extrusion. Microstructural characterization revealed reasonably uniform distribution of Y_2O_3 particulates in the matrix and the presence of nanopores. Thermomechanical analysis revealed significant reduction in CTE of magnesium as a result of presence of yttria nanoparticulates. Mechanical characterization studies revealed that hardness, 0.2% yield strength, ultimate tensile strength, work of fracture and ductility of pure Mg increased when 0.17 and 0.7 vol.% of nano yttria reinforcements are added into Mg matrix. The studies revealed that the best combination of mechanical properties is realized from the composite containing 0.7 volume percentage of yttria.

4.1 Introduction

Magnesium based composites are increasingly getting attention of materials community as a result of their weight saving capabilities [1-3]. The main drawback of magnesium based materials is their low ductility, toughness and stiffness when compared to aluminum based materials. Recently, investigators have indicated that

ductility and work of fracture of magnesium can be increased by using reinforcements such as Mo [4], Ti [5], CNTs [6] and alumina [7]. Most of the work on development of magnesium based materials is done on the samples processed using solidification route [8-10] or powder metallurgy route [11-14]. For magnesium matrix composites, conventional reinforcements such as SiC and Al_2O_3 in particulate form are commonly used. Results of literature search indicated that yttria in particulate form in magnesium matrix has been investigated to a limited extent. Garces *et al.* investigated the microstructure, tensile and compressive properties to correlate the mechanical anisotropy with texture of magnesium matrix reinforced with micron size yttria reinforcements of two different sizes up to 20 volume percent [14]. Dunand *et al.* reported microstructure, room temperature tensile and compressive properties and creep of dispersion-strengthened-cast magnesium (DSC-Mg) containing 30 volume percent of submicron size Y_2O_3 particulates [9, 10]. Nano size yttria particles have been used as reinforcement only in the case of titanium matrix and not in magnesium matrix. The titanium composites were made using solidification processing and the amount of yttria was varied from 0.3 to 0.7wt.%. Attempts were made in that study to establish interrelationship between hardness and tensile tests [15].

The results of literature research reveal that no attempt is made to synthesize Mg/Y_2O_3 formulations using energy efficient microwave assisted powder metallurgy route and where the yttria particulate length scale is in nanometers. Accordingly, the present study was aimed at synthesizing Mg/Y_2O_3 composites using powder metallurgy route incorporating innovative microwave assisted rapid sintering coupled with hot extrusion. The synthesized materials were characterized for physical,

microstructural and mechanical properties. Particular emphasis was placed to study the effect of increasing presence of nano Y_2O_3 particulates in magnesium matrix.

4.2 Results

4.2.1 Macrostructure

The results of macrostructural characterization on the compacted and extruded monolithic and composite samples did not reveal presence of any macrodefects. The outer surfaces were smooth and free of circumferential cracks.

4.2.2 Density Measurements

The density and porosity measurements conducted on the extruded magnesium and its composite samples are listed in Table 4.1. The amount of porosity level in all samples remained below 1% indicating the near net shape forming capability of the processing methodology adopted in this study.

4.2.3 Microstructural Characterization

The results of microstructural characterization revealed uniform distribution of nanosized Y_2O_3 particulates in the case of Mg/0.17%Y_2O_3 (Figure 4.1a) and fairly uniform distribution of nanosized Y_2O_3 particulates with a few clusters in the case of Mg/0.7%Y_2O_3 (Figure 4.1b) samples. The identity of the Y_2O_3 particulates was confirmed through EDS point analysis (Figure 4.2). Nanopores were observed in all the composite samples. The results of grain size and aspect ratio of the extruded

samples are shown in Table 4.1. Near-equiaxed grain morphology was observed for both monolithic and reinforced samples.

Table 4.1 Results of density, porosity and grain morphology determinations.

Material	Reinforcement		Density (g/cm^3)	Porosity (vol.%)	Grain characteristics	
	wt.%	vol.%			Size (μm)	Aspect ratio*
Mg	-	-	1.74 ± 0.01	0.13	20 ± 3	1.4 ± 0.1
Mg/Y_2O_3	0.5	0.17	1.73 ± 0.01	0.87	19 ± 3	1.4 ± 0.2
Mg/Y_2O_3	2.0	0.70	1.76 ± 0.01	0.35	18 ± 3	1.4 ± 0.2

* Aspect ratio is measured by dividing the maximum dimension of the grain by the minimum dimension of the grain.

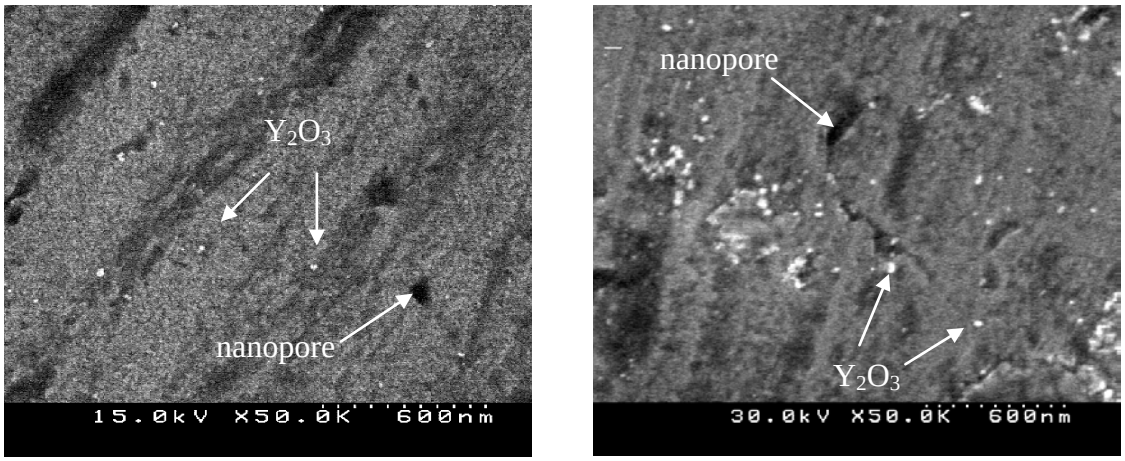

(a) (b)

Figure 4.1. Representative FESEM micrographs showing reinforcement distribution of Y_2O_3 particulates and presence of nanopores in the case of: (a) Mg/0.17Y_2O_3 and (b) Mg/0.7Y_2O_3.

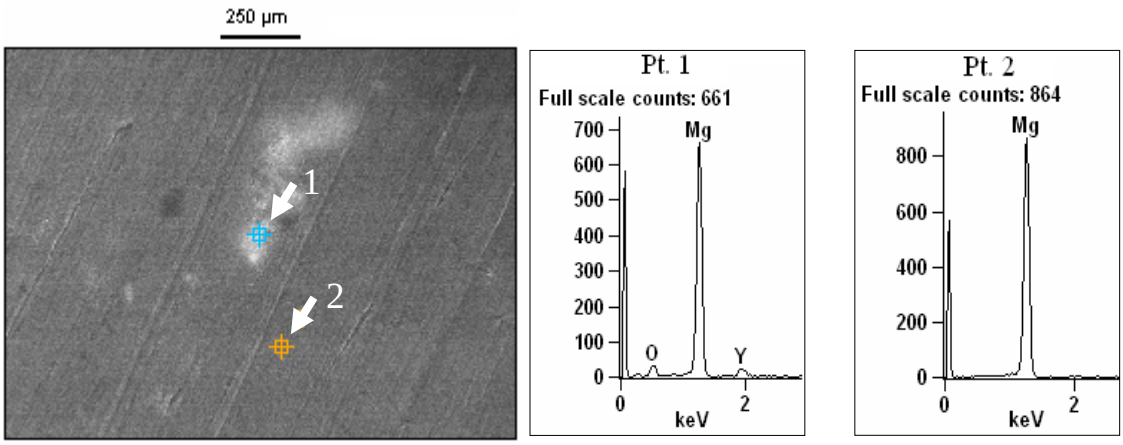

(a)

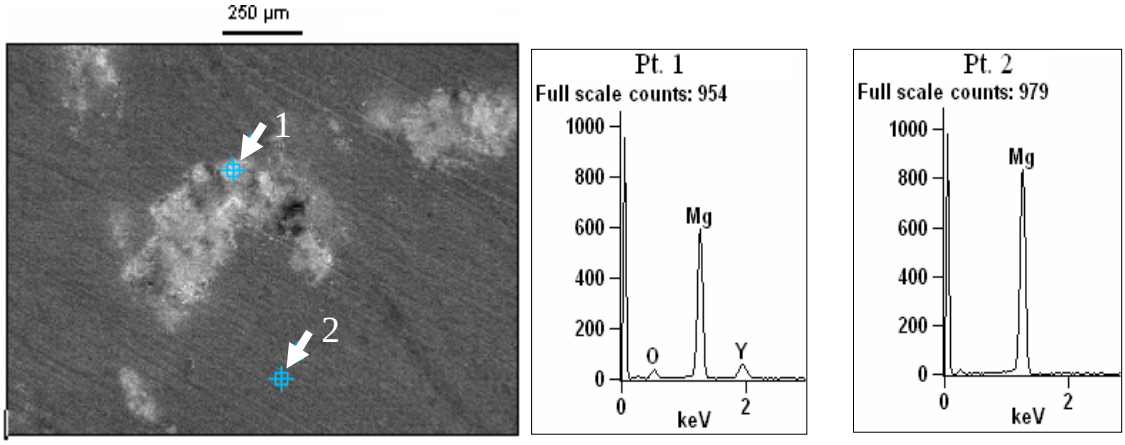

(b)

Figure 4.2. EDS analysis showing the presence of Y_2O_3 particulates in the case of: (a) Mg/0.17Y_2O_3 and (b) Mg/0.7Y_2O_3.

4.2.4 X-Ray Diffraction Studies

The results of X-ray diffraction studies are shown in Figure 4.3. No matching peaks of Y_2O_3, MgO, or other related phases were observed in any samples. The absence of the peaks except for that of magnesium may be attributed to the low volume fraction (less than 0.7%) of these phases.

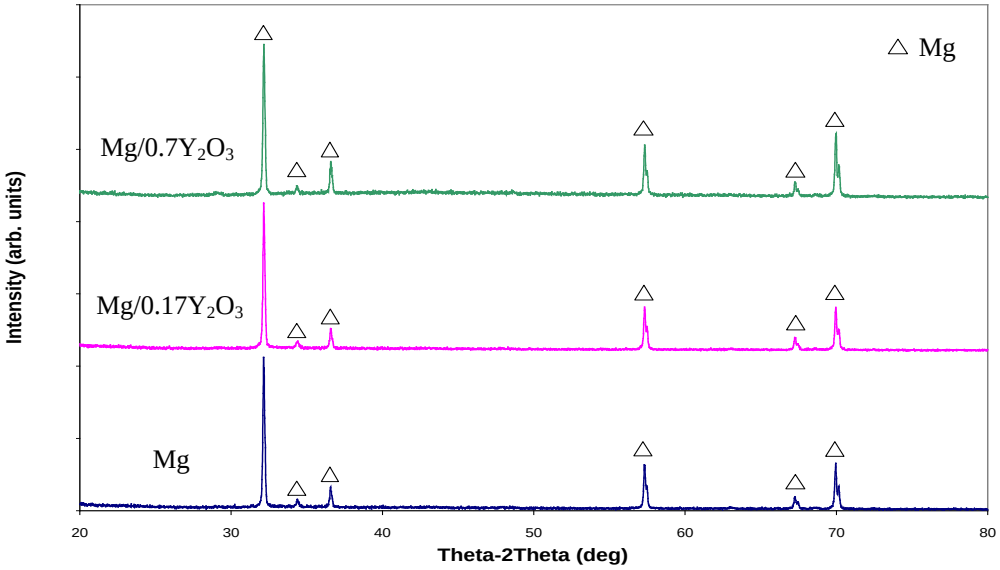

Figure 4.3. X-Ray diffractograms of Mg and Mg/Y_2O_3 samples.

4.2.5 Coefficient of Thermal Expansion

The results of coefficient of thermal expansion (CTE) measurements obtained from monolithic and composite samples are shown in Table 4.2. The results revealed: (a) reduction in CTE of magnesium as a result of presence of Y_2O_3 and (b) marginal reduction in average CTE with an increase in Y_2O_3 amount from 0.17 vol.% to 0.7 vol.%.

Table 4.2 Results of CTE and microhardness measurements.

Material	Experimental CTE ($\times 10^{-6}$/ºC)	Microhardness (HV)
Mg	28.2 ± 0.0	37 ± 2.0
$Mg/0.17\%Y_2O_3$	21.3 ± 0.1	38 ± 0.4
$Mg/0.7\%Y_2O_3$	20.8 ± 0.6	45 ± 2.0

4.2.6 Mechanical Behavior

The results of microhardness measurements conducted on Mg and Mg/Y_2O_3 samples are listed in Table 4.2 and representative stress-strain curves of Mg and Mg/Y_2O_3 samples are shown in Figure 4.4. The results show a significant change in hardness values of pure magnesium when 0.7 vol.%Y_2O_3 was present in matrix. The results from ambient temperature tensile testing are listed in Table 4.3. The tensile property results revealed that Mg/Y_2O_3 nanocomposite samples exhibit superior combination of 0.2% yield strength, UTS and ductility when compared to pure magnesium samples. The increasing trend of overall mechanical properties is observed with increasing volume percentage of nanosized Y_2O_3 particulate reinforcement.

Table 4.3 Results of ambient temperature tensile properties.

Materials	Reinforcement		0.2%YS (MPa)	UTS (MPa)	Ductility (%)	Work of fracture (MJ/m^3)
	wt.%	vol.%				
Mg	-	-	134 ± 7	193 ± 1	7.5 ± 2.5	12.9 ± 4.8
Mg/Y_2O_3	0.5	0.17	144 ± 2	214 ± 4	8.0 ± 2.8	16.6 ± 4.2
Mg/Y_2O_3	2.0	0.70	157 ± 10	244 ± 1	8.6 ± 1.2	21.8 ± 3.1
Mg/Y_2O_3 [a] [14]	-	5.0	238 [d]	-	4	-
Mg/Y_2O_3 [b] [14]	-	5.0	229 [d]	-	3.5	-
Mg/Y_2O_3 [c] [9]	-	30.0	230 [e]	230 [e]	0	-

[a] particle size of < 1μ.
[b] micron sized particles.
[c] submicron sized particles.
[d] value estimated from graph.
[e] samples failed prematurely in the elastic range.

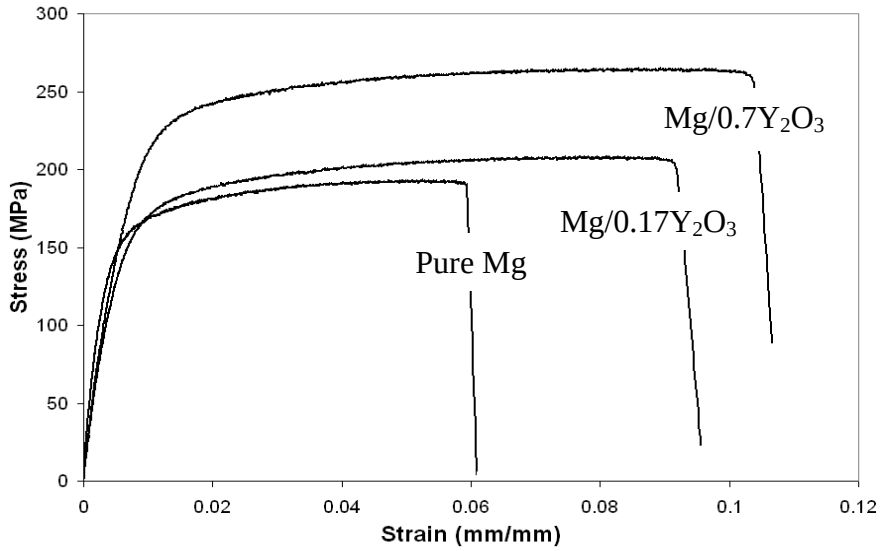

Figure 4.4. Representative stress-strain curves of pure Mg and Mg/Y_2O_3 nanocomposites.

4.2.7 Fractography

Tensile fracture surfaces of Mg and Mg/Y_2O_3 samples are shown in Figure 4.5. Fracture surface of Mg samples indicates the presence of cleavage steps and microscopically rough features. Fracture studies conducted on the composites samples revealed mixed mode failure showing more evidences of matrix plastic deformation.

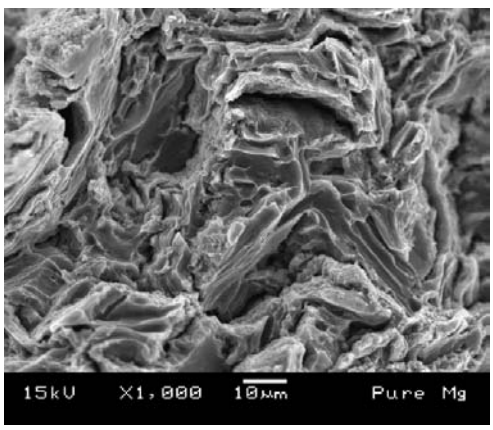

(a)

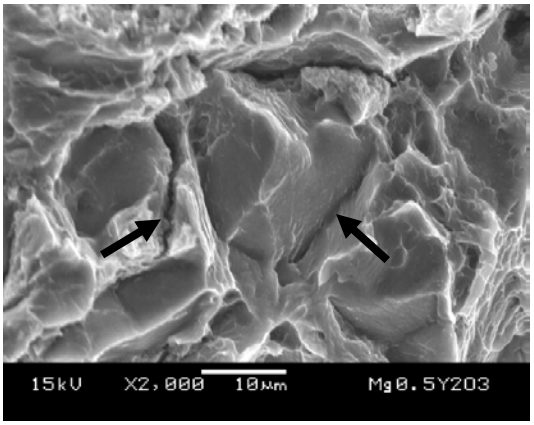

(b)

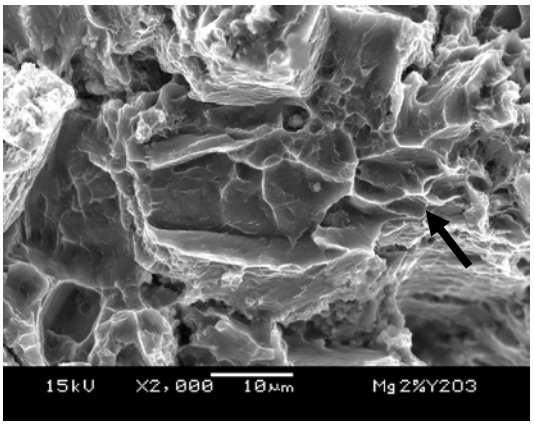

(c)

Figure 4.5. Representative fractrographs showing: (a) brittle failure in pure Mg, (b) intergranular crack propagation in the case of $Mg/0.17\%Y_2O_3$ and (c) some dimple like features in the case of $Mg/0.7\%Y_2O_3$.

4.3 Discussion

4.3.1 Synthesis of Mg and Mg/Y_2O_3 Nanocomposites

Synthesis of monolithic and Mg/Y_2O_3 nanocomposites has been successfully accomplished using powder metallurgy route incorporating microwave assisted rapid sintering technique and hot extrusion. The density of both monolithic and composite samples was greater than 99% indicating the appropriateness of the processing steps and parameters. In particular, the results revealed that energy efficient microwave

sintering instead of conventional sintering can be used. It may be noted that normal sintering time (heating-holding-cooling) for a 35-mm billet is about 3 hours while it took only 13 min in microwave. This translates to a cut in ~92.8% of sintering time.

4.3.2 Microstructure

The studies conducted on the extruded samples revealed near equiaxed grain shape (see Table 4.1). Grain size measurements of the nanocomposite samples revealed a reduction in average matrix grain size with increasing volume percentage of nanosized Y_2O_3 particulates. The reduction in grain size, however, was marginal and within the standard deviation of each other. The distribution of Y_2O_3 particulates was relatively more uniform at low volume percentages (0.17 vol.%) and the presence of clusters was evident at high volume percentages (0.7 vol.%) (Figure 4.1). The results thus suggest that the blending parameters need to be further optimized for high volume percentage of Y_2O_3 particulates. The results are, however, encouraging considering the difference in size of Mg powder (60-300μm) and Y_2O_3 particulates (30-50nm). Microstructural characterization further revealed the presence of almost equiaxed nanopores (see Figure 4.1). The pores were not necessarily located with particulate clusters. The volume fraction of porosity was also limited (see Figure 4.1 and Table 4.1) and indicate the appropriateness of blending, microwave sintering and extrusion parameters [17, 18].

4.3.3 Coefficient of Thermal Expansion

The reduction in average coefficient of thermal expansion (CTE) of composite samples can be attributed to the presence of nano Y_2O_3 reinforcements which has lower CTE value ($7.6x10^{-6}K^{-1}$) [19] when compared to pure Mg ($28.9x10^{-6}K^{-1}$) [20]. The results suggest the existence of good microstructural conditions (distribution and interfacial integrity) in terms of presence of Y_2O_3 particulates. The results obtained in this study thus reveal that good thermal stability can be obtained by the addition of nanosized Y_2O_3 particulate reinforcement to the magnesium matrix. Variation in CTE with the change in amount of Y_2O_3 particulates from 0.17 to 0.7 vol.% was marginal and can be attributed to the relatively poor distribution of Y_2O_3 particulates in the case of Mg/0.7 vol.%Y_2O_3 (see Figure 4.1 and Table 4.2).

4.3.4 Mechanical Behavior

The results of hardness measurements reveal that 0.17 vol.%Y_2O_3 was not sufficient to suitably increase the hardness while 0.7 vol.%Y_2O_3 was able to increase the hardness by about 22%. The results thus suggest that the amount of Y_2O_3 up to 0.7 vol.% in matrix is advantageous to increase the resistance to localized plastic deformation [21].

The results of room temperature tensile testing reveal an increase in 0.2% yield strength, UTS, ductility and work of fracture with an increase in the amount of nanosized Y_2O_3 particulates in the magnesium matrix. The best combination of yield and tensile strengths and ductility are observed in the case of Mg/0.7vol.%Y_2O_3 samples. The increase in 0.2%YS can be estimated using the following equation, [22]

$$\sigma_{my} = \sigma_{m0} + \Delta\sigma \quad (1)$$

where σ_{my} and σ_{m0} are yield strength of the reinforced and unreinforced matrix, respectively and $\Delta\sigma$, the total increment in yield stress of the matrix is given by [23]

$$\Delta\sigma = \sqrt{(\Delta\sigma_{EM})^2 + (\Delta\sigma_{CTE})^2} \quad (2)$$

where $\Delta\sigma_{EM}$ and $\Delta\sigma_{CTE}$ are the incremental stresses due to elastic modulus (EM) mismatch and the coefficient of thermal expansion (CTE) mismatch between the matrix and reinforcement. According to the Taylor dislocation strengthening mechanisms, these stresses can be determined as [22]

$$\Delta\sigma_{EM} = \sqrt{3}\alpha\mu_m b\sqrt{\rho_G^{EM}} \quad (3)$$

$$\Delta\sigma_{CTE} = \sqrt{3}\beta\mu_m b\sqrt{\rho_G^{CTE}} \quad (4)$$

where μ_m is the shear modulus of the matrix, *b* is Burgers vector and α and β are the two dislocation strengthening coefficients. The presence of reinforcement particles causes incompatibility in deformation in the matrix through the geometrically necessary dislocations stored near the surfaces of particles. These dislocations are assumed to be generated mainly from the differences in elastic modulus and CTE between Mg matrix and Y_2O_3 particulate reinforcement. The geometrically necessary dislocation density due to elastic modulus mismatch can be estimated by [24]

$$\rho_G^{EM} = \frac{4\gamma}{b\lambda} \quad (5)$$

where γ is the plastic shear strain and λ is the local length scale of the deformation field. For particulate reinforced composites, λ is related to the interparticle distance

and considered to be approximately equal to *r/f*, where *r* is the particle radius and *f* is the volume fraction of the particles.

When the composites are cooled from the elevated processing temperature, misfit strains or deformations are produced due to the differential thermal contraction at the Mg-Y_2O_3 interface [25, 26]. Thus, high dislocation density is generated around the particulate reinforcement due to the large difference in CTE between the matrix and reinforcements. These geometrically necessary dislocations needed for the accommodation of thermal misfit strains can be estimated by [27]

$$\rho_{\mathrm{G}}^{\mathrm{CTE}} = \frac{A\varepsilon V_{\mathrm{p}}}{b(1-V_{\mathrm{p}})d} \tag{6}$$

where A is a geometric constant, b is the Burgers vector, d is the diameter of the particle, V_{p} is the particle volume fraction and ε is the thermal misfit strain between the matrix and reinforcement. Mismatch deformations due to large difference in CTE are sufficient to produce geometrically necessary dislocations in the vicinity of the reinforcement during microwave assisted sintering method in which temperature was increased up to near melting temperature of the matrix during sintering and then the temperature was reduced to room temperature through convection cooling. From the above equation, it can also be seen that the smaller the diameter of the particulates and the higher the volume fraction of the reinforcement the higher will be the dislocation density in the matrix. By virtue of significant difference in elastic modulus of Y_2O_3 (177.6 GPa) [28] and Mg (44.7 GPa) [20] (Eq. 5) and nanosize of Y_2O_3 (Eq. 6), an increase in dislocation density is expected with increasing amount of Y_2O_3 particles based on fundamental principles. This also indicates a corresponding increase in

$\Delta\sigma_{EM}$ and $\Delta\sigma_{CTE}$ thus leading to an increase in yield strength of composite samples (Eqs. 1-4 and Table 4.3). An improvement of ~17% in 0.2%YS and ~26% in UTS over that of pure magnesium was attained with the addition of 0.7 vol.% Y_2O_3 particulates in the current investigation.

It may further be noted that the increase in strength due to grain size effect can be neglected in the present study due to the extremely limited decrease in grain size due to presence of Y_2O_3 particulates. A comparison of tensile properties of submicron and micron size Y_2O_3 reinforced Mg indicate that much higher level of ductility can be realized using nano-sized Y_2O_3 particulates as reinforcement (see Table 4.3) (9, 14). Mg/Y_2O_3 nanocomposites also show the potential of light weight due to lower density (lower amount of Y_2O_3) and also the potential to exhibit higher specific mechanical properties when compared to Mg/Y_2O_3 formulations having Y_2O_3 in micron and submicron length scales (higher amount of Y_2O_3) (see Table 4.3). Mg/Y_2O_3 nanocomposite samples exhibited an increase in ductility with the increasing presence of Y_2O_3 particulates (see Table 4.3). This can primarily be attributed to: a) the activation of non basal slip system [29] and b) tendency of Y_2O_3 particulates to enhance cross slip [21]. In past studies similar observations were made when Ti [5], nano size Al_2O_3 [30] and carbon nanotube [6] were used as reinforcements. In past studies it was also indicated that both precipitation and dispersion have the ability to enhance cross-slip tendency [21].

4.3.5 Fracture Behavior

The fracture surface observed in Mg sample indicates presence of cleavage steps and a visible microscopic rough surface (Figure 4.5). This can be attributed to HCP structure of magnesium with limited slip systems and hence ductility [31]. With the increasing presence of Y_2O_3 particulates, intergranular cracks (Figure 4.5b) and dimple like features (Figure 4.5c) were observed. The presence of limited intergranular cracks is associated with the increase in ductility consistent with the previous findings [32]. The presence of dimple like features may be attributed to the formation of tiny voids in the Mg/Y_2O_3 interfacial zone under tensile mode of deformation and their subsequent coalescence. Further work is continuing in this area.

4.4 Conclusions

1. Conventional solid state powder metallurgy technique incorporating rapid microwave sintering and hot extrusion can be successfully used to synthesize near dense Mg composites containing nano Y_2O_3 particulates.
2. Distribution of reinforcement was dependent on amount of Y_2O_3 particulates. Porosity was minimal and nanopores were observed.
3. The increasing presence of nanosize Y_2O_3 particulates leads to an increase in 0.2%YS, UTS, ductility and work of fracture. Coefficient of thermal expansion showed reverse trend indicating an increase in thermal stability.

4.5 References

[1] A. Evans, C.S. Marchi and A. Mortensen, *Metal Matrix Composites in Industry: An Introduction and a Survey*, Boston, Kluwer Academic Publishers, 2003.

[2] D.J. Lloyd, Int. Mater. Rev., 39 (1994) 1-23.

[3] I.A. Ibrahim, F.A. Mohamed and E.J. Lavernia, J. Mater. Sci., 26 (1991) 1137-1156.

[4] W.L.E. Wong and M. Gupta, Adv. Eng. Mater., 7 (2005) 250-256.

[5] P. Pérez, G. Garcés and P. Adeva, Comp. Sci. Tech., 64 (2004) 145-151.

[6] C.S. Goh, J. Wei, L.C. Lee and M. Gupta, Nanotech., 17 (2006) 7-12.

[7] S.F. Hassan and M. Gupta, Mater. Sci. Tech., 20 (2004) 1383-1388.

[8] A. Luo, Canad. Metall. Quarterly, 35 (1996) 375-383.

[9] B.Q. Han and D.C. Dunand, Mater. Sci. Eng. A, 277 (2000) 297-304.

[10] B.Q. Han and D.C Dunand, Mater. Sci. Eng. A, 300 (2001) 235-244.

[11] H. Ferkel and B.L. Mordike, Mater. Sci. Eng. A, 298 (2001) 193-199.

[12] Q.C. Jiang, H.Y. Wang, B.X. Ma, Y. Wang and F. Zhao, J. Alloys Compd., 386 (2005) 177-181.

[13] H.Y. Wang, Q.C. Jiang, Y. Wang, B.X. Ma and F. Zhao, Mater. Letters, 58 (2004) 3509-3513.

[14] G. Graces, M. Rodriguez, P. Perez and P. Adeva, Mater. Sci. Eng. A, 419 (2006) 357-364.

[15] V. Castro, T. Leguey, A. Munoz, M.A. Monger and R. Pareja, Mater. Sci. Eng. A, 400-401 (2005) 345-348.

[16] F. Thummler and R. Oberacker, *An Introduction to Powder Metallurgy*, London, Institute of Materials, 1993.

[17] M. Gupta and W.L.E. Wong, Script Mater., 52 (2005) 479-483.

[18] W.L.E. Wong, S. Karthik and M. Gupta, Mater. Sci. Tech., 21 (2005) 1063-1070.

[19] R. Morrell, *Handbook of properties of technical & engineering ceramics*. London, HMSO, 1985.

[20] A. Buch, *Pure metals properties: A scientific-technical handbook*, Materials Park, Ohio, ASM International, London, Freund Publishing House, 1999.

[21] P.O. Kettunen, V.T. Kuokkala, *Plastic deformation and strain hardening*, Enfield, N. H, Trans Tech, 2002.

[22] L.H. Dai, Z. Ling and Y.L. Bai, Comp. Sci. Tech., 61 (2001) 1057-1063.

[23] T.W. Clyne and P.J. Withers, *An Introduction to Metal Matrix Composites*, New York, NY, USA, Cambridge University Press, 1993.

[24] N.A. Fleck, G.M. Muller, M.F. Ashby and J.W. Hutchinson, Acta Metall. Mater., 42 (1994) 475-487.

[25] R.J. Arsenault and N. Shi, Mater. Sci. Eng., 81 (1986) 175-187.

[26] M. Taya, K.E. Lulay and D.J. Lloyd, Acta Metall. Mater., 39 (1991) 73-87.

[27] N. Chawla and K.K. Chawla, *Metal Matrix Composites*, New York, Springer Science + Business Media Inc., 2006, p.197.

[28] Website: http://www.ceramics.nist.gov/srd/summary/Y2O3.htm, last assessed in July 2009.

[29] J. Koike, T. Kobayashi, T. Mukai, H. Watanabe, M. Suzuki, K. Maruyama and K. Higashi, Acta Mater., 51 (2003) 2055-2065.

[30] S.F. Hassan and M. Gupta, Mater. Sci. Eng. A, 392 (2005) 163-168.

[31] R.E. Reed-Hill and R. Abbaschian, *Physical metallurgy principles*, 3rd ed., Boston, PWS-Kent Pub., 1992.

[32] W. Yang and W.B. Lee. *Mesoplasticity and its application*, Germany, Springer-Verlag, 1993.

CHAPTER 5

EFFECT OF HEATING RATE ON Mg AND Mg/Y_2O_3 NANOCOMPOSITE DURING HYBRID MICROWAVE SINTERING

The work presented in this chapter is published. The citation is as follows:

K.S. Tun and M. Gupta, "Effect of heating rate during hybrid microwave sintering on the tensile properties of magnesium and Mg/Y_2O_3 nanocomposite", J. Alloys Compd., 466 (2008) 140-145.

CHAPTER 5

EFFECT OF HEATING RATE ON Mg AND Mg/Y_2O_3 NANOCOMPOSITE DURING HYBRID MICROWAVE SINTERING

Summary

In this chapter, effect of heating rate during hybrid microwave sintering is critically investigated. Mg/0.7vol.%Y_2O_3 was chosen as it revealed the best overall tensile properties (*Chapter 4*). Accordingly, pure magnesium and Mg/0.7vol.%Y_2O_3 nanocomposite were microwave sintered using heating rates of 49˚C/min and 20˚C/min. Results obtained from extruded rods revealed that average hardness and strengths of both Mg and Mg/Y_2O_3 samples were higher when they were sintered at higher heating rate. Ductility of pure Mg, however, reduced at higher heating rate while it remained similar for Mg/Y_2O_3 nanocomposite. An attempt is made in this chapter to correlate tensile properties with the end microstructural features of the samples sintered at two different heating rates.

5.1 Introduction

Powder metallurgy (PM) is one of the near net shape processing methods commonly used for fabricating engineering components based on metal based materials [1-3]. The PM method usually involves mixing of powders, compaction and solid state sintering followed by secondary consolidation process such as extrusion.

Among these steps, sintering is a very important step due to its ability to evolve microstructural features that govern the end properties [4].

Sintering can be done in a number of ways using radiant, plasma, induction and microwave heating sources [4]. Among these methods, microwave sintering is emerging as a rapid, energy efficient and environment friendly technique [5-8]. In microwave heating volumetric heating of materials is realized as a result of conversion of electromagnetic energy to thermal energy. Till about 1990s, most of the work on microwave heating and sintering was applied for the processing of ceramic materials [8, 9-11] and only limited research was conducted on investigating interaction between microwave and metal based materials [12-15]. Results of literature search indicated that limited investigations have been made to study the effect of sintering temperature and time on the microstructure and properties of metallic materials [16-17] and no studies have been made to investigate the effect of heating rate during microwave sintering of light weight metal such as magnesium and its nanocomposites.

Accordingly, the main aim of the present study was to synthesize pure magnesium and its nanocomposite using hybrid microwave sintering approach using a 2.45 GHz multimode microwave furnace. Particular emphasis was placed to study the effect of heating rate during sintering on microstructure and mechanical properties of pure magnesium and a Mg/Y_2O_3 nanocomposite.

5.2 Results

5.2.1 Macrostructure

The results of macrostructural characterization conducted on microwave sintered samples at high heating rate did not show any sintering defects such as shrinkage cavity and cracking indicating homogeneous heating. It may be noted that circumferential cracks can originate at high heating rates especially when the heat generation is inhomogeneous [19]. Following extrusion, Mg and Mg/Y_2O_3 samples also did not reveal presence of any macrodefects. The outer surfaces were smooth and free of circumferential cracks. For Mg and Mg/Y_2O_3 sintered at low heating rate, the outer surfaces were comparatively rougher. The surfaces of extruded rods were smooth except for the last portion which showed the presence of shallow circumferential cracks. This portion was not used for characterization.

5.2.2 Density Measurements

The density and porosity measurements conducted on the extruded magnesium and its composite samples for different heating rates are listed in Table 5.1. The results show that the densities of magnesium and composite samples at different heating rates are within standard deviation of each other. The porosity level decreases with increasing heating rate for both pure magnesium and composite samples. The highest porosity percentage was observed in Mg/Y_2O_3 sample sintered at low heating rate.

Table 5.1 Results of density, porosity and pore and grain morphologies.

Material	Heating rate (˚C/min)	Experimental Density (g/cm^3)	Porosity (vol.%)	Pore characteristics*		Grain characteristics*	
				Size (μm)	Aspect ratio	Size (μm)	Aspect ratio
Mg	49	1.738±0.007	0.13	0.4±0.3	2.2±0.8	20±3	1.4±0.1
Mg	20	1.734±0.002	0.33	0.2±0.2	2.1±0.9	36±9	1.4±0.3
Mg/.7Y_2O_3	49	1.757±0.006	0.35	0.3±0.2	2.0±0.7	18±3	1.4±0.2
Mg/.7Y_2O_3	20	1.754±0.002	0.49	1.1±0.6	2.3±1.1	29±8	1.4±0.3

* More than 100 pores and grains were used for measurements.

The results of pore morphology measurements show that there was no significant change in pore size in the case of magnesium for both heating rates whereas larger pores (micron size pores) were observed in composite sample sintered at low heating rate when compared to composite sample sintered at high heating rate (Table 5.1). The aspect ratio of pores remained in 2.0-2.3 range for both magnesium and composite samples for both heating rates.

5.2.3 Microstructural Characterization

The results of grain size and aspect ratio of the extruded samples are shown in Table 5.1. The results of grain morphology indicate that grain coarsening was pronounced in samples sintered at low heating rate (Table 5.1 and Figure 5.1).

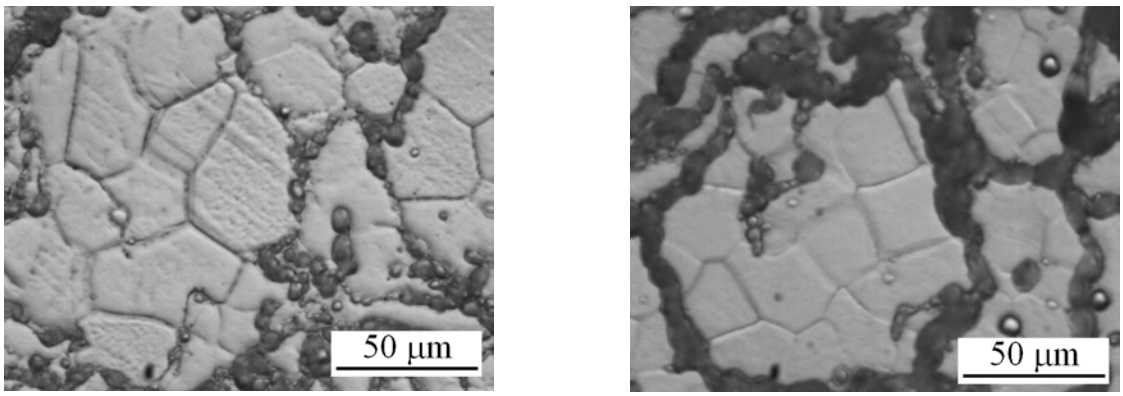

(a) (b)

Figure 5.1. Representative micrographs showing grain morphology of: (a) pure Mg and (b) Mg/Y_2O_3 sintered at low heating rate.

Near equiaxed grain morphology was observed in both monolithic and reinforced samples for different heating rates. The results of microstructural characterization conducted on the composite samples revealed relatively uniform distribution of nanosized yttria particulates with minimal presence of clusters (Y_2O_3 particulates together but not fused with each other) in the case of samples sintered at high heating rate (Figure 5.2a) and poorly distributed yttria particulates with presence of clusters and agglomerated region (Y_2O_3 particulates fused with each other) in the case of samples sintered at low heating rate (Figure 5.2c). It was observed from the FESEM micrographs (Figure 5.2) that particles were distributed everywhere inside the samples, either along the grain boundaries or inside the grains for samples sintered at both low and high heating rates. In composite samples sintered at high heating rate, Y_2O_3 particles were well decorated along the particle/grain boundary with minute pores (Table 5.1 and Figure 5.2b). On the contrary, particle clusters or agglomerates with larger size pores along the particle/grain boundary were more predominantly

observed in the composite samples sintered at low heating rate (Table 5.1 and Figure 5.2d).

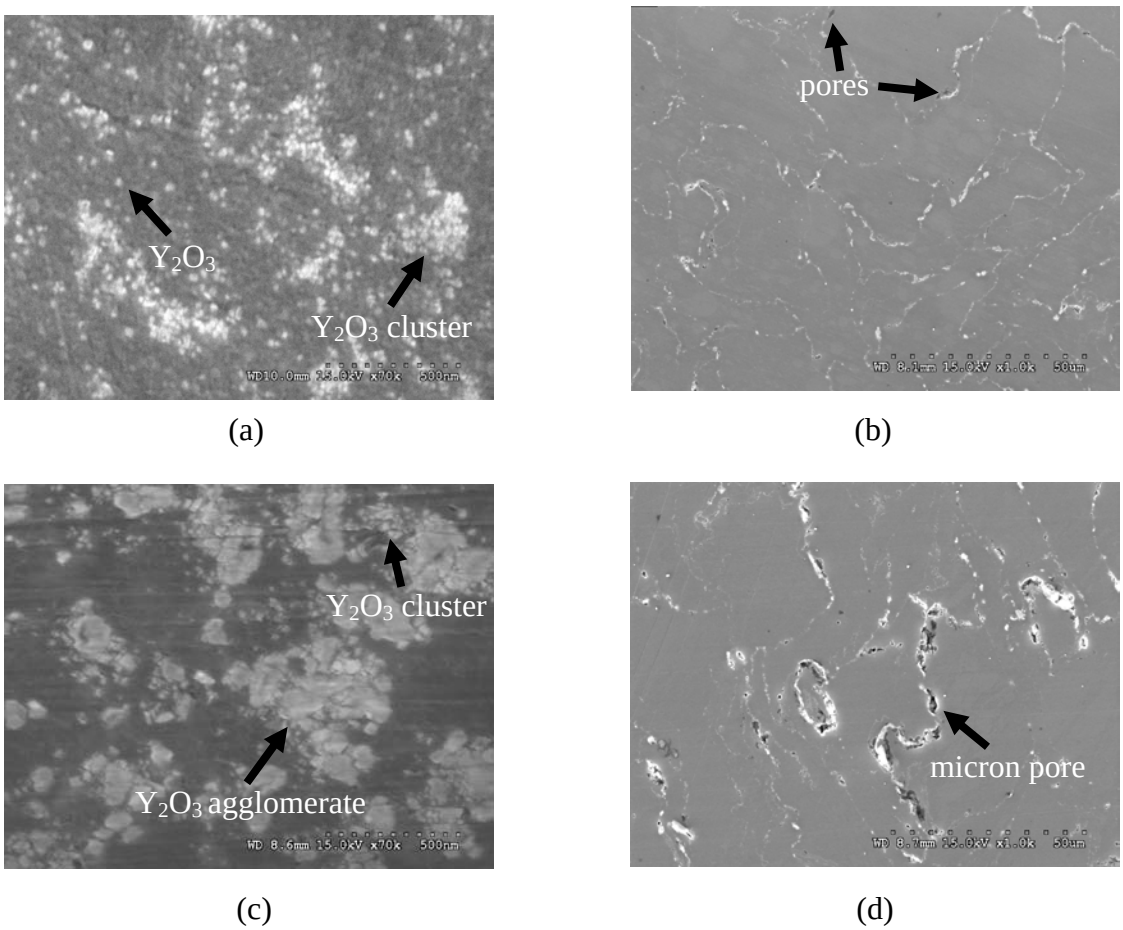

Figure 5.2. Representative FESEM micrographs showing: (a) particulate distribution and (b) presence of minimal pores in Mg/Y_2O_3 sample sintered at high heating rate, and (c) particulate clusters and agglomerates and (d) presence of micron pores in Mg/Y_2O_3 sample sintered at low heating rate.

5.2.4 Mechanical Behavior

The results of microhardness measurements conducted on polished extruded samples are listed in Table 5.2. The results show a noticeable change in hardness values of pure magnesium when 0.7vol.%Y_2O_3 was present in matrix in the case of samples sintered at higher heating rate. When compared with high heating rate

samples, similar hardness value of pure magnesium and significant decrease in hardness of composite sample were observed in low heating rate samples. The results of room temperature tensile testing are listed in Table 5.2. The results revealed, in common, an increase in strength for both pure Mg and Mg/0.7vol.%Y_2O_3 samples when they are sintered at high heating rate.

Table 5.2 Results of microhardness and room temperature tensile properties.

Material	Heating rate (˚C/min)	Microhardness (HV)	0.2%YS (MPa)	UTS (MPa)	Failure Strain (%)
Mg	49	37 ± 2	134 ± 7	193 ± 1	6.9 ± 2.5
Mg	20	36 ± 2	116 ± 17	186 ± 21	11.3 ± 1.0
Mg/0.7Y_2O_3	49	45 ± 2	157 ± 10	244 ± 1	9.1 ± 0.6
Mg/0.7Y_2O_3	20	38 ± 1	111 ± 10	175 ± 8	9.2 ± 0.5
Mg [18]	PM*	37 ± 1	105 ± 0	150 ± 1	5.0 ± 0.7

*PM indicates Powder Metallurgy incorporating conventional sintering.

5.2.5 Fractography

Tensile fracture surfaces of Mg and Mg/Y_2O_3 samples sintered at different heating rates are shown in Figure 5.3. Fracture surface of magnesium sintered at low heating rate shows the evidence of more plastic deformation (Figures 5.3(a and b)). For composites samples, intergranular fracture (Figure 5.3c) and cleavage fracture (Figure 5.3d) were observed.

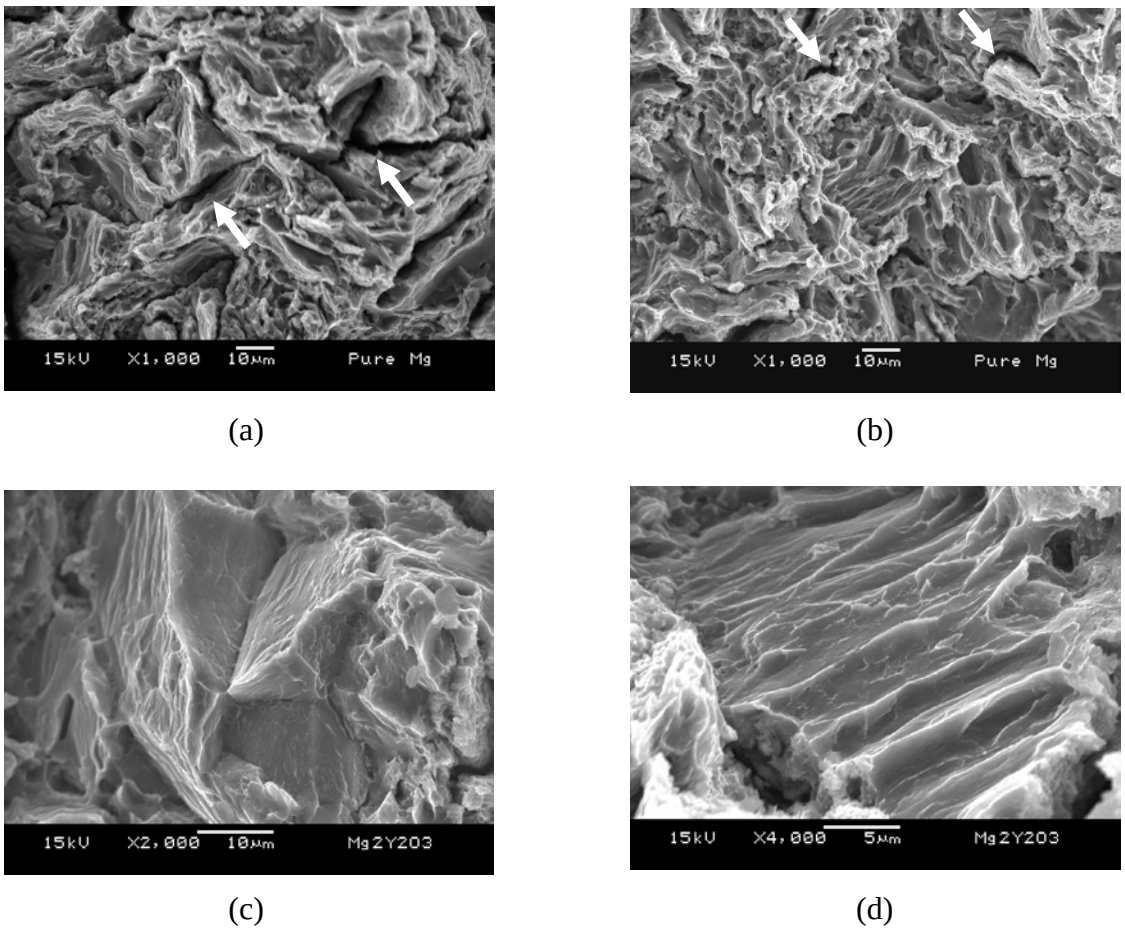

(a) (b)

(c) (d)

Figure 5.3. Representative fractographs showing: (a) fracture surface of Mg sintered at high heating rate, (b) fracture surface of Mg sintered at low heating rate, (c) intergranular fracture in Mg/Y_2O_3 sintered at high heating rate and (c) ductile cleavage in Mg/Y_2O_3 sintered at low heating rate.

5.3 Discussion

5.3.1 Densification Behavior

Monolithic Mg and Mg/Y_2O_3 composite were successfully synthesized using powder metallurgy route incorporating hybrid microwave sintering with heating rates of 49˚C/min and 20˚C/min respectively. The density of samples sintered at both heating rates was retained above 99% of theoretical density indicating that hybrid microwave sintering used in this study can offer highly dense samples regardless of

heating rate. The results of porosity measurements indicate that high heating rate during sintering lead to lower amount of porosity in both the monolithic and reinforced samples (Table 5.1). Results suggest that densification is favored when the samples are sintered at high heating rate using microwaves. Further work using different metallic matrices is continuing in this area.

5.3.2 Microstructural Observations

The studies conducted on extruded samples sintered at low and high heating rates revealed near equiaxed grain morphology. For both pure magnesium and composite samples the larger grain size was observed for the samples that were sintered at low heating rate. Similar trend of grain coarsening in uranium dioxide sintered pellets with decreasing heating rate was also observed by Yang et al. [19]. Saitou [15] investigated sintering mechanism of microwave and electric furnace using different metal powder compacts. He reported that microwave radiation does not change the sintering mechanism. In accordance with his observation, it takes longer time to reach the desired sintering temperature for low heating rate sample leading to more grain growth. When the grain size of pure magnesium was compared with that of composite samples, marginal decrease in grain size was observed for both heating rates. It can be correlated with the fact that there was pinning effect of particulates on grain growth although it was only marginal and statistically insignificant. The standard deviation of grain size for low heating rate samples was higher than that for high heating rate samples indicating relatively more microstructural non-uniformity in samples that were sintered at low heating rate. From FESEM micrographs, predominance of agglomerated (fused) Y_2O_3 particulates was observed in composite

samples sintered at low heating rate when compared to samples sintered at high heating rate in which fairly well-distributed particulates and clusters was observed. For samples sintered at low heating rate, nano-sized particulate clusters tends to agglomerate (fused Y_2O_3 particulates) under longer exposure time while particle agglomeration was restricted when the sintering was carried out at high heating rate. These observations are consistent with the observations of other investigators [16]. Lloyd et al. [20] reported that secondary fabrication, such as extrusion, can modify the particle distribution but complete declustering cannot be achieved even at the highest extrusion ratios. Following extrusion, relatively uniform particle distribution with presence of particle clusters (Figure 5.2a) is observed in composite samples sintered at high heating rate. For composite sample sintered at low heating rate, the particles that were agglomerated could not be broken down as their size still remained in submicron length scale (Figure 5.2 c).

5.3.3 Mechanical Behavior

For both heating rates, there is an increase in average hardness value of composite samples over pure magnesium. This can be attributed to the grain refinement and presence of yttria particles in the case of composite samples (see Table 5.1). The marginal increment of hardness in the case of composite sample sintered at low heating rate when compared to pure Mg can be attributed to the poor distribution of yttria particulates with formation of clusters and agglomerates in the microstructure. Within pure magnesium and composite samples, the microhardness value realized for samples sintered at high heating rate is higher when compared to that of samples

sintered at low heating rate. This may be attributed to lower porosity and grain refinement observed in the samples sintered at high heating rate.

The results of room temperature tensile testing indicate that an increase in 0.2%YS and UTS in the case of pure Mg and Mg/Y_2O_3 can be realized using high heating rate during sintering. The results are consistent with the microstructural observations which revealed that high heating rate during sintering leads to: a) decrease in amount of porosity (Table 5.1) [21], b) reduction in grain size (Table 5.1) [22], c) increased uniformity of microstructure in terms of grain size distribution (low standard deviation in grain size) (Table 5.1) and d) presence of more individual Y_2O_3 particulates rather than agglomerated (fused) nanoparticulates in the case of composite sample causing a more uniform distribution of reinforcing particulates [2, 3]. Ductility in the case of composite samples was found to be independent of heating rate during sintering while it was clearly superior for pure Mg sintered at low heating rate. The exact mechanisms that lead to increase in ductility of Mg sintered at low heating are not clear and further work is continuing in this area. A comparison of tensile properties of pure Mg samples with the conventionally sintered Mg sample [18] revealed that superior combination of tensile properties can be obtained using microwave sintering irrespective of the heating rate during microwave sintering.

5.3.4 Fracture Behavior

Tensile fracture surface of pure magnesium sintered at high heating rate revealed: a) bigger and numerous cracks and b) larger cleavage steps when compared to the samples sintered at low heating rate. These features are consistent with the high strength levels and lower ductility exhibited by Mg sample sintered at high heating rate

(Table 5.2 and Figures 5.3(a and b)). In the case of composite samples, presence of intergranular fracture (Figure 5.3c) [23] and ductile cleavage fracture (Figure 5.3d) [24] was observed. These features are consistent with the reasonable level of ductility exhibited by composite samples and are in accordance with the similar observations made by researchers earlier [23, 24].

5.4 Conclusions

1. Near dense Mg and Mg/Y_2O_3 nanocomposite can be synthesized using hybrid microwave sintering approach and with sintering heat rates of 49˚C/min and 20˚C/min.
2. Grain coarsening is pronounced when samples are sintered at low heating rate leading to decrease in yield and tensile strength when compared to samples sintered at higher heating rate.
3. For pure Mg, high heating rate is desirable to achieve higher yield and tensile strength with moderate ductility while low heating rate is desirable to achieve higher ductility while maintaining reasonable yield and tensile strength.
4. For Mg/Y_2O_3 nanocomposite, high heating rate is recommended for realizing superior combination of tensile properties.

5.5 References

[1] R.M. German, *Powder Metallurgy Science*, 2nd ed., Princeton, N.J., USA, Metal Powder Industries Federation, 1994.

[2] D.J. Lloyd, Int. Mater. Rev., 39 (1994) 1-23.

[3] I.A. Ibrahim, F.A. Mohamed and E.J. Lavernia, J. Mater. Sci., 26 (1991) 1137-1156.

[4] R.A. German, *Sintering Theory and Practice*, New York, John Wiley & Sons Inc., 1996.

[5] D.E. Clark and W.H. Sutton, Annul. Rev. Mater. Sci., 26 (1996) 299-331.

[6] D. Agrawal, J. Cheng and R. Roy, Innovative Processing/Synthesis: Glasses, Composites IV, Am. Ceramic Soc. Publ., (2000) 273-284.

[7] A. Upadhyaya, G. Sethi and D. Agrawal, Microwave Sintering of Cu-12Sn alloy in Sintering 2003 Conference, 15-17 September 2003, Penn State University, Pennsylvania, USA.

[8] A. Chatterjee, T. Basak and K.G. Ayappa, AIChE Journal, 44 (1998) 2302-2311.

[9] Z. Xie, C. Wang, X. Fan and Y. Huang, Mater. Letters, 38 (1999) 190-196.

[10] A.W. Fliflet, R.W. Bruce, A.K. Kinkead, R.P. Fischer, D. Lewis, R. Rayne, B. Bender, L.K. Kurihara, G.M. Chow, P.E. Schoen, IEEE Trans. on plasma Sci., 24 (1996) 1041-1049.

[11] D.K. Agrawal, Current Opinion in Solid State & Mater. Sci., 3 (1998) 480-486.

[12] R. Roy, D. Agrawal, J. Cheng and S. Gedevanishvili, Nature, 399 (1999) 668-670.

[13] R.M. Anklekar, D.K. Agrawal and R.

[14] Roy, Powder Metall., 44 (2001) 355-362.

[15] E. Breval, J.P. Cheng, D.K. Agrawal, P. Gigl, M. Dennis, R. Roy and A.J. Papworth, Mater. Sci. Eng. A, 391 (2005) 285-295.

[16] K. Saitou, Scripta Mater., 54 (2006) 875-879.

[17] Y. Fang, D.K. Agrawal, R. Roy, P. Angerer and G. Skandan, Proceedings of the Microwave Sintering of Nano-phase MgO, TiO_2 and Cu Metal Powders in Sintering 2003 Conference, 15–17 September 2003, Penn State University, Pennsylvania, USA.

[18] S.S. Panda, A. Upadhyaya and D. Agrawal, J. Mater. Sci., 42 (2007) 966-978.

[19] M. Gupta and W.L.E. Wong, Scripta Mater., 52 (2005) 479-483.

[20] J.H. Yang, K.W. Song, Y.W. Lee, J.H. Kim, K.W. Kang, K.S. Kim and Y.H. Jung, J. Nuclear Mater., 325 (2004) 210-216.

[21] D.J. Lloyd, H. Lagace, A. McLeod and P.L. Morris, Mater. Sci. Eng. A, 107 (1989) 73-80.

[22] G.F. Bocchini, The Int. J. Powder Metall., 22 (1986) 185-202.

[23] V. Novikov, *Grain Growth and Control of Microstructure and Texture in Polycrystalline Materials*, Boca Raton, CRC Press, 1997.

[24] W. Yang and W.B. Lee, *Mesoplasticity and Its Application*, Germany, Springer-Verlag, 1993.

[25] A. Puskar, *Microplasticity and Failure of Metallic Materials*, New York, Elsevier, 1989.

CHAPTER 6

EFFECT OF EXTRUSION RATIO ON MICROWAVE SINTERED Mg AND Mg/Y_2O_3 NANOCOMPOSITE

The work presented in this chapter is published. The citation is as follows:

K.S. Tun and M. Gupta, "Effect of extrusion ratio on microstructure and mechanical properties of microwave-sintered magnesium and Mg/Y_2O_3 nanocomposite", J. Mater. Sci., 43 (2008) 4503–4511.

CHAPTER 6

EFFECT OF EXTRUSION RATIO ON MICROWAVE SINTERED Mg AND Mg/Y_2O_3 NANOCOMPOSITE

Summary

In this chapter, extrusion ratio (secondary processing parameter) was optimized to realize best combination of properties in the case of microwave sintered magnesium nanocomposites. This study establishes that extrusion ratio has a critical role in enhancing microstructural and mechanical characteristics of commercially pure magnesium and a magnesium based nanocomposite. The study reveals that best microstructural and mechanical characteristics can be achieved in a Mg/Y_2O_3 nanocomposite provided it is extruded at a ratio higher than a critical extrusion ratio (19:1). An extrusion ratio at 25:1 is found to be the ratio in the present study which leads to significant enhancement in microstructural characteristics (low porosity and good distribution of particulates) and mechanical properties (microhardness, 0.2% YS and UTS) of Mg/0.7vol.%Y_2O_3 nanocomposite. Results of this study also show very close relationship between microhardness and strengths (0.2%YS and UTS) for both pure magnesium and Mg/Y_2O_3 composite extruded at different extrusion ratios.

6.1 Introduction

Magnesium based materials are excellent candidates for structural applications with a tremendous potential to reduce green house gas emission due to their light weight. These materials have certain limitations such as low elastic modulus and

ductility which can be circumvented by the use of composite technology [1, 2]. Commonly, reinforcement is used in particulate form to realize low cost and isotropic properties. In recent years, several attempts have been made to use different types of particulates (metals and ceramic) and in different length scales [3-12]. Particulate reinforcement in nano length scales such as alumina and yttria have shown the potential to increase the combination of tensile strengths and ductility [3, 4, 12]. Whilst there have been a number of studies to tailor the properties of magnesium using different types and amount of reinforcement, there has been no attempt made to study the effect of the level of deformation such as extrusion ratio on the microstructure and tensile properties of commercially pure magnesium and magnesium based nanocomposites. Limited studies exist only on unreinforced alloys such as AZ31 [13], AZ31B [14] and AZ91 [15], and AZ91/SiC composite with micron size particulates [15].

Accordingly, the primary aim of the present study was to study the effect of extrusion ratio on the microstructure and tensile properties of powder metallurgy processed pure magnesium and a magnesium based nanocomposite. Microwave sintering which has a capability to cut the energy consumption up to 90% was used during the powder metallurgy processing.

6.2 Results

6.2.1 Macrostructure

The results of macrostructural characterization revealed that the outer surface of compacted and sintered billets of both magnesium and magnesium nanocomposites

showed no macroscopically observable signs of cracking and warping. After extrusion, the extruded rods were smooth and free of surface cracks except for the sample extruded at an extrusion ratio of 12:1 in which shallow circumferential cracks were observed in some portion of the rods.

6.2.2 Density Measurements

The results of density and porosity measurements for pure magnesium and magnesium composite samples extruded at different extrusion ratios are shown in Figure 6.1. The results revealed an increase in density, and therefore a decrease in porosity, with an increase in extrusion ratio for both monolithic and reinforced samples. The highest porosity, which is more than 1 percent, was observed in the composite sample extruded at the lowest extrusion ratio (12:1). In all cases, the porosity of the composite samples was higher than that of the equivalent monolithic samples (Figure 6.1b).

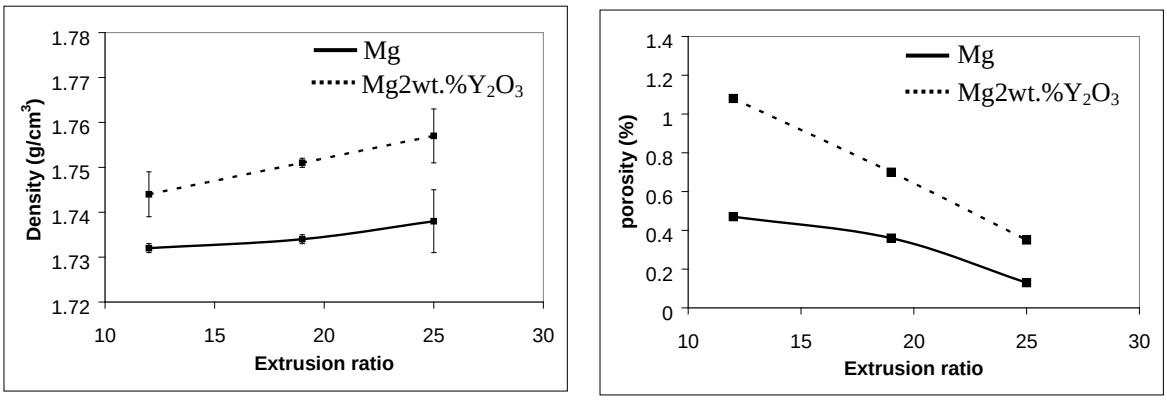

(a) (b)

Figure 6.1. Effect of extrusion ratio on: (a) density and (b) porosity.

6.2.3 Microstructural Characterization

The results of grain morphology measurements for the samples extruded at different extrusion ratios are shown in Table 6.1 and Figure 6.2. It was observed that the average grain size decreases with increasing extrusion ratio for both pure magnesium and the composite samples. As the extrusion ratio increases, the distribution of grain size also becomes more homogeneous for both monolithic and composite samples. This is evident from the reduction in standard deviations in the grain size of monolithic and composite samples. When the grain size of the pure magnesium is compared to that of magnesium nanocomposites extruded at different extrusion ratios, average grain size in composite samples was smaller than that in pure sample. Considering standard deviation, the difference in grain size of monolithic and composite samples can be considered statistically insignificant.

Table 6.1 Results of grain morphology determinations.

Materials	Extrusion Ratio	Grain characteristics	
		Size (μm)	Aspect ratio
Mg	12:1	37 ± 11	1.6 ± 0.4
Mg	19:1	31 ± 8	1.6 ± 0.3
Mg	25:1	20 ± 3	1.4 ± 0.1
Mg/0.7vol.%Y_2O_3	12:1	35 ± 9	1.6 ± 0.4
Mg/0.7vol.%Y_2O_3	19:1	28 ± 6	1.6 ± 0.3
Mg/0.7vol.%Y_2O_3	25:1	18 ± 3	1.4 ± 0.2

Extrusion ratio	12:1	19:1	25:1
Mg	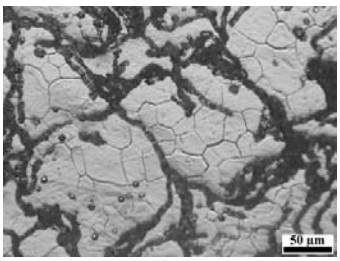	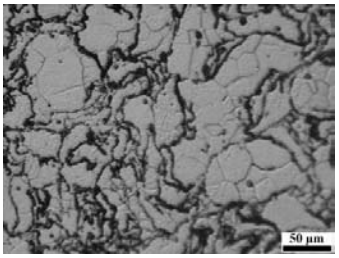	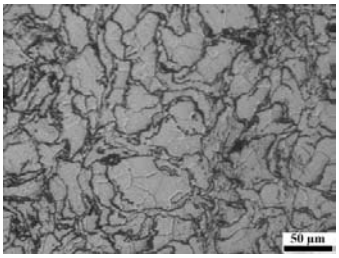
Mg/Y_2O_3	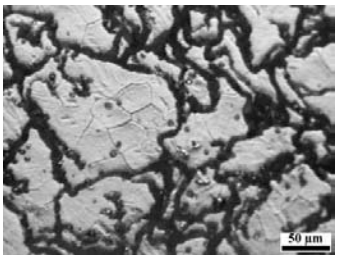	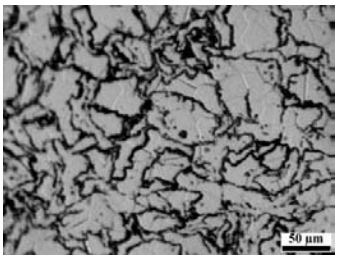	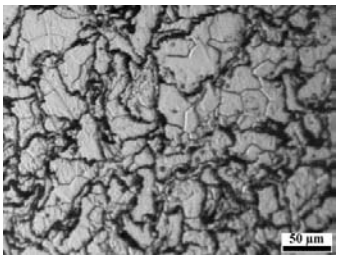

Figure 6.2. Optical micrographs showing grain morphology of pure magnesium and magnesium nanocomposites extruded at different extrusion ratios.

FESEM micrographs revealing the distribution of nano yttria particulates in magnesium matrix for the composite samples extruded at different extrusion ratios are shown in Figure 6.3. An improvement in uniformity of reinforcement particulate distribution with increasing extrusion ratio can be discerned. Non-uniform distribution of nano yttria particulates with the presence of numerous particulate clusters in large bundle was found in the sample extruded at an extrusion ratio of 12:1 while nano yttria particulates were reasonably well distributed in the sample extruded at extrusion ratio of 25:1 (Figures 6.3 (a and c)).

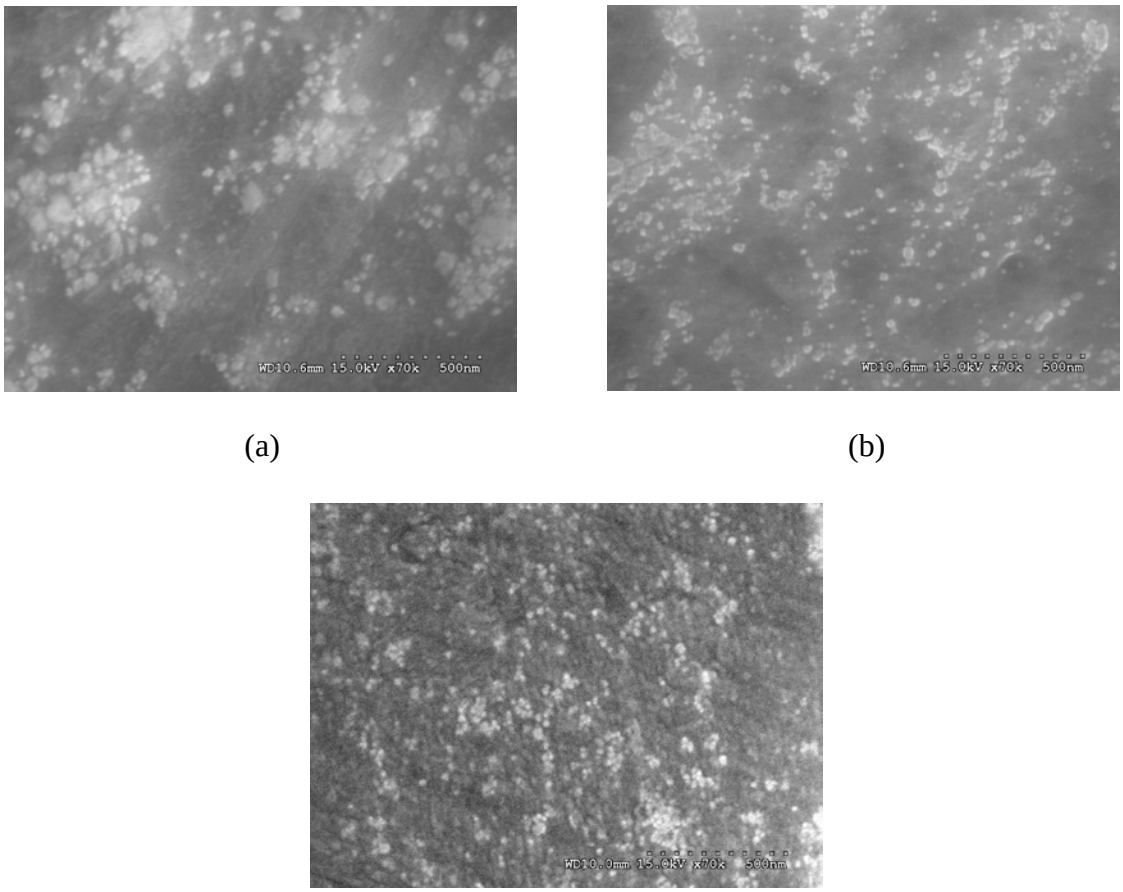

(a) (b)

(c)

Figure 6.3. FESEM micrographs showing particle distribution in Mg/Y_2O_3 nanocomposites extruded at extrusion ratio of: (a) 12:1, (b) 19:1 and (c) 25:1.

6.2.4 Mechanical Behavior

The results of microhardness measurements and room temperature tensile properties are shown in Figures 6.4 and 6.5. It was observed that microhardness increases with an increase in extrusion ratio for both monolithic and composite samples (Figure 6.4). In both samples, the microhardness increases only slightly when the extrusion ratio increases from 12:1 to 19:1, but shows a sharp rise when the extrusion ratio was increased to 25:1.

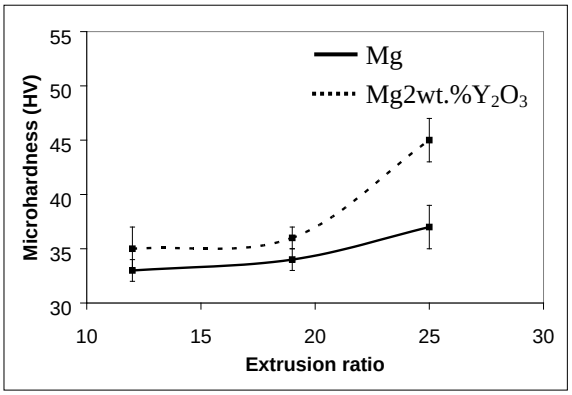

Figure 6.4. Effect of extrusion ratio on microhardness.

Results of room temperature tensile testing revealed an increase in 0.2%YS and UTS with an increase in extrusion ratio for both monolithic and composite samples, again with the greatest increase occurring as the extrusion ratio increased from 19:1 to 25:1. The ductility peaked at an extrusion ratio of 19:1 (Figure 6.5). Significant decrease in ductility was observed in the case of pure magnesium, whilst the peak ductility value was maintained in the case of magnesium nanocomposite.

6.2.5 Fractography

Figure 6.6 shows the fractographs taken from the tensile fracture surfaces of pure magnesium and magnesium nanocomposites. In the case of pure magnesium, typical brittle fracture was observed in the sample extruded at the highest extrusion ratio of 25:1 whereas some localized plastic deformation with formation of dimple like features was observed in the samples extruded at lower extrusion ratios. In the case of composite samples, the fracture surfaces show evidence of plastic deformation, with

the formation of dimple like features in the samples extruded at higher extrusion ratios, while micron size yttria particulate clusters were observed in the fracture surface of the sample extruded at lowest extrusion ratio (12:1).

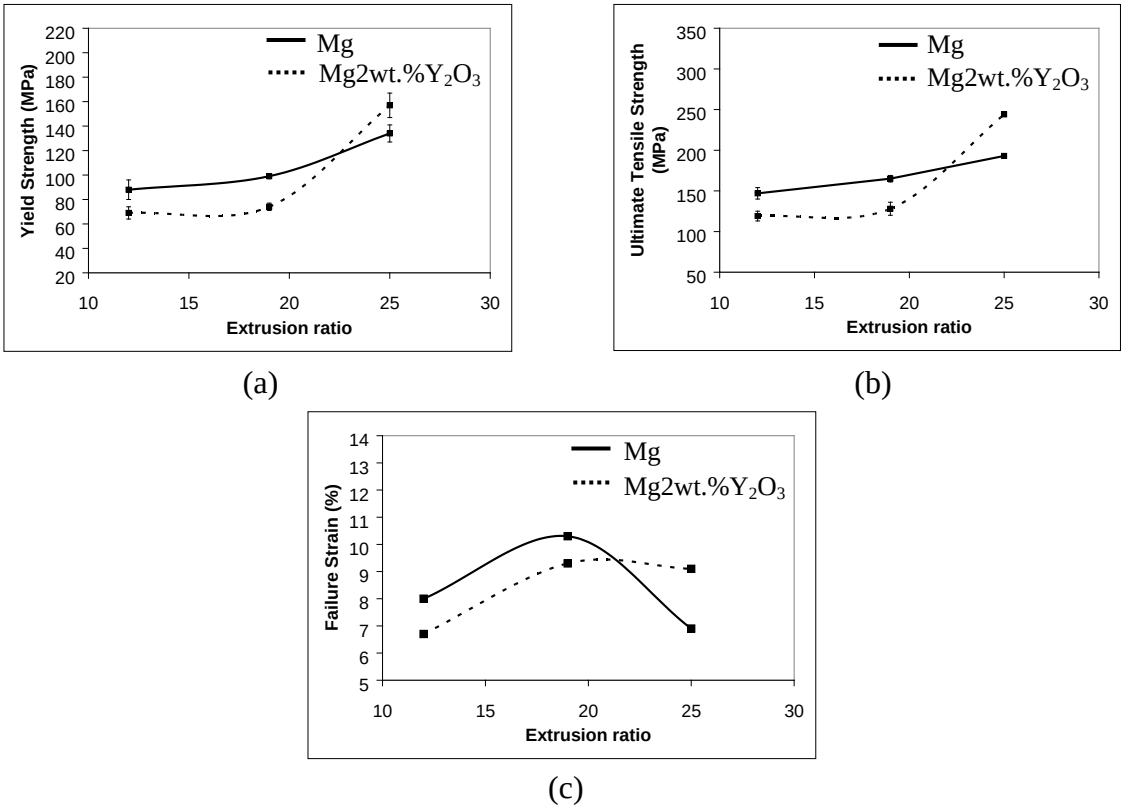

Figure 6.5. Effect of extrusion ratio on: (a) 0.2% yield strength, (b) ultimate tensile strength and (c) failure strain.

Extrusion ratio	12:1	19:1	25:1
Mg	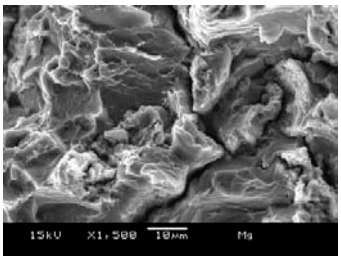	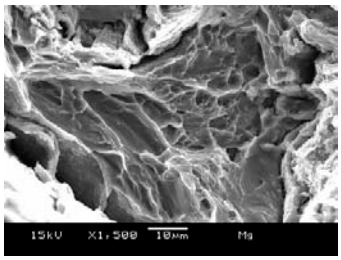	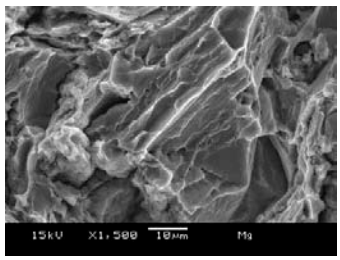
Mg/Y_2O_3	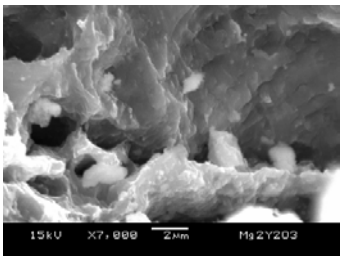	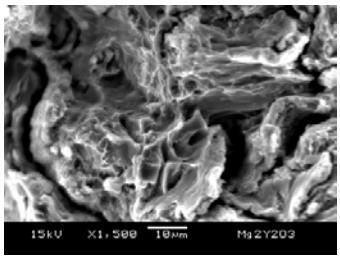	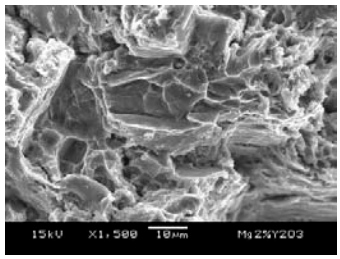

Figure 6.6. Representative tensile fracture surfaces of pure magnesium and magnesium nanocomposites extruded at different extrusion ratios.

6.3 Discussion

6.3.1 Densification Behavior

The results from the current investigation, which show an increasing trend in density with increasing extrusion ratio for both pure magnesium and the magnesium nanocomposite samples, are reasonably in agreement with the previous study [17] in which an increase in density of glassy alloy compact with increasing extrusion ratio was reported. Lloyd reported that the use of high extrusion ratio can lead to more contact and good bonding between powder particles [1]. As the extrusion ratio increases, the degree of workability or deformability of the materials increases leading to an improvement in bonding between particles as a result of an increase in the extent of particle contact contributing to progressively higher density of samples. In

accordance with the density results, the porosity of samples decreased with increasing extrusion ratio. Although the decrease in porosity was steady in pure samples, a steep decrease in porosity was observed in composite samples with increasing extrusion ratio. This can be attributed to the breakdown of Y_2O_3 particulate clusters and a minimization of the particulate cluster associated porosity (see Figure 6.3) [1]. Presence of higher porosity in composite samples when compared to monolithic samples can be attributed to the presence of the particle and cluster associated porosity. These findings are similar to the observations made on composites containing micron size particulates [18, 19].

6.3.2 Microstructural Evolution

Grain size determinations in monolithic and composite samples revealed the following:

(a) Decrease in average grain size with an increase in extrusion ratio (Table 6.1 and Figure 6.2).

(b) Increase in homogeneity of grain size (Table 6.1).

(c) Null effect of presence of nanoparticulates on grain size.

The decrease in grain size with increase in extrusion ratio can be attributed to an increased level of deformation, and these results are consistent with the results obtained on AZ31 and AZ31B commercial magnesium alloys [13, 14]. Grain distribution curves shown in Figures 6.7a and 6.7b also support the results shown in Table 6.1. The increase in homogeneity of grain size with an increase in extrusion ratio (smaller standard deviations for the mean grain size) indicates that the thermal

exposure following the complete recrystallization of the matrix was limited, inhibiting the tendency for abnormal grain growth (Table 6.1).

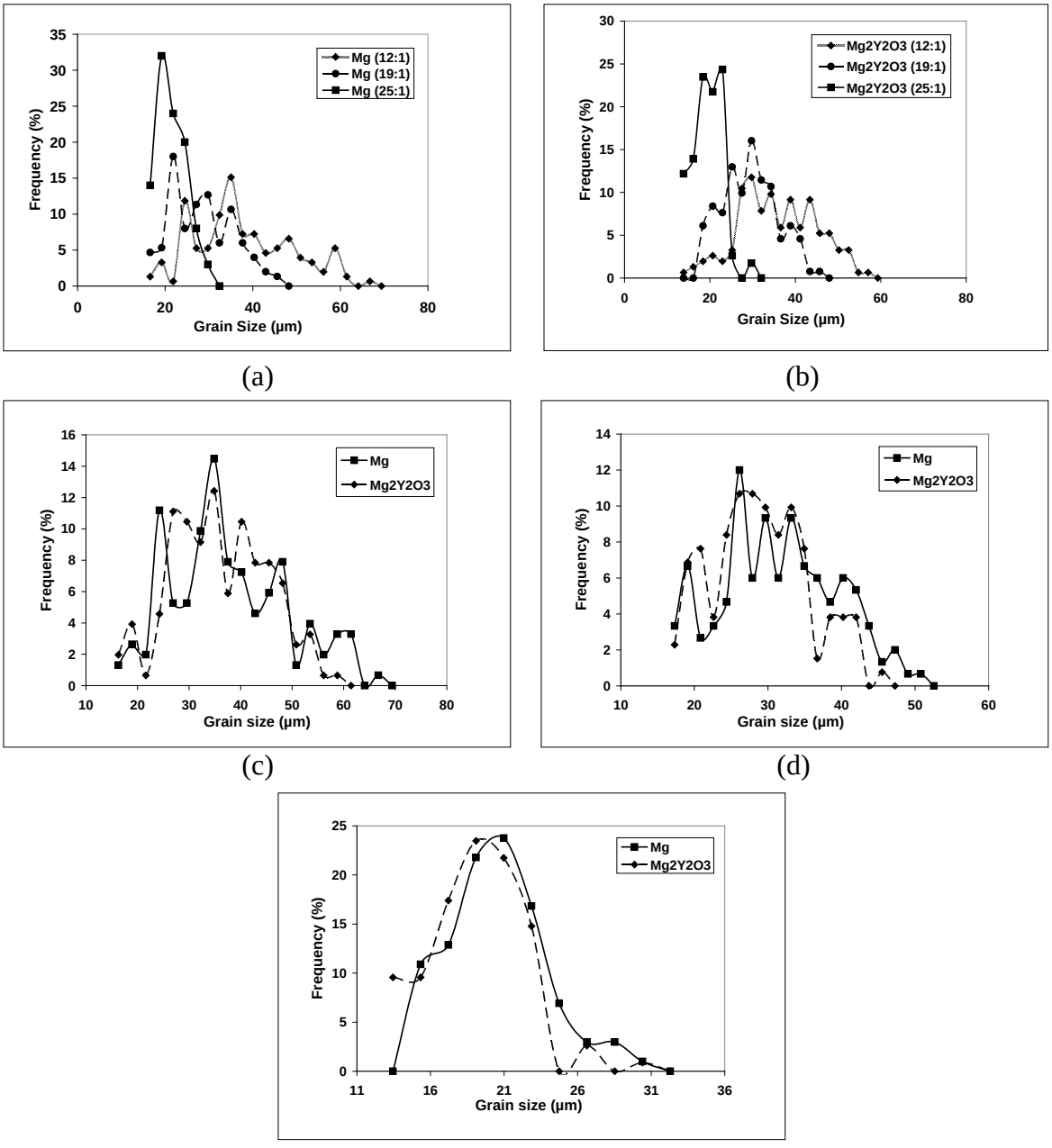

Figure 6.7. Grain size distribution at different extrusion ratio for: (a) pure magnesium samples, (b) magnesium nanocomposite samples, and grain size distribution for pure magnesium and magnesium nanocomposite at extrusion ratio of: (c) 12:1, (d) 19:1 and (e) 25:1.

6.3.3 Mechanical Behavior

The results of microhardness measurements revealed that increasing the extrusion ratio leads to an increase in average microhardness of pure magnesium and magnesium nanocomposites. This can be attributed to: a) improvement in distribution of Y_2O_3 particulates, b) progressively decreasing average grain size (Table 6.1) and c) reduction in amount of porosity (Figure 6.1) [26] with increasing extrusion ratio. The marginally higher microhardness of composite samples when compared to the monolithic samples at extrusion ratios of 12:1 and 19:1 can be attributed to the non-uniform presence of Y_2O_3 particulates while a significant increase in hardness at 25:1 extrusion ratio in case of Mg/ Y_2O_3 composite can be attributed to the improved distribution of Y_2O_3 particulates. The results of microhardness measurements are consistent with results of microstructural characterization showing a clear improvement in distribution of Y_2O_3 at 25:1 extrusion ratio (Figure 6.3c). The increase in hardness with increasing extrusion ratio can partly be attributed to a reduction in grain size, however, the results revealed (Figure 6.4) that an ~36% reduction in grain size in case of pure Mg (from extrusion ratio 19:1 to 25:1) leads to only marginal improvement in hardness further suggesting the dominant role played by the distribution of reinforcement in improving the hardness in case of composite samples.

It is well established that yield and tensile strengths normally increase with increasing extrusion ratio. Previous investigations on the effect of extrusion ratio on yield strength and/or ultimate tensile strength of aluminum alloys [27, 28], magnesium alloys [13-15] and magnesium alloy matrix composite [15] confirmed such a trend. The present study further confirms this trend for commercially pure magnesium and Mg/Y_2O_3 nanocomposite. The increase in yield and tensile strengths of monolithic and

composite samples can be attributed to two common factors: a) reduction in matrix grain size through classical Hall-Petch relationship and b) decrease in amount of porosity with increasing extrusion ratio. Since the presence of pores, especially in powder processed materials, can greatly influence the mechanical properties of materials [29], the use of an extrusion process with appropriately high extrusion ratios is very effective in reducing porosity content and thus realizing higher strength levels in materials. The degradation of strength due to increasing amount of porosity has been reported in the literature [18, 19, 29]. In addition, an increase in strengths of magnesium nanocomposites with increasing extrusion ratio can further be explained by the improvement in the distribution of yttria particulates in the magnesium matrix [15]. At extrusion ratios of 12:1 and 19:1, the strength values obtained in composite samples are similar and lower than those of the pure samples. The presence of the yttria particulates in magnesium matrix seems to degrade the properties of the composites because of the presence of particulate clusters, which remain due to the low extrusion ratio used (see Figures 6.3(a and b)). When the extrusion ratio is increased from 19:1 to 25:1, both 0.2%YS and UTS increased significantly and exceeded that of pure Mg and this can be attributed primarily to the improvement in the distribution of Y_2O_3 particulates (Figure 6.3c). This suggests that an extrusion ratio higher than a certain critical value is needed for efficient breakdown of particulate clusters particularly for powder processed composite materials containing reinforcement in nano length scale.

Earlier investigations have revealed that in the case of magnesium alloys, an increase in extrusion ratio leads to an increase in ductility [13, 14]. In the present study, monolithic and composite samples showed an increase in ductility only when

the extrusion ratio increases from 12:1 to 19:1. This increment in ductility may be attributed to the refinement in grain size [13, 14, 30] and low porosity percentage observed in the samples as extrusion ratio increases. The maximum ductility value was observed at critical extrusion ratio of 19:1 for both pure magnesium and nanocomposite samples. Especially for pure magnesium [31] and magnesium alloys [13, 14], the reduction in grain size is one of the most effective microstructural modification for improving both strength and ductility. However, a further increase in extrusion ratio from 19:1 to 25:1 led to a significant decrease in ductility of magnesium even though a finer grain and a lower porosity were achieved in the sample. The reduction in ductility with a decrease in grain size resulting from increased plastic deformation in the equal-channel angular pressed (ECAP) pure Mg was also observed in another study [32]. Kim [33] reported that a rapid material failure can occur due to the heterogeneity of void size even if the void volume fraction is low. This might be the cause of the low ductility with reduced porosity in pure magnesium in the current study. In the case of the composite sample, ductility remained similar when the extrusion ratio increased from 19:1 to 25:1 (Figure 6.5c). The ductility of composite sample was higher than that of pure sample at extrusion ratio of 25:1. This may be attributed to the presence and homogenous distribution of nano particulates in magnesium matrix [1, 12, 34]. Furthermore, lower ductility values exhibited by composite samples when compared to pure sample at extrusion ratios of 12:1 and 19:1 can be attributed primarily to the presence of particulate associated defects in the microstructure such as high porosity and formation of relatively large number of particulate clusters due to a relatively lower degree of plastic deformation at lower extrusion ratios [34].

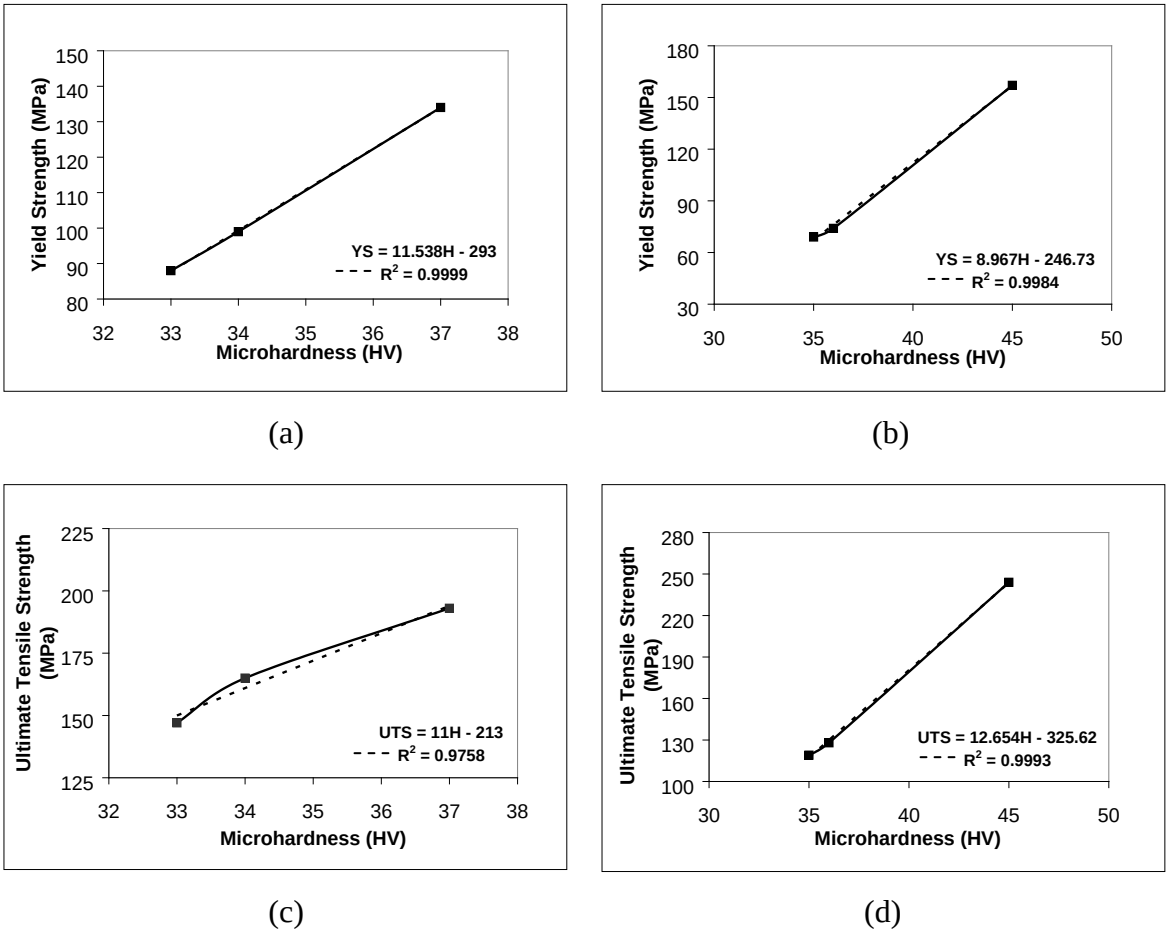

Figure 6.8. Relationship between microhardness and yield strength for: (a) Mg and (b) Mg/Y_2O_3 nanocomposite, and microhardness and ultimate tensile strength for: (c) Mg and (d) Mg/Y_2O_3 nanocomposite at different extrusion ratios.

The results of the present study also revealed an excellent agreement between microhardness and strength of pure magnesium and Mg/Y_2O_3 composite (see Figure 6.8). The expressions with the degree of curve fit are shown below:

Pure Mg

$YS = 11.538H - 293 \qquad R^2 = 0.9999 \qquad (1)$

$UTS = 11H – 213 \qquad R^2 = 0.9758 \qquad (2)$

$\underline{Mg/Y_2O_3}$

$YS = 8.967H - 246.73$ $R^2 = 0.9984$ (3)

$UTS = 12.654H - 325.62$ $R^2 = 0.9993$ (4)

where H, YS and UTS represents microhardness, yield strength and ultimate tensile strength respectively. These near perfect relationships suggest that for a given formulation the variation in processing can be assessed by hardness measurements which can be further correlated clearly with the tensile strengths.

6.3.4 Fractography

From the fractographic analysis, pure Mg extruded at an extrusion ratio of 25:1 fails predominantly in a brittle manner, showing the presence of cleavage steps. This is a common failure mode in hexagonally close packed magnesium. For magnesium samples extruded at lower extrusion ratios, localized plastic deformation zones on the fracture surface of the sample were observed indicating a relatively more ductile mode of failure (Figure 6.6). In the composite samples extruded at higher extrusion ratios of 19:1 and 25:1, observation of some plastic deformation in the tensile fractographs can be correlated with higher tensile ductility of the samples (Figure 6.5). Both monolithic and composite samples extruded at 12:1 extrusion ratio showed the presence of cracks on fracture surface suggesting the presence of unacceptable porosity related defects in the samples contributing to crack initiation and propagation at lower level of tensile plastic deformation.

6.4 Conclusions

1. Synthesis of monolithic Mg and Mg/Y_2O_3 nanocomposite can be successfully accomplished by using a microwave sintering approach followed by hot extrusion at different extrusion ratios.
2. An increase in extrusion ratio leads to an increase in density and reduction in porosity irrespective of the type of sample.
3. An increase in extrusion ratio leads to an improvement in homogeneity of microstructure in terms of grain morphology and reinforcement distribution. The best distribution of nano size Y_2O_3 particulates was realized at an extrusion ratio of 25:1.
4. Microhardness and strengths for both samples increased with increasing extrusion ratio. The greatest increase in both hardness and strength occurred in composite sample when extrusion ratio was increased from 19:1 to 25:1. This increment is attributed to the homogenization in microstructure in terms of grain size and particulate distribution.
5. At critical extrusion ratio of 19:1, both pure and composite samples showed maximum ductility. Further increase in extrusion ratio was not effective for ductility enhancement.

6.5 References

[1] D.J. Lloyd, Int. Mater. Rev., 39 (1994) 1-23.

[2] A. Evans, C.S. Marchi and A. Mortensen, *Metal matrix composites in industry: An introduction and a survey*, Boston, Kluwer Academic, 2003.

[3] C.S. Goh, J. Wei, L.C. Lee and M. Gupta, Acta. Mater., 55 (2007) 5115-5121.

[4] S.F. Hassan and M. Gupta, Mater. Sci. Eng. A, 392 (2005) 163-168.

[5] W.L.E. Wong and M. Gupta, Comp. Sci. Tech., 67 (2007) 1541-1552.

[6] P. Perez, G. Garces and P. Adeva, Comp. Sci. Tech., 64 (2004) 145-151.

[7] H. Ferkel and B.L. Mordike, Mater. Sci. Eng. A, 298 (2001) 193-199.

[8] Q.C. Jiang, H.Y. Wang, B.X. Ma, Y. Wang and F. Zhao, J. Alloys Compd., 386 (2005) 177-181.

[9] H.Y. Wang, Q.C Jiang, Y. Wang, B.X. Ma and F. Zhao, Mater. Letters, 58 (2004) 3509-3513.

[10] G. Garces, M. Rodriguez, P. Perez and P. Adeva, Mater. Sci. Eng. A, 419 (2006) 357-364.

[11] Z. Xiuqing, W. Haowei, L. Lihua, T. Xinying and M. Naiheng, Mater. Letters, 59 (2005) 2105-2109.

[12] S.F. Hassan and M. Gupta, J. Alloys Compd., 429 (2007) 176-183.

[13] Y. Chen, Q. Wang, J. Peng, C. Zhai and W. Ding, J. Mater. Process. Tech., 182 (2007) 281-285.

[14] T. Murai, S. Matsuoka, S. Miyamoto and Y. Oki, J. Mater. Process. Tech., 141 (2003) 207-212.

[15] D.M. Lee, B.K. Suh, B.G. Kim, J.S. Lee and C.H. Lee, Mater. Sci. Tech., 13 (1997) 590-595.

[16] M. Gupta and W.L.E. Wong, Scripta Mater., 52 (2005) 479-483.

[17] Y. Kawamura, H. Kato, A. Inoue and T. Masumoto, Mater. Sci. Eng., 219 (1996) 39-43.

[18] U. Cocen and K. Onel, Comp. Sci. Tech., 62 (2002) 275-282.

[19] C. Tekmen, I. Ozdemir, U. Cocen and K. Onel, Mater. Sci. Eng. A, 360 (2003) 365-371.

[20] B. Inem, Mater. Sci. Eng. A, 197 (1995) 91-95.

[21] X.J. Wang, K. Wu, H.F. Zhang, W.H. Huang, H. Chang, W.M. Gan, M.Y. Zheng and D.L. Peng, Mater. Sci. Eng. A, 465 (2007) 78-84.

[22] R.D. Doherty, D.A. Hughes, F.J. Humphreys, J.J. Jonas, D.J. Jensen, M.E. Kassner, W.E. King, T.R. McNelley, H.J. McQueen and A.D. Rollett, Mater. Sci. Eng. A, 238 (1997) 219-274.

[23] R.A. Shahani and T.W. Clyne, Mater. Sci. Eng. A, 135 (1991) 281-285.

[24] M. Gupta, R. Sikand and A.K. Gupta, Scripta Metall. Mater., 30 (1994) 1343-1348.

[25] D.J. Lloyd, H. Lagace, A. McLeod and P.L. Morris, Mater. Sci. Eng. A, 107 (1989) 73-80.

[26] G.F. Bocchini, Inter. J. Powder Metal., 22 (1986) 185-202.

[27] S. Karabay, M. Zeren and M. Yilmaz, J. Mater. Process. Tech., 135 (2003) 101-108.

[28] S. Karabay, M. Yilmaz and M. Zeren, J. Mater. Process. Tech., 160 (2005) 138-147.

[29] R.M. German, *Powder Metallurgy Science*, 2nd ed., Princeton, Metal Powder Industries Federation, 1994.

[30] X.L. Wang, Y. Yu and E.D. Wang, Mater. Sci. Forum, 488-489 (2005) 535-538.

[31] C.S. Robert, *Magnesium and its alloys*, New York, Wiley, 1960.

[32] A. Yamashita, Z. Horita and T.G. Langdon, Mater. Sci. Eng. A, 300 (2001) 142

[33] T.W. Kim, Scripta Mater., 55 (2006) 1115-1118.

[34] D.L. McDanels, Met. Trans. A, 16A (1985) 1105-1115.

CHAPTER 7

DEVELOPMENT OF Mg/(Y_2O_3+Cu) HYBRID NANOCOMPOSITES

The work presented in this chapter is published. The citation is as follows:

K.S. Tun, M. Gupta and T.S. Srivatsan, "Investigating the Influence of Hybrid (Yttria+Copper) Nanoparticulate Reinforcements on Microstructural Development and Tensile Response of Magnesium", Mater. Sci. Tech., 26 (2010) 87-94.

CHAPTER 7

DEVELOPMENT OF Mg/(Y_2O_3+Cu) HYBRID NANOCOMPOSITES

Summary

In this chapter, development of Mg/(ceramic+metal) hybrid nanocomposites to further enhance the properties of Mg/0.7vol.%Y_2O_3 nanocomposite is addressed. Hybrid nanocomposites were prepared by using a fixed amount of 0.7vol.%Y_2O_3 and different amounts of nano-copper particulates (0.3vol.%, 0.6vol.% and 1.0vol.%) in monolithic magnesium. Both the monolithic magnesium and magnesium nanocomposites were synthesized using the blend-press-sinter powder metallurgy technique followed by hot extrusion. Materials were sintered using microwaves at an optimized heating rate of 49°C/min and extrusion was carried out at an optimum extrusion ratio of 25:1. Test results revealed that both strength and ductility of pure magnesium increased with the addition of yttria and a hybrid reinforcement mixture of yttria and copper nano-particulates. The best combination of properties in uniaxial tension was obtained for the Mg/(0.7vol.%Y_2O_3+0.3vol.%Cu) hybrid nanocomposite. The observed improvement in properties is attributed to synergistic influences of a noticeable reduction in grain size of the hybrid nanocomposite, coexistence of both Y_2O_3 and copper to a reasonable extent, and a fairly uniform distribution of the reinforcement particulates and intermetallics. A scientific attempt is made in this study to highlight the significance of using hybrid reinforcements, at nano-length scale, in a pure magnesium matrix to obtain a noticeable increase in tensile properties.

7.1 Introduction

Of the most widely chosen and used metallic materials, magnesium is rated as being one of the lightest that can be safely chosen and put to use in a spectrum of structural applications [1]. With a density of 1.74 g/cc, magnesium is 35.6% lighter than its contender aluminum and 61.3% lighter than the competing non-ferrous metal titanium [2]. However, its atomic structure coupled with a low core potential and bivalency, arising from the 2s orbit electrons, restricts the physical characteristics of unalloyed magnesium and magnesium-base alloys. In particular, the magnesium-base alloys suffer from high chemical reactivity, which results in inferior corrosion resistance. Also, a hexagonal close-packed crystal structure, with a limited number of slip systems, results in limitations to enhanced strengthening coupled with a noticeable degradation in ductility or deformability. Consequently, the widespread use of magnesium-base alloys, particularly the ingot metallurgy (IM) processed, has been restricted by the competing and mutually interactive influences of poor oxidation and corrosion resistance, low thermal stability, poor formability and low strength levels. Furthermore, a number of the alloying additions, such as: molybdenum, titanium and chromium have high melting points that far exceed the boiling point of magnesium and consequently, alloying by the traditional methods was difficult and has its limitations. The commonly chosen and used alloying elements exhibit limited solid solubility in magnesium and tend to form intermetallic compounds as a direct result of the electro-positive nature of magnesium [3]. These limitations can be easily overcome by the application of powder metallurgy techniques. Despite several noticeable limitations a few notable advantages of magnesium and its alloy counterparts are its superior

mechanical properties to include specific strength (σ/ρ) and specific stiffness (E/ρ), while its disadvantages include low stiffness (E), limited ductility (ε_f) and poor fracture toughness [4]. Few recent studies have attempted to enhance the strength of magnesium through a careful use of copper and nickel particulates [5-7] but at the expense of ductility. Similarly, lithium was successfully used to enhance ductility but with a concurrent reduction in strength [1]. A simultaneous increase in both strength and ductility of magnesium was made possible by using ceramic particulates such as alumina [8], yttria [9, 10] and silicon carbide [11] at nano-length scale. This improvement was realized irrespective of the type of processing technique used for the metal and its alloy counterparts.

A careful and comprehensive examination of the published literature reveals that no attempt has been made to improve the mechanical properties of magnesium using hybrid reinforcements (metal + ceramic) at the nano-length scale. Accordingly, the present study was undertaken with the primary objective of investigating microstructural development and mechanical behavior of magnesium due to the simultaneous presence of copper and yttria at the nano-length scale. The test results are benchmarked against samples of pure magnesium and Mg/Yttria samples.

7.2 Results and Discussion

7.2.1 Macrostructure

From the macrostructural characterization studies, the surface of as-sintered samples revealed no observable macroscopic defects, such as, cracking and warped surfaces, indicating the innate capability of the microwave sintering method as a viable

alternative to conventional sintering for the purpose of sintering both the metal and metal-based nanocomposites. Following extrusion, no distinct evidence of structural defects was distinctly evident and directly observed on the surface of the extruded rods. The results of macrostructural characterization studies are consistent with the earlier observations made on microwave sintered and/or extruded materials such as magnesium, aluminum and lead-free solder [5, 11, 12].

7.2.2 Density and Porosity Measurements

In the present study, hybrid microwave sintering technique was successfully applied to sinter pure magnesium and magnesium nanocomposites, with the intent of achieving savings in both cost and energy [13]. The results of density, porosity and grain morphology measurements of synthesized materials are summarized in Table 7.1. Density measurements revealed low porosity level in all of the samples. The density values obtained for all the samples was above 99% of the theoretical density providing evidence for the ability of the processing route and appropriateness of the processing parameters used in this study to fabricate near-dense samples. From the porosity measurements, an increase in the percentage of porosity was observed in nanocomposite samples when compared to Mg. The addition of reinforcements to the magnesium metal matrix leads to the formation and presence of pores at the matrix-reinforcement interfaces and/or within the clusters of the reinforcing particulates.

Table 7.1 Results of density, porosity and grain morphology determinations.

Material	Reinforcement (vol.%)		Theoretical Density (g/cm^3)	Experimental Density (g/cm^3)	Porosity (vol.%)	Grain Characteristics	
	Y_2O_3	Cu				Size (μm)	Aspect ratio
Mg	-	-	1.740	1.738±0.007	0.13	20±3	1.4±0.1
Mg/Y_2O_3	0.7	-	1.763	1.757±0.006	0.35	18±3	1.4±0.2
Mg/(Y_2O_3+Cu)	0.7	0.3	1.784	1.775±0.001	0.45	9±5	1.6±0.4
Mg/(Y_2O_3+Cu)	0.7	0.6	1.806	1.792±0.004	0.77	9±4	1.5±0.3
Mg/(Y_2O_3+Cu)	0.7	1.0	1.835	1.825±0.002	0.62	8±4	1.5±0.3

The tendency to form clusters cannot be avoided with the use of nano particulate reinforcements because of their inherent high surface energy. An increase in porosity of the magnesium-base composites due to the addition of an increasing amount of copper nanoparticulates was reported in an earlier study [5]. Relatively higher amount of porosity was observed in the magnesium hybrid nanocomposites and this can be attributed to the simultaneous presence of both the yttria and copper particulates in the matrix. Additional research work is presently in progress with the aim of investigating the formation and specific location of pores in the composite samples.

7.2.3 Initial Microstructure

7.2.3.1 Characterization of Grains

Results from grain size measurements (Table 7.1) reveal the grain size to decrease significantly when the hybrid reinforcements are incorporated into the magnesium matrix. For the case of the Mg/Yttria nanocomposite, an insignificant

reduction in grain size was observed. This can be attributed to the low amount of yttria particulates (0.7vol.%) that are incapable of restricting grain growth. In a related study [14], investigators showed effective grain boundary pinning by the nanoparticulates when their amount was high enough (2vol.%). A noticeable reduction in grain size of the hybrid reinforcements can be attributed to an increase in volume fraction of the obstacles that facilitate pinning the grain growth. An increase in the number of obstacles arises from the addition of copper, which exhibits limited solid solubility [15] in magnesium coupled with a strong tendency to form intermetallics. The presence of yttria particulates together with Cu-based phases at the grain boundaries appears to be the primary cause for refinement in grain size in the case of hybrid composites. The presence of intermetallics was confirmed by EDS analysis (Figure 7.1a). The intermetallics were seen as coarse and bright particles whereas the yttria particulates are fine and pale in color due to the much higher brightness of intermetallics (Figure 7.1b). Both the yttria particulates and intermetallics (ranging from nano to a few submicron in size) were found within the grain and along the grain boundaries (Figure 7.1). It can also be observed from the FESEM micrographs that the presence of intermetallics at the grain boundary (Figure 7.1c) does aid in pinning the grain growth in addition to yttria particulates, which are located at the grain boundary (Figure 7.1b). In addition, the presence of copper agglomerates was also observed along the grain boundary regions (Figure 7.2a), indicating an involvement of copper in enabling grain boundary pinning. Results of the present study are consistent with an earlier study [5] that demonstrated the capability of copper nanoparticulates to reduce the grain size of magnesium.

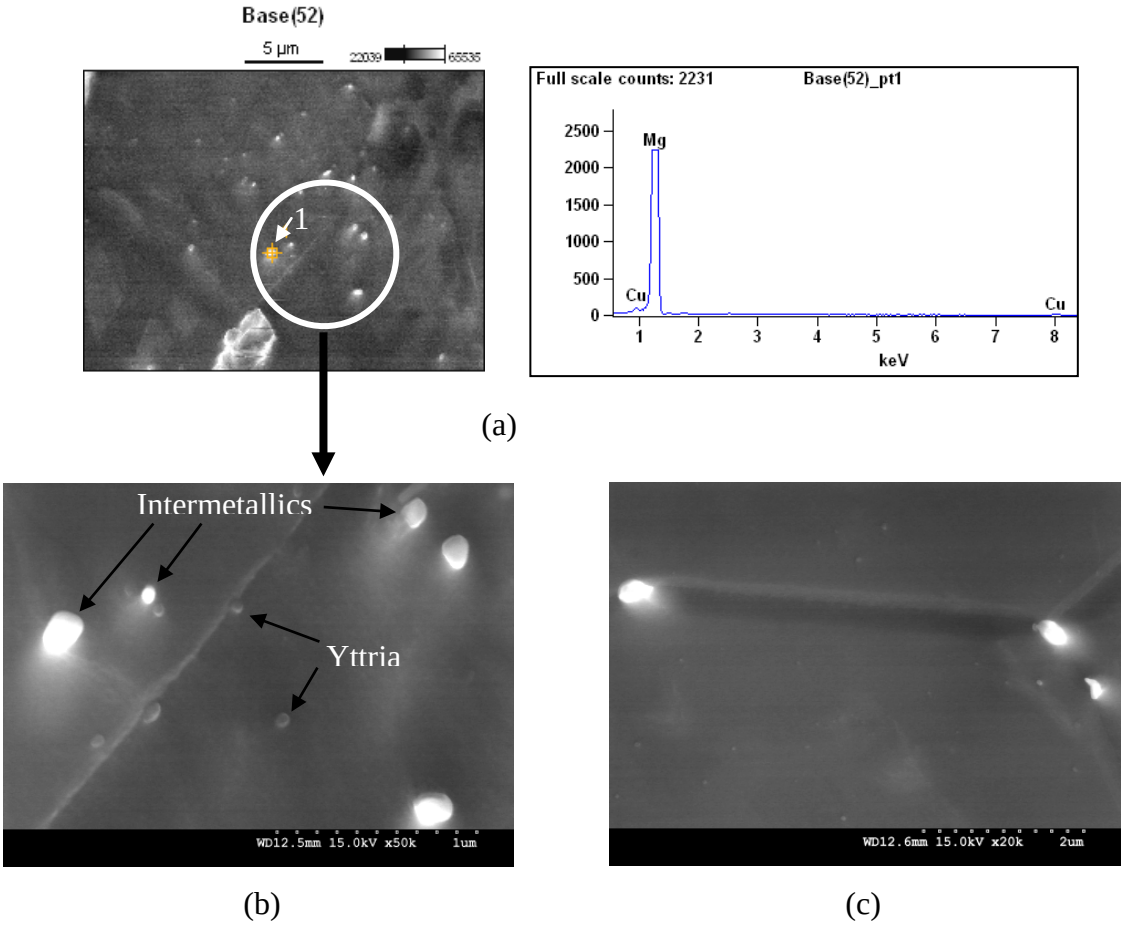

Figure 7.1. Representative micrographs showing the presence of: (a) intermetallics using EDS analysis, (b) yttria particulates and (c) intermetallics at grain boundary in Mg/(0.7Y_2O_3+0.3Cu) hybrid nanocomposite.

Furthermore, results of present study also reveal that the grain size was not decreased any further with an increasing presence of the copper particulates within hybrid nanocomposites (Table 7.1). This could be due to a saturation of the amount of obstacles at the grain boundary region coupled with the formation of clusters of copper particles (Figure 7.2). The results also reveal the presence of singular or hybrid reinforcements did not appreciably affect the aspect ratio of the grain and that the grains were near-equiaxed in all of the samples (Table 7.1).

7.2.3.2 Distribution of Reinforcement

To investigate the distribution of reinforcement particulates as well as intermetallics in the hybrid nanocomposites, microstructure of the etched and polished samples was analyzed using FESEM. For the Mg/(0.7Y_2O_3+0.3Cu) hybrid nanocomposite, most of copper particulates were present in the form of agglomerates and clusters (Figure 7.2 and Figure 7.3a) both at the grain boundary and in the grain interior (Figure 7.2), indicating a reasonable distribution of the clustered/agglomerated copper particulates in the magnesium metal matrix.

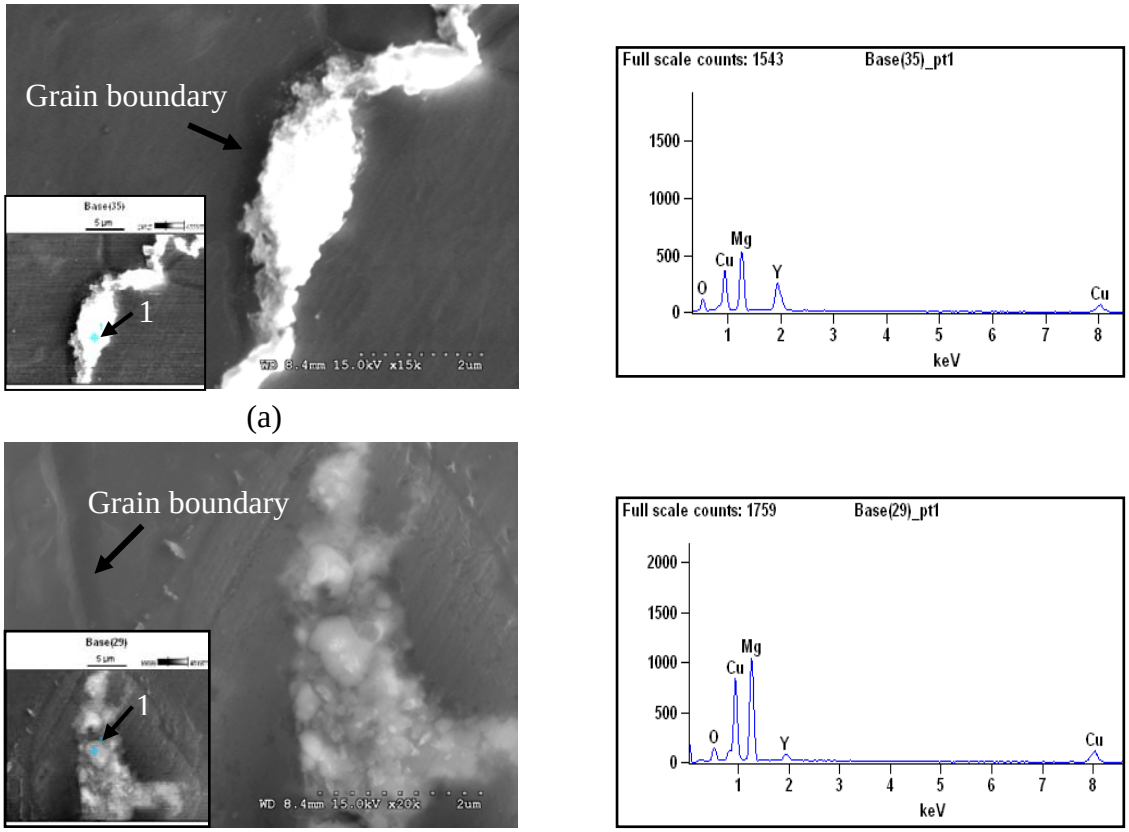

Figure 7.2. Representative micrographs showing: (a) continual network of copper agglomerates along the grain boundary and (b) copper clusters/agglomerates at grain interior in Mg/(0.7Y_2O_3+0.3Cu) hybrid nanocomposite.

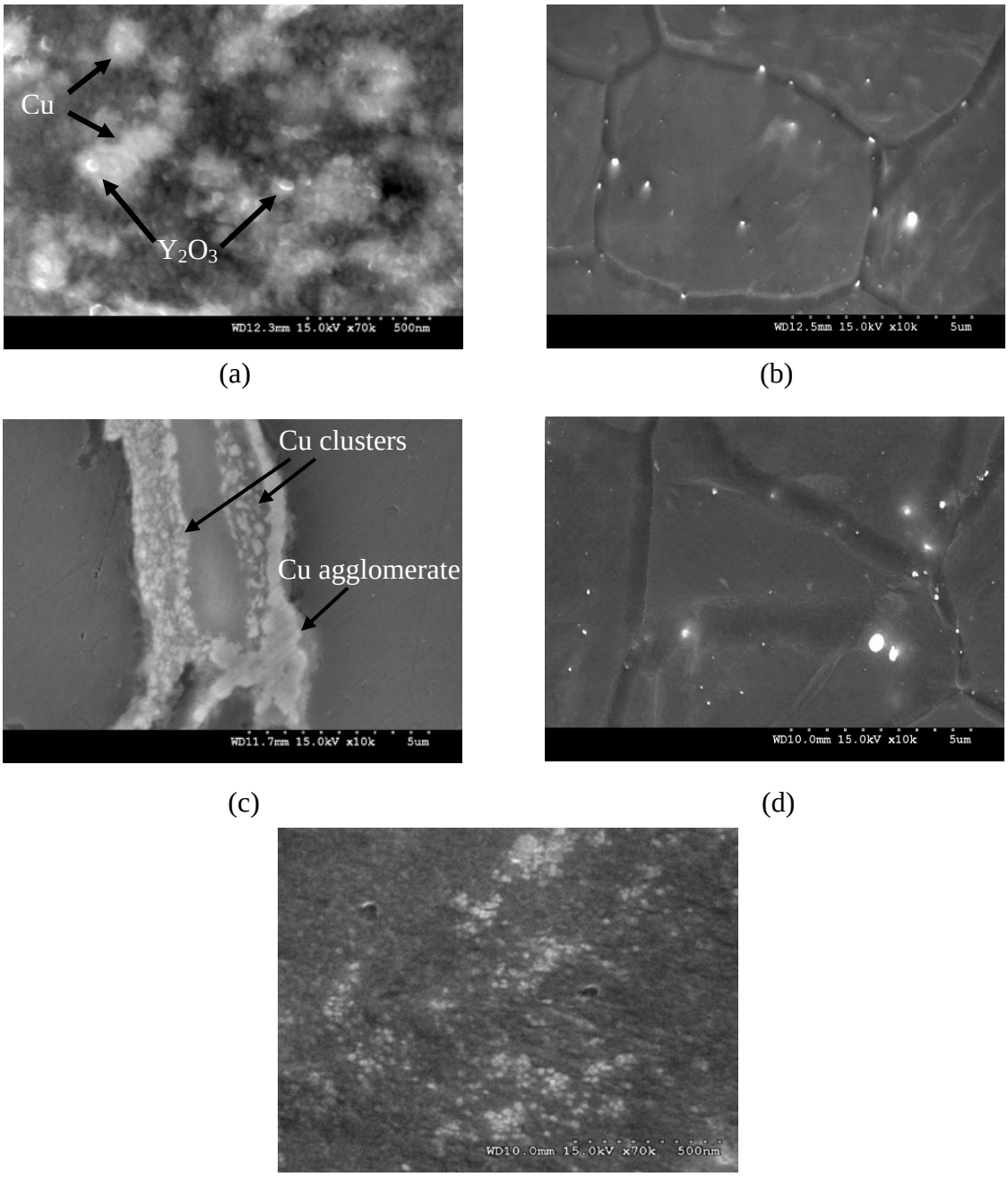

Figure 7.3. Representative micrographs showing: (a) coexistence of yttria and copper, (b) the distribution of intermetallics in Mg/(0.7Y_2O_3+0.3Cu) hybrid nanocomposite, (c) presence of copper clusters and coarse copper agglomerate, (d) the distribution of intermetallics in Mg/(0.7Y_2O_3+0.6Cu) hybrid nanocomposites and (e) the distribution of yttria in Mg/0.7Y_2O_3 nanocomposite.

Microstructural observations revealed a higher tendency of the copper particulates to form clusters and agglomerates when compared to yttria particulates (Figure 7.3). The yttria particulates were present both individually and in combination with the copper clusters (Figure 7.3a). Hence, in view of the uniform distribution of yttria particulates, Cu clusters and intermetallics (Figures 7.1 and 7.3b) the microstructure can be considered to be homogeneous in case of Mg/($0.7Y_2O_3$+0.3Cu) hybrid composite. For the Mg/ ($0.7Y_2O_3$+0.6Cu) hybrid nanocomposite, the size of copper agglomerates was coarse (Figure 7.3c) and the presence of copper clusters can also be found in combination with copper agglomerates. However, the yttria and intermetallics were found to be well dispersed in the Mg metal matrix (Figure 7.3d). When compared to Mg/ ($0.7Y_2O_3$+0.3Cu) composite, the size of intermetallics was nearly the same as observed in the Mg/ ($0.7Y_2O_3$+0.6Cu) composite.

7.2.4 Tensile Behavior

The results of room temperature tensile properties are summarized in Table 7.2. It is observed from the results that an improvement in both strength and failure strain is seen for the magnesium nanocomposites. For the case of the Mg/Yttria nanocomposite, the addition of nano ceramic particulates to the magnesium matrix enabled in achieving increments in both strength and ductility of the composite. This observation is in agreement with the findings of other researchers [8-11]. A detailed explanation for the strengthening mechanism of the Mg/Yttria system can be found elsewhere [16]. The addition of nano yttria and copper particulates to the magnesium matrix was observed to increase 0.2 % yield strength, improve the failure strain, and enhance the work of fracture in Mg/($0.7Y_2O_3$+0.3Cu) and Mg/($0.7Y_2O_3$+0.6Cu)

nanocomposite compositions. However, the ultimate tensile strength increased only for the Mg/ ($0.7Y_2O_3$+0.3Cu) hybrid nanocomposite. The addition of 1vol.% Cu in Mg/$0.7Y_2O_3$ composition led to a decrease in both 0.2%YS and UTS with similar ductility level when compared to Mg/$0.7Y_2O_3$ nanocomposite.

Table 7.2 Results of room temperature tensile properties.

Material	0.2%YS (MPa)	UTS (MPa)	Failure Strain (%)	Work of fracture (MJ/m^3)
Mg	134 ± 7	193 ± 1	6.9 ± 2.5	12.9 ± 4.8
Mg/$0.7Y_2O_3$	157 ± 10	244 ± 1	9.1 ± 0.6	21.8 ± 3.1
Mg/($0.7Y_2O_3$+0.3Cu)	215 ± 20	270 ± 22	11.1 ± 1.0	29.8 ± 2.7
Mg/($0.7Y_2O_3$+0.6Cu)	179 ± 7	231 ± 13	11.1 ± 0.7	25.4 ± 0.9
Mg/($0.7Y_2O_3$+1.0Cu)	148 ± 11	200 ± 10	10.2 ± 1.0	20.3 ± 1.9

The observed improvement in 0.2% yield strength of the hybrid nanocomposite is attributed to the independent and/or synergistic influences of the following:

(a) An Orowan strengthening mechanism due to the presence of hard yttria and copper nanoparticulates in the magnesium matrix.

(b) The strain misfit between the magnesium matrix and the particulate reinforcements.

(c) Difference in Coefficient of Thermal Expansion (CTE) between the metal matrix and the reinforcing particulates, especially due to a well dispersed yttria nanoparticulates in the magnesium metal matrix.

(d) Grain size strengthening arising from grain refinement.

(e) An additional strengthening effect provided by the presence of hard intermetallic phases formed as a result of the addition of copper [17].

According to the previous investigation [18], Orowan strengthening mechanism can be effective only when the particle diameter (assuming equiaxed particles) is less than 1 μm. In addition to particle size, a uniform dispersion of particles is preferred in order to have more particles to take part in strengthening the metal matrix [19]. For the Mg/(0.7Y_2O_3+0.3Cu) composite, Orowan strengthening mechanism was well or ably assisted by the presence of evenly dispersed yttria nanoparticulates and copper clusters/agglomerates as their size was less than 1 μm (Figure 7.3a). Furthermore, the observed increase in strength can be attributed to the presence of well dispersed intermetallics. It has been established in earlier studies that owing to their high strength and hardness, reasonably dispersed intermetallics can assist in strengthening of the matrix material in the same manner as particulate reinforcements [17, 19]. The observed decrease in strength of the Mg/(0.7Y_2O_3+0.6Cu) composite when compared to Mg/ (0.7Y_2O_3+0.3Cu) composite can be attributed to a coarsening of the copper clusters/agglomerates leading to a reduction in the Orowan strengthening effect.

The observed improvement in yield strength of the hybrid nanocomposites (containing 0.3 and 0.6 vol.% Cu) when compared to Mg/0.7%Y_2O_3 nanocomposite can be attributed to the increasing presence of obstacles to resist plastic deformation of the matrix. Due to the presence of sufficiently stronger and harder yttria and copper nanoparticulates when compared to the magnesium matrix, an incompatibility in deformation (strain misfit) arises between the soft and plastically deforming metal matrix and the hard and elastically deforming particulate reinforcements. As a result,

the density of geometrically necessary dislocations increases in the matrix to accommodate the misfit strain resulting in strengthening of the composites [20]. Furthermore, the presence of hard intermetallics also assists in strengthening of the hybrid nanocomposites based on misfit strain. Similarly, an incompatibility in deformation is generated in the immediate vicinity of the reinforcement particulates due to intrinsic differences in coefficient of thermal expansion (CTE) between the metal matrix and particulate reinforcements, contributing to generation of dislocations near the matrix-reinforcement interfaces with a concurrent increase in strength of the material [21, 22]. Since the difference between CTE of magnesium (28.9 x 10^{-6}/°K [23]) and yttria (7.6 x 10^{-6}/°K [24]) is larger than that of magnesium and copper (18.3 x 10^{-6}/°K [23]), strengthening of the hybrid nanocomposites through CTE mismatch is believed to emerge mainly from thermal expansion mismatch between magnesium and the well dispersed yttria while less contribution is expected from the presence of copper particulates.

Another important factor which influences the increase in yield strength of hybrid nanocomposites is grain refinement. Previous studies have also shown the effect of grain refinement in improving the strength of magnesium and magnesium nanocomposites [5, 8-10, 25]. With the presence of additional reinforcements (i.e., copper and copper-related intermetallics), other than yttria, in magnesium hybrid nanocomposites the effective number of obstacles that resist grain growth becomes higher resulting in a decrease in grain size with increasing number of grain boundaries. As the grain size decreases, the hybrid nanocomposites were strengthened in accordance with the classical Hall-Petch relationship. Again, strengthening of material from the presence of grain boundaries fundamentally comes from mutual disturbance

to slip between the grains coupled with impediments to the motion of dislocations across the grain boundary [19].

Within hybrid nanocomposite formulations, the average grain size obtained was almost the same although the amount of copper increased from 0.3vol.% to 1.0vol.% while the amount of yttria remained the same (0.7vol.%). However, the increasing presence of copper particulates in Mg/(0.7Y_2O_3+0.6Cu) hybrid nanocomposite caused an adverse effect on the distribution of copper in the matrix with a tendency to form coarse copper agglomerates (see Figure 7.3c). This effect results in a decrease in both 0.2% yield strength and ultimate tensile strength of Mg/(0.7Y_2O_3+0.6Cu) and Mg/(0.7Y_2O_3+1.0Cu) when compared to the Mg/(0.7Y_2O_3+0.3Cu) hybrid nanocomposite. Another factor which contributes to the reduction in strength is the presence of higher porosity level in this composite formulation (see Table 7.1).

Although a high porosity level (but not beyond 1 vol.%) was observed in the hybrid nanocomposite formulations (see Table 7.1), the best ductility (in terms of failure strain) was attained in these nanocomposites. An improvement in ductility arising from the addition of copper to Mg/Zn alloy system was reported in an earlier study [26] but not for composite system. The increase in ductility in the case of hybrid nanocomposite can be attributed to the independent or mutually interactive influences of the following:

(a) Presence of intrinsically ductile copper particulates in the metal matrix.

(b) Reduction in grain size of the matrix (Table 7.1) [8, 9, 27].

(c) Coexistence of Y_2O_3 and Cu in the microstructure resulting in enhanced compatibility of the composite Y_2O_3/Cu phase with the magnesium metal matrix (see Figures 7.2 and 7.3a).

Among the hybrid nanocomposites, an increase in amount of copper from 0.3 to 0.1 volume percentage did not appreciably affect the ductility. This is attributed to an increase in clustering of the Cu particulates coupled with an increase in size of the agglomerates. Further work is continuing in this area.

7.2.5 Fractography

Figure 7.4 shows the SEM fractographs of the tensile fracture surface of monolithic and composite samples. From the fractograph of pure magnesium (Figure 7.4a), brittle failure associated with the presence of typical cleavage features was seen on the fracture surface since magnesium has a HCP crystal structure. Formation and presence of microscopic cracks and their propagation through the microstructure was readily seen and is indicative of the restricted plastic deformation at the microscopic level. In contrast, for the composite samples, the fracture surface revealed an evidence of ductile failure with the presence of fine dimples of varying size and overall microscopically fine fracture surfaces. In case of the Mg/Yttria nanocomposite, the fracture surface was microscopically finer than that of pure magnesium with evidence of localized dimple formation suggesting the occurrence of localized microplastic deformation (Figure 7.4b). Fracture of the composite can be considered as mixed mode. However, for the hybrid nanocomposite a large volume fraction of dimples and an overall fine fracture surface was observed (Figure 7.4c). This observation can be easily correlated with the higher ductility observed during tensile testing (see Table

7.2) and a relatively homogenous distribution of the key microstructural features as observed in the microstructural characterization studies.

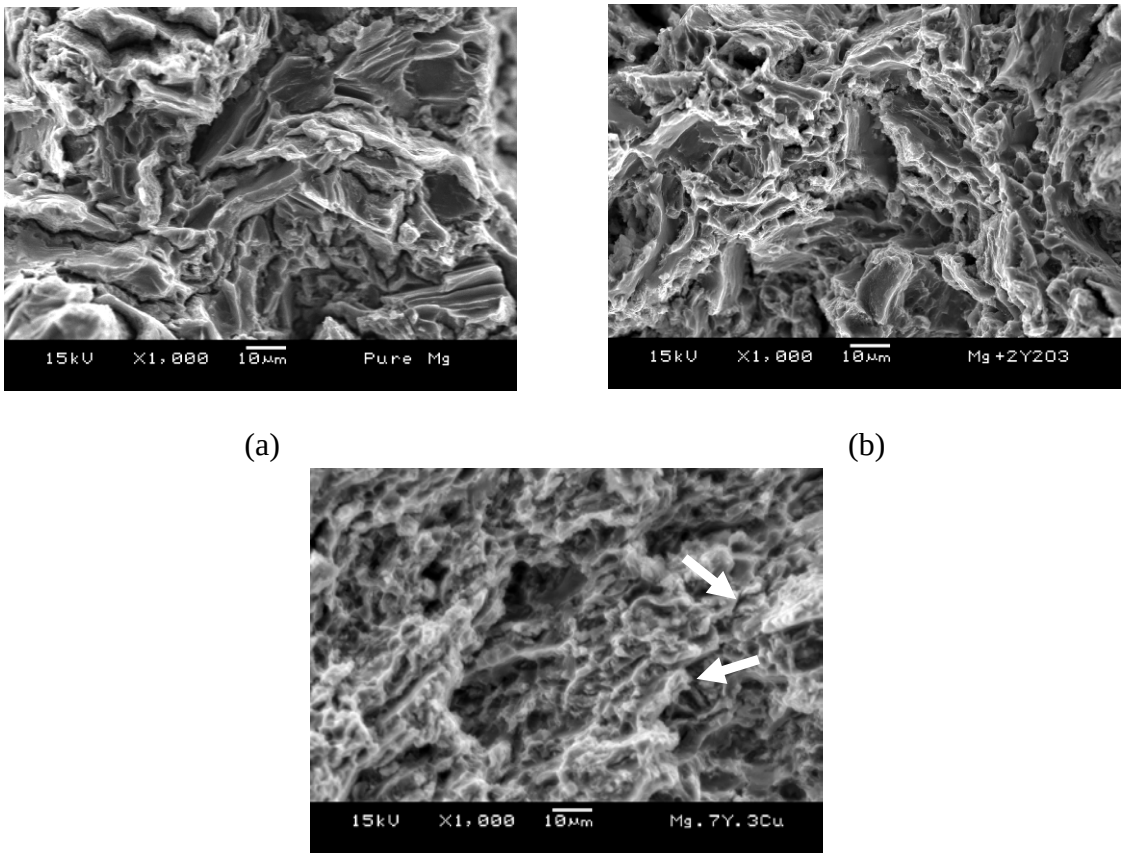

(a) (b)

(c)

Figure 7.4. Representative fractographs showing: (a) brittle failure in Mg, (b) brittle-ductile mix-mode failure in Mg/Yttria nanocomposite, (c) ductile failure in Mg/(0.7Y_2O_3+0.3Cu) hybrid nanocomposite.

The formation and presence of dimples on the fracture surface comes from the presence of fine particulates in the matrix. It may be noted that the particulates, as small as 5nm, favor the formation of dimples through the nucleation of voids at the matrix-particulate interfaces [19]. The observation of more dimples in hybrid nanocomposites can be attributed to an increasing presence of uniformly dispersed yttria and Cu phases/agglomerates/clusters in the magnesium matrix. Furthermore, the presence of smaller and much fewer microscopic cracks (marked by arrow) in the

hybrid nanocomposite (Figure 7.4c) unlike in pure magnesium are indicative of the increased yield strength and tensile strength of the hybrid composites (Table 7.2). In addition, the observed improvement in tensile ductility of the hybrid nanocomposites can be correlated with an activation of the non-basal slip systems observed from the tensile fractographs (Figure 7.5a) [9, 28].

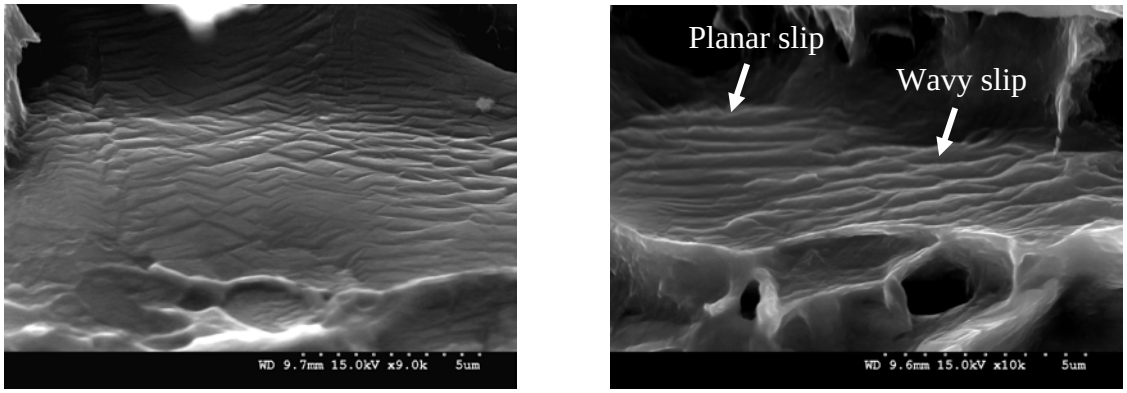

(a) (b)

Figure 7.5. Representative fractographs showing: (a) the activation of basal and non-basal slips and (b) the planar and wavy slip patterns in Mg/(0.7Y_2O_3+0.3Cu).

In this fractograph, the observation of uneven lines can be related to an activation of the basal and non-basal slip systems. From figure 7.5b, an activation of basal slip in the form of planar slip, and cross slip in the form of wavy slip was also observed [19, 28, 29]. The occurrence of cross slip can be attributed to the presence of nano length scale phases such as yttria in the magnesium matrix [30]. According to Dieter [19], the formation of fine wavy slip is an indication of homogenous deformation and an optimum ductility can be obtained while overall strength of the material is maintained. The results are consistent with microstructural characterization

studies, which revealed a fairly uniform distribution of reinforcements, intermetallics and other features in the metal matrix.

7.3 Conclusions

Based on a careful and comprehensive study aimed at understanding the influence of hybrid nanoparticulate reinforcements (a mixture of yttria and copper) on microstructural development and tensile properties of magnesium, the following conclusions can be drawn:

1. Monolithic magnesium and magnesium nanocomposites were successfully synthesized using the hybrid microwave sintering approach, which enables lower production cost for powder metallurgy processed materials.
2. A marginal reduction in grain size was observed for the magnesium nanocomposite containing yttria nanoparticulates while a significant reduction in grain size was observed for the magnesium hybrid nanocomposites containing yttria and copper nanoparticulates.
3. Microstructural characterization studies revealed a uniform distribution of yttria and intermetallics in Mg matrix while copper particulates were mostly observed in clustered/agglomerated form together with yttria particulates.
4. Agglomeration of copper particulates was more pronounced but the size of intermetallics remained the same with an increasing presence of copper nanoparticulates in hybrid nanocomposites.

5. Reinforcing with yttria as well as both yttria and copper nanoparticulates led to an increase in both strength and ductility of the composite material formulation.
6. A significant improvement in ductility was observed for the hybrid nanocomposite formulations suggesting the efficiency of hybrid reinforcement methodology.
7. The best combination of tensile properties was realized from the magnesium hybrid nanocomposite containing 0.7vol.% yttria and 0.3vol.% copper nanoparticulates.

7.4 References

[1] B.L. Mordike and T. Ebert, Mater. Sci. Eng. A, 302 (2001) 37-45.

[2] F.H. Froes, Y.W. Kim and S. Krishnamurthy, Mater. Sci. Eng. A, 117 (1989) 19-29.

[3] S. K. Das and L.A. Davis, Mater. Sci. Eng., 98 (1988) 1-12.

[4] K.U. Kainer and F. Bush, *Magnesium Alloys and Technologies*, Cambridge, Weinheim, Wiley-VCH, 2003, p. 2.

[5] W.L.E. Wong and M. Gupta, Comp. Sci. Tech., 67 (2007) 1541-1552.

[6] S.F. Hassan and M. Gupta, Mater. Sci. Tech., 19(2003) 253-259.

[7] S.F. Hassan and M. Gupta, J. Alloys Compd., 335 (2002) L10–L15.

[8] S.F. Hassan and M. Gupta, Mater. Sci. Eng. A, 392 (2005) 163-168.

[9] S.F. Hassan and M. Gupta, J. Alloys Compd.**,** 429 (2007) 176-183.

[10] C.S. Goh, J. Wei, L.C. Lee and M. Gupta, Acta Mater., 55 (2007) 5115-5121.

[11] W.L.E. Wong and M. Gupta, Adv. Eng. Mater., 8 (2006) 735-740.

[12] M. Gupta and W.L.E. Wong, Scripta Mater., 52 (2005) 479-483.

[13] W.L.E. Wong and M. Gupta, Adv. Eng. Mater., 9 (2007) 902-909.

[14] Y.C. Kang and S.L.Chan, Mater. Chem. Phy., 85 (2004) 438-443.

[15] H. Okanoto (editor), *Desk handbook: Phase diagrams for binary alloys*, Ohio Park, USA, ASM International, 2001, p. 301.

[16] K.S. Tun and M. Gupta, Comp. Sci. Tech., 67 (2007) 2657-2664.

[17] J.H. Westbrook, *Intermetallic Compounds*, New York, John Wiley & Sons, 1967, p. 471.

[18] W.S. Miller and F.J. Humphreys, Scripta Metall. Mater., 25 (1991) 33-38.

[19] G.E. Dieter, *Mechanical Metallurgy*, UK, McGraw-Hill, 1988, p. 214.

[20] M. Kouzeli and A. Mortensen, Acta Mater., 50 (2002) 39-51.

[21] D.C. Dunand and A. Mortensen, Mater. Sci. Eng. A, 144 (1991) 179-188.

[22] Z. Zhang and D.L. Chen, Scripta Mater., 54 (2006) 1321-1326.

[23] A. Buch, *Pure metals properties: A scientific-technical handbook*, Materials Park, Ohio, ASM International, London, Freund Publishing House, 1999.

[24] R. Morrell, *Handbook of properties of technical & engineering ceramics*, London, HMSO, 1985.

[25] H. Ferkel, B.L. Mordike, Mater. Sci. Eng., 298 (2001) 193-199.

[26] I.J. Polmear, *Light Alloys: Metallurgy of the Light Metals*, London, Edward Arnold, 1989, p. 185.

[27] C.S. Robert, *Magnesium and its alloys*, New York, Wiley, 1960.

[28] P. Pérez, G. Garcés and P. Adeva, Comp. Sci. Tech., 64 (2004) 145-151.

[29] J.C. Williams, A. W. Thompson and R.G. Baggerly, Scripta Metall., 8 (1974) 625-630.

[30] P.O. Kettunen and V.T. Kuokkala, *Plastic deformation and strain hardening*, Enfield, N. H, Trans Tech, 2002.

CHAPTER 8

DEVELOPMENT OF Mg/(Y_2O_3+Ni) HYBRID NANOCOMPOSITES

The work presented in this chapter is published. The citation is as follows:

K.S. Tun and M. Gupta, "Development of Magnesium/(Yttria+Nickel) Hybrid Nanocomposites Using Hybrid Microwave Sintering: Microstructure and Tensile Properties", J. Alloys Compd., 487 (2009) 76-82.

CHAPTER 8

DEVELOPMENT OF Mg/(Y_2O_3+Ni) HYBRID NANOCOMPOSITES

Summary

In this chapter, nickel nanoparticulates were used as the hybrid reinforcement with yttria nanoparticulates in pure magnesium to investigate the role of hybrid reinforcement (ceramic+metal) methodology in enhancing tensile response of magnesium. Powder metallurgy incorporating microwave sintering was used as the processing technique. Mg/0.7vol.%Y_2O_3 nanocomposite was chosen as main reference point based on the first part of investigation (*Chapter 4*). Nickel nanoparticulates in the range of 0.3-1.0 volume percent were used to hybridize the nanosize Y_2O_3 reinforcement. Tensile results revealed an increase in 0.2% YS and UTS of Mg/(Y_2O_3+Ni) hybrid nanocomposites when compared to pure Mg and Mg/0.7Y_2O_3. Mg/(0.7Y_2O_3+0.6Ni) nanocomposite showed a simultaneous improvement in both strengths (0.2%YS and UTS) and average ductility when compared to Mg and Mg/0.7Y_2O_3. Emphasis is placed in this part of study to highlight the capability of metallic and ceramic hybrid reinforcements to improve overall tensile response of magnesium when used in right amounts.

8.1 Introduction

The ability of particulate reinforced metal matrix composites (PMMCs) to exhibit isotropic and improved mechanical properties at a relatively low production cost had been instrumental in making them attractive candidates for widespread

engineering applications. Among PMMCs, extensive research has been focused on the development of aluminum and magnesium based composites due to their light weight. For reinforcing phase, ceramic particulates like silicon carbide and alumina are often used due to their low cost and easy availability [1]. In recent years, magnesium is getting tremendous attention to replace aluminum due to its capability to offer similar strength levels and ~35% weight saving. One of the drawbacks of conventional magnesium composite systems is lack of enough deformability at room temperature although they show reasonably high strength levels. These composite systems involve magnesium reinforced with micron sized ceramic particulates [1-3] and metal particulates at both micron [4-6] and nano [7] length scales. Recently, studies have shown that variation of strength and ductility of magnesium can be realized through the use of ceramic reinforcements at nano length scale [8-12]. While a significant improvement in ductility was realized in these studies, the increment in strength was only marginal for them to compete against some of the existing and commercially available magnesium alloys [13]. In the present study, an attempt is made to realize a simultaneous increase in strength and ductility of magnesium by hybridizing the ceramic reinforcement (Y_2O_3) at nano length scale with a metallic reinforcement (Ni) also at nano length scale. In earlier studies, capability of nickel to enhance significantly the strength of magnesium at the expense of ductility has been established [5, 6]. In the said study, micron size nickel additions were made and no ceramic reinforcements were used.

The hybrid composites in the present study were synthesized using powder metallurgy route coupled with hybrid microwave sintering method. Microwave sintering was used due to its capability to reduce energy consumption and the sintering

time significantly [14-18]. Focus is placed in this part of study to correlate the tensile properties with the microstructural characteristics arising due to co-presence of yttria and nickel reinforcements. The properties of hybrid composites are benchmarked against that of pure Mg and Mg/Y_2O_3 nanocomposite to justify their development.

8.2 Results

8.2.1 Macrostructure

Macroscopic observations conducted on compacted and sintered surfaces of magnesium and magnesium nanocomposite samples showed no defects such as cracking and shrinkage cavities. The surfaces were smooth and defect free at macroscopic level. The surfaces of extruded rods were also free of extrusion defects.

8.2.2 Density and Porosity

Table 8.1 shows the results of density and porosity measurements. All composite samples exhibited higher porosity level than that of pure magnesium. However, no definite trend of porosity values was observed with increasing presence of reinforcements in magnesium matrix. The amount of porosity was below 0.5 vol.% for all composites.

Table 8.1 Results of density, porosity and grain morphology determinations.

Materials	Theoretical Density (g/cm^3)	Experimental Density (g/cm^3)	Porosity (vol.%)	Grain Characteristics	
				Size (μm)	Aspect ratio
Mg	1.740	1.738 ± 0.007	0.13	20 ± 3	1.4 ± 0.1
Mg/Y_2O_3	1.763	1.757 ± 0.006	0.35	18 ± 3	1.4 ± 0.2
Mg/(0.7Y_2O_3+0.3Ni)	1.785	1.778 ± 0.002	0.34	9 ± 3	1.4 ± 0.3
Mg/(0.7Y_2O_3+0.6Ni)	1.806	1.802 ± 0.002	0.21	6 ± 2	1.4 ± 0.3
Mg/(0.7Y_2O_3+1.0Ni)	1.835	1.829 ± 0.002	0.30	5 ± 2	1.5 ± 0.3

8.2.3 Microstructure

The results of grain morphology measurements are shown in Table 8.1. The matrix grain size was not reduced significantly with the presence of singular reinforcement (yttria). The presence of hybrid reinforcements (yttria+nickel) in pure magnesium led to a remarkable decrease in grain size. Within hybrid composites, average grain size decreased marginally with an increase in amount of nickel. The results also revealed that presence of singular and hybrid reinforcements did not affect the aspect ratio of magnesium grains.

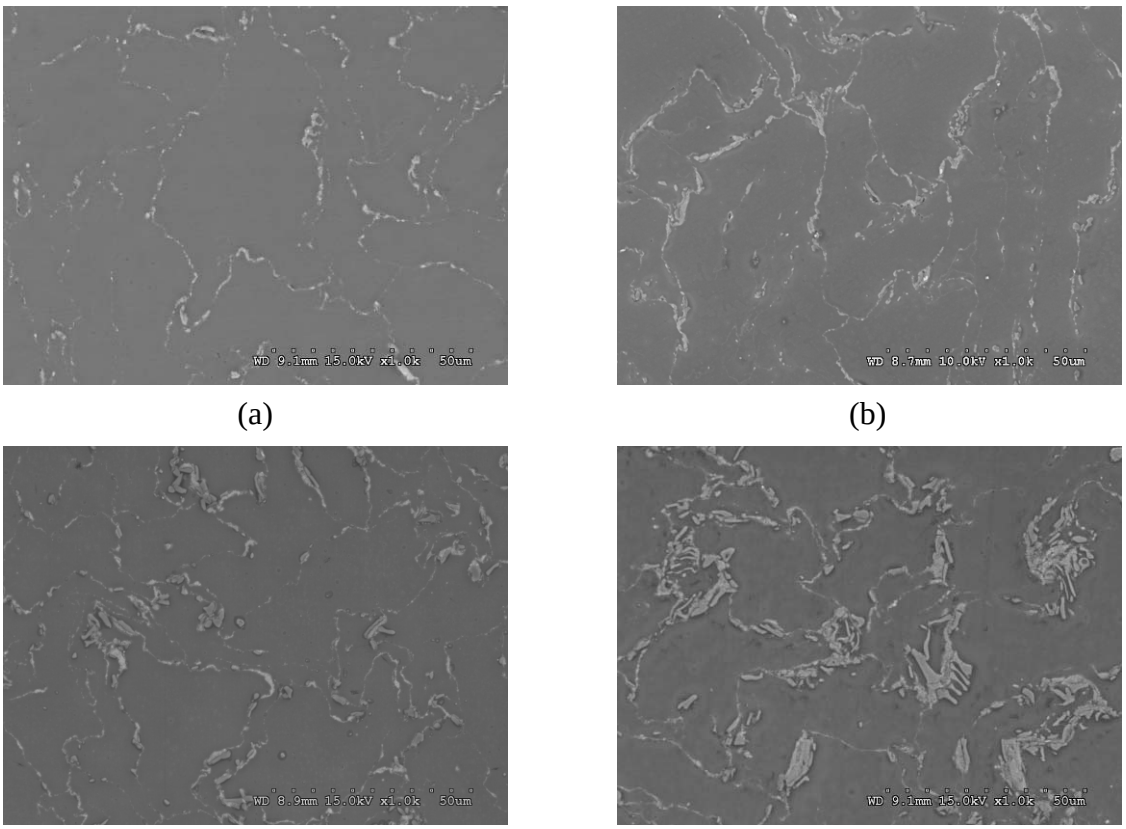

Figure 8.1. Representative FESEM micrographs showing distribution of: (a) yttria particulates in Mg/Y_2O_3 nanocomposite, and reinforcement (yttria+nickel) and intermetallic phases in (b) Mg/(0.7Y_2O_3+0.3Ni), (c) Mg/(0.7Y_2O_3+0.6Ni) and (d) Mg/(0.7Y_2O_3+1.0Ni) hybrid nanocomposites.

Figure 8.1a shows the grain boundary segregated distribution of yttria in Mg/Y_2O_3 nanocomposite and figures 8.1(b-d) show the continual network of reinforcement (Y_2O_3 and Ni) and intermetallic (Mg_2Ni) phases along grain boundaries in Mg/(Y_2O_3+Ni) hybrid nanocomposites.

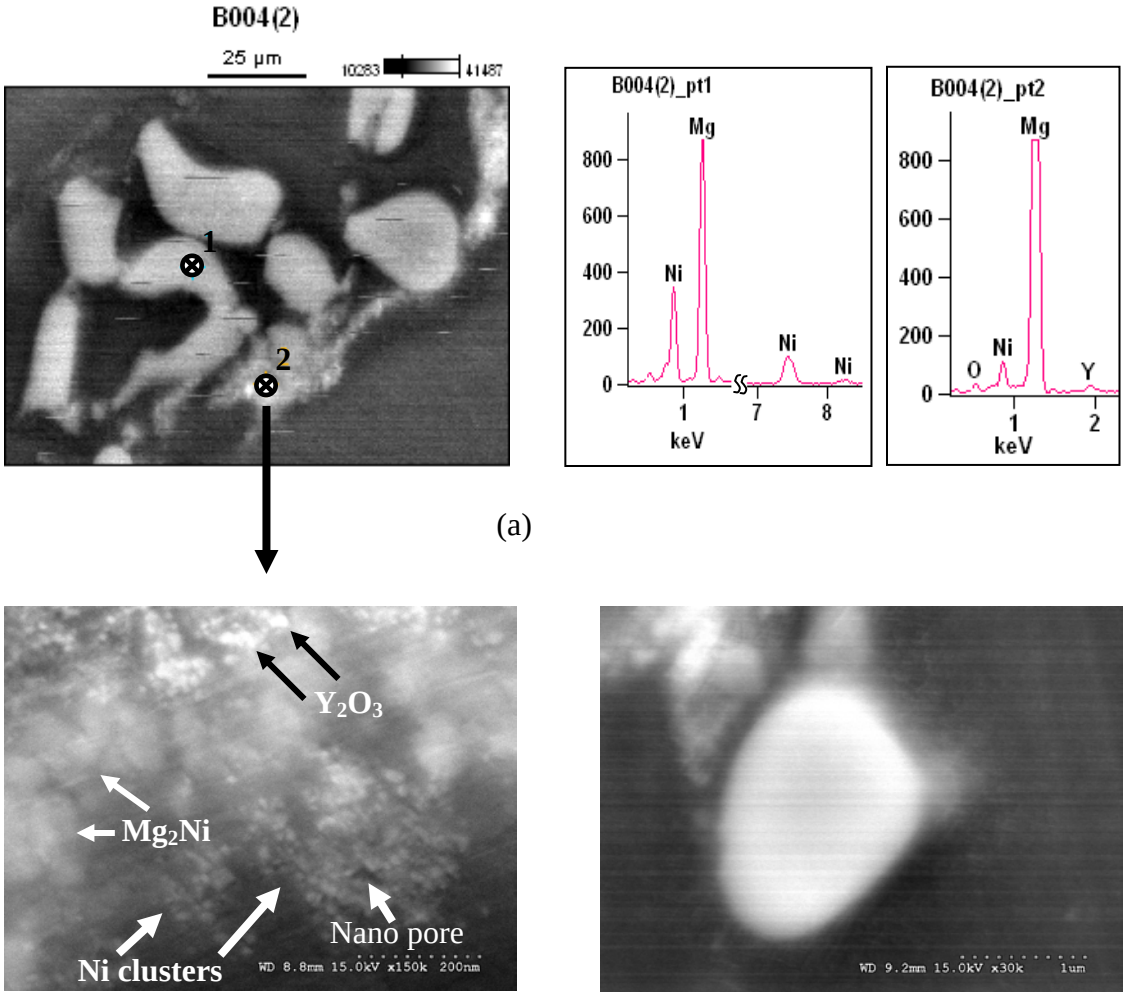

Figure 8.2. Micrographs showing the presence of nickel, yttria and Mg_2Ni intermetallics in Mg matrix (a) by using EDS analyses and (b) at high magnification, and (c) interfacial integrity between Mg_2Ni phase and Mg matrix in Mg/(0.7Y_2O_3+0.6Ni) hybrid nanocomposite.

The presence of Mg_2Ni intermetallic phase at point 1 and the co-presence of Y_2O_3, Ni and Mg_2Ni phases at point 2 were analyzed using EDS (Figure 8.2a). The weak

intensity of Ni peak at point 2 in figure 8.2a can be explained by the presence of relatively small nickel nanoparticulate clusters observed at high magnification. XRD analysis also showed the appearance of Ni and Mg_2Ni phases in hybrid nanocomposite samples (Figure 8.3). In addition, increasing presence of intermetallic clusters with increasing amount of nickel particulates in hybrid nanocomposites was observed from the micrographs.

8.2.4 X-ray Diffraction Studies

The results of X-ray diffraction studies are shown in Figure 8.3. No matching peaks of Y_2O_3 and MgO phases were observed in any samples. However, matching peaks for Ni and Mg_2Ni phases were observed in hybrid nanocomposite samples.

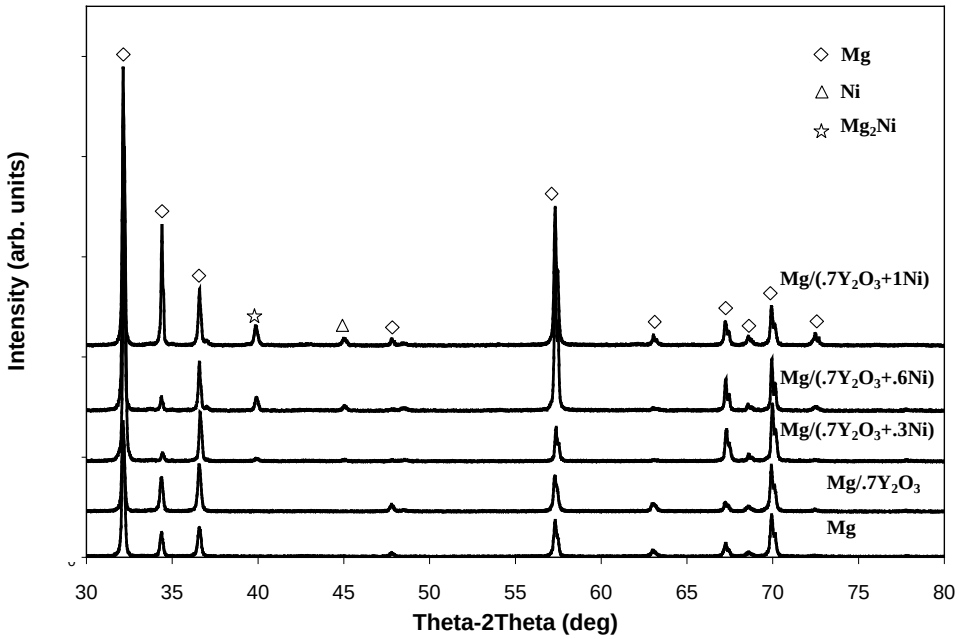

Figure 8.3. XRD patterns of Mg, Mg/Y_2O_3 nanocomposite and Mg/(Y_2O_3+Ni) hybrid nanocomposites.

8.2.5 Microhardness

Microhardness measurements taken from the polished surfaces of pure and reinforced magnesium samples are summarized in Table 8.2. From the results, a significant increase in microhardness of magnesium was observed with addition of singular reinforcement (yttria) as well as hybrid reinforcements (yttria+nickel) in magnesium matrix.

Table 8.2 Results of microhardness and room temperature tensile properties.

Materials	Microhard-ness (HV)	0.2%YS (MPa)	UTS (MPa)	Failure Strain (%)	Work of Fracture (MJ/m^3)
Mg	37 ± 2	134 ± 7	193 ± 1	6.9 ± 2.5	12.9 ± 4.8
Mg/0.7Y_2O_3	45 ± 2	157 ± 10	244 ± 1	9.1 ± 0.6	21.8 ± 3.1
Mg/(0.7Y_2O_3+0.3Ni)	54 ± 4	221 ± 7	262 ± 6	9.0 ± 0.9	23.7 ± 2.1
Mg/(0.7Y_2O_3+0.6Ni)	60 ± 4	232 ± 8	272 ± 2	9.5 ± 0.9	25.9 ± 2.3
Mg/(0.7Y_2O_3+1.0Ni)	63 ± 4	228 ± 8	271 ± 6	5.5 ± 0.7	15.4 ± 2.3
Mg/1.11Y_2O_3 [9]	51 ± 1	153 ± 3	195 ± 2	9.1 ± 0.2 [a]	15.2 ± 0.3
Mg/1.0Y_2O_3 [11]	-	151 ± 5	222 ± 4	6.8 ± 0.5[a]	-
Mg/(0.3SiC+0.7Al_2O_3) [39]	48 ± 1	165 ± 1	206 ± 5	4 ± 2	-

[a] denotes ductility in percent.

8.2.6 Tensile Properties

The results of room temperature tensile properties are shown in Table 8.2. From the results, magnesium reinforced with singular (yttria) as well as hybrid (yttria+nickel) nanoparticulates showed an improvement in both 0.2% yield and ultimate tensile strengths when compared to pure magnesium. Also, failure strain of magnesium was enhanced in nanocomposites formulations except for Mg/(0.7Y_2O_3+l.0Ni) hybrid nanocomposite.

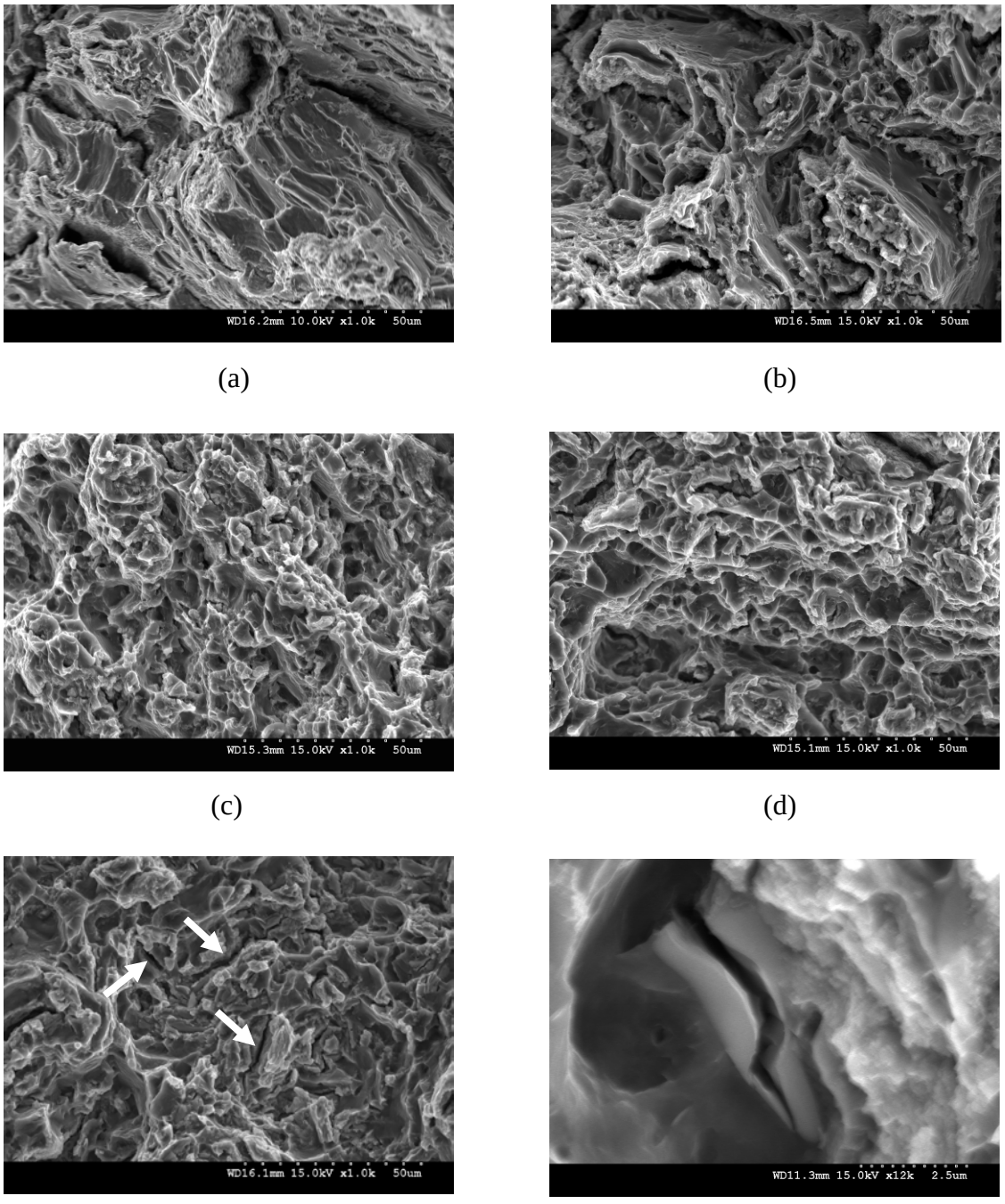

Figure 8.4. SEM fractographs showing: (a) cleavage failure in pure Mg, (b) localized dimple like structure in Mg/0.7Y_2O_3, uniform dimple like features in (c) Mg/(0.7Y_2O_3+0.3Ni) and (d) Mg/(0.7Y_2O_3+0.6Ni), and with predominant crack formations (marked by arrows) (e) and cracking of Mg_2Ni intermetallic (f) in Mg/(0.7Y_2O_3+1.0Ni).

8.2.7 Tensile Failure Analysis

Fractographs taken from the tensile fracture surfaces of pure magnesium and magnesium nanocomposite samples are shown in figure 8.4. Typical brittle fracture was observed in failed magnesium sample (Figure 8.4a) whereas for composite samples the fracture surfaces showed evidence of enhanced plastic deformation (Figures 8.4(b-d)). Brittle failure showing multiple crack formations (Figure 8.4e) and cracking of intermetallic (Mg_2Ni) phase was observed in the case of Mg/(0.7Y_2O_3+1.0Ni) hybrid nanocomposite formulation (Figure 8.4f).

8.3 Discussion

8.3.1 Synthesis of Materials

Successful synthesis of commercially pure magnesium and magnesium nanocomposites was accomplished using powder metallurgy route where materials were sintered using hybrid microwave sintering method followed by hot extrusion. From the present study, highly dense materials were resulted through microwave sintering and secondary consolidation (Table 8.1). All synthesized unreinforced and reinforced magnesium samples showed densities above 99% of theoretical density. This can be attributed to the coupled effects of: (a) using hybrid microwave sintering method which has proven to fabricate highly dense samples [12, 18, 19] and (b) suitability of extrusion ratio used [20]. Synthesized materials also exhibited good mechanical properties (Table 8.2) owing to low porosity [21].

8.3.2 Microstructural Analysis

The addition of hybrid ceramic and metal reinforcements on the microstructure of magnesium is discussed in terms of: (a) grain size reduction, (b) distribution of reinforcements (Y_2O_3 and Ni) and intermetallics (Mg_2Ni) in Mg matrix, (c) interfacial integrity between Mg matrix and Mg_2Ni phase and (d) porosity.

As compared to pure magnesium, an overall reduction in grain size was observed in hybrid composite samples. The addition of yttria and nickel particulates as hybrid reinforcements to pure magnesium is found to have significant effect than that of yttria on the reduction in average matrix grain size. According to well known Zener relation [11, 22], pinning mechanism at grain boundary is favorable with the presence of very fine particulates at a relatively high volume fraction in the matrix material. In the present study, a marginal reduction in average grain size was attained although nano-length scale yttria particulates were used in Mg/Y_2O_3 nanocomposite. This implies that the amount of yttria (0.7vol.%) added to magnesium matrix was not enough to inhibit the matrix grain growth. With the use of ceramic and metal nanoparticulate reinforcements in hybrid nanocomposites, adding only 0.3 vol.% of nickel nanoparticulates to $Mg/0.7Y_2O_3$ formulation provides an average grain size reduction of 55% over pure magnesium (Table 8.1). Related studies [7, 23] also showed a significant grain size reduction due to the use of metal nanoparticulate reinforcements in pure magnesium. According to Mg-Ni phase diagram and the sintering temperature used in the present study (643°C), Mg_2Ni is the favorable intermetallic phase formed between Mg and Ni [24]. Based on the previous study [25] solid state reaction between Mg and Ni took place at the low temperature which is even lower than Mg-Ni eutectic temperature (506°C). In another related studies, only

Mg_2Ni phase was formed when the constituent Mg and Ni powders were synthesized at 670°C [26] and 750°C (1023K) [27]. It indicates that reaction product between Mg and Ni can readily form through solid phase processing and the product formed is confirmed to be Mg_2Ni intermetallic at low temperatures up to 750°C. Studies [5, 6] on solidification processed Mg/Ni composites using micron size nickel particles also reported the formation of Mg_2Ni phase. The formation of Mg_2Ni in Mg/(Y_2O_3+Ni) system in the present study is thus consistent with the observation of other research groups [25-27]. The formation of Mg_2Ni intermetallic in hybrid nanocomposites further assisted in grain boundary pinning in addition to yttria and nickel reinforcements in magnesium matrix. When singular reinforcement at nano length scale is present in the matrix, the tendency to form clusters is unavoidable and relatively large amount of reinforcements is needed to effectively refine the matrix grain size [28]. From the present study, intermetallics formed in hybrid nanocomposites (Figures 8.1(b-d)) were relatively abundant and favorably distributed together with reinforcement phases. The grain refinement thus observed in hybrid composites can primarily be attributed to the presence of Mg_2Ni phase. The result further indicates that increase in Ni content from 0.3 to 1 vol.% did not affect the magnesium grain size significantly considering the standard deviation. The results from grain morphology measurements also revealed that there was no significant difference in grain aspect ratio for both pure and reinforced magnesium samples. Near equiaxed grain morphology was observed in all samples (Table 8.1). This can be attributed to the suitability of extrusion parameters (extrusion ratio and temperature) in facilitating full recrystallization of magnesium matrix.

The distribution of Y_2O_3 and Ni nano particulates, and Mg_2Ni was predominantly at grain boundaries (Figures 8.1 and 8.2) and in the form of clusters. Nickel particulates were not totally consumed as can be discerned from XRD results (Figure 8.3). In related studies targeted to synthesize Mg_2Ni using solid state process, presence of unreacted nickel and magnesium were similarly observed [26, 27]. Among hybrid nanocomposites, an increase in size and amount of intermetallic clusters with increasing presence of nickel particulates in the samples was observed. However, these localized clusters were evenly distributed and no evidence of cluster associated porosity was found in the micrographs. The development of homogeneous microstructure in relation to second phase distribution can be attributed to the suitability of parameters during blending and extrusion steps. The ability of these steps in the development of microstructure in the case of composites has been identified and established before [1]. It was also observed that intermetallic phase (Mg_2Ni) formed in hybrid nanocomposites was predominantly in micron size length scale. Mg_2Ni phase exhibited good interfacial bonding with Mg matrix assessed in terms of absence of pores and debonding (Figure 8.2c) at the interface. Results of this study further confirm good compatibility between Mg matrix and Mg_2Ni intermetallics [5, 6, 29]. The result of microstructural characterization further revealed the presence of nano pores in the clusters containing Y_2O_3, Ni and Mg_2Ni phases (Figure 8.2b). The presence of isolated porosity observed through microstructural characterization is consistent with the porosity levels computed using density results (Table 8.1).

8.3.3 Mechanical Behavior

8.3.3.1 Microhardness

Microhardness measurements revealed that the addition of both singular (yttria) and hybrid (yttria+nickel) nanoparticulates in magnesium matrix shows a noticeable improvement in average microhardness of magnesium. This can be generally attributed to: (a) presence and fairly well distribution of harder and stronger second phases in magnesium matrix, (b) an increase in resistance to localized matrix deformation due to the presence of Y_2O_3, Ni and Mg_2Ni and (c) reduction in matrix grain size. With addition of 0.7vol.% yttria reinforcement in magnesium matrix, 22% improvement in microhardness over that of pure magnesium was achieved. When 0.3vol.% nickel was present in Mg/0.7Y_2O_3 formulation, microhardness increased up to 46% as compared to that of pure magnesium. This shows the effectiveness of hybrid (ceramic+metal) reinforcements and the presence of properly distributed and well bonded Mg_2Ni intermetallic phase in Mg matrix. The increase in hardness of hybrid composites with an increase in amount of Ni can primarily be attributed to the increasing presence of Mg_2Ni phase which served to harden the magnesium matrix [30].

8.3.3.2 Tensile Properties

Mechanical behavior of magnesium and magnesium nanocomposites was assessed in terms of tensile tests at room temperature. The results from tensile testing revealed that the use of yttria nanoparticulate reinforcements in pure magnesium led to a significant improvement in 0.2% yield strength and ultimate tensile strength of pure magnesium. The addition of nickel as hybrid reinforcement in a fixed Mg/0.7Y_2O_3 composition led to a simultaneous improvement in both 0.2% yield strength and

ultimate tensile strength when compared to that of Mg and Mg/Y_2O_3 nanocomposite formulation.

An increase in 0.2% yield strength and ultimate tensile strength of Mg/(Y_2O_3+Ni) hybrid nanocomposites can primarily be attributed to the following:

(a) An effective load transfer from matrix to harder and stronger second phases (Y_2O_3, Ni and Mg_2Ni) [9, 10].

(b) Orowan strengthening due to the presence of yttria and nickel reinforcements at nanolength scale [31].

(c) Strain misfit between matrix and reinforcements [32].

(d) Difference in coefficient of thermal expansion (CTE) between Mg matrix and reinforcements [33-36].

(e) Strengthening effect through refinement in matrix grain size (Table 8.1) [7, 37, 38].

(f) Additional strengthening from Mg_2Ni intermetallics [30].

The results reveal the clear significance of addition of Ni nanoparticulates in improving strength levels till 0.6 volume percent. Formation of Mg_2Ni and its excellent interfacial integrity with Mg matrix (Figure 8.2c) appeared to be crucial factor. The results of tensile testing also revealed that failure strain of Mg increased due to the presence of Y_2O_3 and addition of Ni to the extent of 0.6 Ni did not adversely affected it (see Table 8.2). The results of present study reveal minimal effect of grain size reduction on the failure strain of hybrid composites (Tables 8.1 and 8.2). The reduction in ductility of Mg/(0.7Y_2O_3+1.0Ni) can be attributed to the increased clustering of intermetallic phase at the micron length scale.

Comparing magnesium reinforced with total of 1vol.% hybrid reinforcements, Mg/(0.7Y_2O_3+0.3Ni), with conventional PM processed Mg/1.11vol%Y_2O_3 [9] and Mg/1vol.%Y_2O_3 [11], superior improvement in both 0.2%yield strength and ultimate tensile strength was realized from the current composite formulation. Likewise, comparatively high level of yield and tensile strengths was realized from the abovementioned hybrid nanocomposite as compared to the strengths of magnesium reinforced with hybrid ceramic nanoparticulates of 0.3vol.%SiC and 0.7vol.%Al_2O_3 (total of 1vol.%) [39]. For the deformability of the materials in terms of failure strain or ductility, Mg/(0.7Y_2O_3+0.3Ni) hybrid nanocomposite is more deformable than that of other Mg nanocomposites in references [11, 39] except for reference [9] in which similar deformability level was reported as compared to the present result. The results thus reveal that hybrid composites containing metal and ceramic particulates exhibit superior overall tensile behavior when compared to conventional and hybrid nanocomposites containing ceramic reinforcements.

8.3.4 Tensile Failure Behavior

Results of fractographic studies revealed predominantly brittle failure of magnesium. Presence of cleavage steps (Figure 8.4a) confirmed the limited plasticity attributed to hcp crystal structure of magnesium. With the presence of yttria particulates in pure magnesium, mode of fracture transformed from brittle manner to quasi-cleavage type fracture (Figure 8.4b). The formation of localized dimple like structure on the fracture surface suggests increased level of plastic deformation. In Mg/(0.7Y_2O_3+0.3Ni) and Mg/(0.7Y_2O_3+0.6Ni) nanocomposite formulations, the formation of dimple like features was predominantly observed (Figures 8.4(c and d)),

indicating their reasonable ability to deform plastically. In Mg/(0.7Y_2O_3+1.0Ni) nanocomposite, numerous cracks were observed on the fracture surface (Figure 8.4e) and could have been catalytic in reducing the plastic deformability (Table 8.2). The presence of cracked Mg_2Ni (Figure 8.4f) suggested good Mg-Mg_2Ni interfacial bonding. All hybrid nanocomposites, in common, revealed refined fracture features (Figures 8.4(c-e)) when compared to magnesium and Mg/Y_2O_3 nanocomposite. Especially when compared to pure Mg which showed microscopically rough fracture features, Mg hybrid nanocomposites exhibit comparatively homogeneous and refined fracture features. This can also be related to refined microstructural features of hybrid composites such as grain size (see Table 8.1).

8.4 Conclusions

1. PM technique incorporating hybrid microwave sintering can be successfully used to synthesize pure magnesium, magnesium-ceramic nanocomposite and magnesium hybrid nanocomposites containing ceramic (Y_2O_3) and metal (Ni) nanoparticulates.
2. Microstructural characterization studies revealed the formation of micron length scale Mg_2Ni intermetallic phase due to the presence of nickel as hybrid reinforcement in Mg/Yttria formulation. Mg_2Ni phase was predominantly located at grain boundaries along with yttria and nickel nanoparticulates.
3. Presence of Ni as hybrid reinforcement assisted reasonably in reducing grain size of Mg.

4. The increase in amount of Ni as hybrid reinforcement led to a progressive increase in hardness of Mg matrix.
5. The addition of hybrid (yttria+nickel) reinforcements in pure magnesium led to a simultaneous increase in both 0.2% yield and ultimate tensile strengths. The ductility of Mg/Y_2O_3 can be retained up to 0.6 volume percent of Ni addition. The best overall tensile properties was realized from $Mg/(0.7Y_2O_3+0.6Ni)$ hybrid nanocomposite formulation.
6. The presence of hybrid reinforcement assisted in refining the fracture features of Mg matrix.

8.5 References

[1] D.J. Lloyd, Int. Mater. Rev., 39 (1994) 1–23.

[2] R.A. Saravanan and M.K. Surappa, Mater. Sci. Eng. A, 276 (2000) 108-116.

[3] S.C.V. Lim and M. Gupta, Mater. Res. Bull., 36 (2001) 2627-2636.

[4] S. F. Hassan and M. Gupta, Mater. Res. Bull., 37 (2002) 377-389.

[5] S. F. Hassan and M. Gupta, J. Mater. Sci., 37 (2002) 2467-2474.

[6] S. F. Hassan and M. Gupta, J. Alloys Compd., 335 (2002) L10-L15.

[7] W.L.E. Wong and M. Gupta, Comp. Sci. Tech., 67 (2007) 1541-1552.

[8] W.L.E. Wong and M. Gupta, Adv. Eng. Mater., 8 (2006) 735-740.

[9] S. F. Hassan and M. Gupta, Trans. ASME, 129 (2007) 462-467.

[10] S. F. Hassan and M. Gupta, Mater. Sci. Eng. A, 392 (2005) 163-168.

[11] C.S. Goh, J. Wei, L.C. Lee and M. Gupta, Acta Mater., 55 (2007) 5115-5121.

[12] K.S. Tun and M. Gupta, Comp. Sci. Tech., 67 (2007) 2657-2664.

[13] ASM Handbook, *Properties of Magnesium Alloys in: Properties and Selection: Non-Ferrous Alloys and Special-Purpose Materials*, Vol. 2, Materials Park, OH, ASM International, 1990, p. 480.

[14] D.E. Clark and W.H. Sutton, Annu. Rev. Mater. Sci., 26 (1996) 299-331.

[15] R. Roy, D. Agrawal, J. Cheng and S. Gedevanishvili, Nature, 399 (1999) 668-670.

[16] K. Saitou, Scripta Mater., 54 (2006) 875-879.

[17] P. Chhillar, D. Agrawal and J.H. Adair, Powder Metall., 51 (2008) 182-187.

[18] M. Gupta and W.L.E. Wong, Scripta Mater., 52 (2005) 479-483.

[19] K.S. Tun and M. Gupta, J. Alloys Compd., 466 (2008) 140-145.

[20] K.S. Tun and M. Gupta, J. Mater. Sci., 43 (2008) 4503-4511.

[21] R.M. German, *Powder metallurgy science*, 2nd ed., Princeton, Metal Powder Industries Federation, 1994.

[22] C.S. Smith, Trans. AIME, 175 (1948) 15-51.

[23] K.S. Tun, M. Gupta and T.S. Srivatsan, Mater. Sci. Tech., available online at 24 April 2009.

[24] ASM Handbook, *Binary Phase Diagram in: Alloy Phase Diagrams*, Vol. 3, Materials Park, OH, ASM International, 1992, p. 281.

[25] M.Y. Tsai, M.H. Chou and C.R. Kao, J. Alloys Compd., 471 (2009) 90-92.

[26] X.J. Chen, T.D. Xia, X.L. Liu, T.Z. Liu and W.J. Zhao, J. Alloys Compd., 426 (2006) 123-130.

[27] A. Wang, H. Liu, B. Ding and Z. Hu, High Pressure Res., 16 (1998) 121-133.

[28] Y.C. Kang and S.L.Chan, Mater. Chem. Phy., 85 (2004) 438-443.

[29] N. Eustathopoulos, M.G. Nicholas and B. Drevet, *Wettability at High Temperatures*, New York, Pergamon, 1999, pp. 175, 187.

[30] J.H. Westbrook, *Intermetallic Compounds*, New York, John Wiley & Sons, 1967, p. 471.

[31] W.S. Miller and F.J. Humphreys, Scripta Metall. Mater., 25(1991) 33-38.

[32] M. Kouzeli and A. Mortensen, Acta Mater., 50 92002) 39-51.

[33] D.C. Dunand and A. Mortensen, Mater. Sci. Eng. A, 144 (1991) 179-188.

[34] Z. Zhang, D.L and Chen, Scripta Mater., 54 (2006) 1321-1326.

[35] A. Buch, *Pure metals properties: A scientific-technical handbook*, Materials Park, Ohio, ASM International, London, Freund Publishing House, 1999.

[36] R. Morrell, *Handbook of properties of technical & engineering ceramics*, London, HMSO, 1985.

[37] S.F. Hassan and M. Gupta, J. Alloys Compd., 429 (2007) 176-183.

[38] S.F. Hassan and M. Gupta, Mater. Sci. Tech., 20 (2004) 1383-1388.

[39] S.K. Thakur, K. Balasubramanian and M. Gupta, Trans. ASME, 129 (2007) 194-199.

CHAPTER 9

COMPRESSIVE PROPERTIES AND DEFORMATION BEHAVIOR OF MAGNESIUM HYBRID NANOCOMPOSITES

Part of the work presented in this chapter is accepted for publication. The citation is as follows:

K.S. Tun and M. Gupta, "Role of Microstructure and Texture on Compressive Strength Improvement of Mg/(Y_2O_3+Cu) Hybrid Nanocomposites", J. Alloys Compd., Accepted on 12 Feb 2010.

CHAPTER 9

COMPRESSIVE PROPERTIES AND DEFORMATION BEHAVIOR OF MAGNESIUM HYBRID NANOCOMPOSITES

Summary

In this chapter, uniaxial compressive response of pure magnesium, Mg/(Y_2O_3+Cu) and Mg/(Y_2O_3+Ni) hybrid nanocomposites are discussed. Results revealed that the presence of hybrid reinforcements led to a significant increase in 0.2% CYS and UCS while the failure strain was compromised. Comparatively low ductility of magnesium hybrid nanocomposites under compressive loading is attributed to the absence of twinning unlike pure magnesium. The variation in compressive properties exhibited by hybrid composites is correlated with the microstructural features and texture effects.

9.1. Introduction

Magnesium based materials are known for their potential as light weight structural materials primarily due to their low density [1]. In recent years, magnesium based nanocomposites have emerged strongly due to their capability to exhibit a good combination of mechanical and oxidation properties [1-4]. Main focus in the published literature is on the development of nanocomposites, their processing, microstructure and tensile properties. Very limited studies have been carried out to study compressive properties of magnesium based composites irrespective of the fact that in many engineering applications magnesium based materials are used to make parts that are loaded in compression [5-11]. Examples include magnesium wheels and seat frames

[12]. This necessitates the importance of understanding the compressive response of magnesium based nanocomposites as they are quite new to scientific community when compared to conventional magnesium alloys. Results of literature search indicate that compressive behavior of magnesium alloys is well reported [5, 13-26] while that of magnesium composites is less reported [9-11]. Among composites, there is only one study in open literature which addresses the compressive response of magnesium based nanocomposites [11]. Considering the ability of particulates at nano length scale to alter the texture of magnesium based materials, the variation in compressive behavior should be expected and investigated. It may be noted that variation in texture can activate the slip and/or twinning systems differently [16, 27]. It may further be noted that no studies have been reported so far to investigate the compressive behavior of hybrid magnesium nanocomposites or to improve the compressive strength of magnesium using hybrid reinforcements (metal+ceramic) at nano length scale.

Accordingly, in the present study, an attempt is made to study the effect of microstructure and texture on the uniaxial compressive behavior of magnesium based hybrid nanocomposites at room temperature. Hybrid reinforcements of (Y_2O_3+Cu) and (Y_2O_3+Ni) at nano length scale are used and cost/energy effective microwave assisted powder metallurgy route is adopted to synthesize materials.

9.2 Mg/(Y_2O_3+Cu) Hybrid Nanocomposites

9.2.1 Results

9.2.1.1 Density and Porosity Measurements

The results of density and porosity measurements are summarized in Table 9.1. Porosity was marginally higher in case of hybrid nanocomposites when compared to monolithic magnesium. No specific trend of porosity was observed with increasing addition of reinforcements within composite samples.

Table 9.1 Results of density, porosity and grain size measurements.

Material	Reinforcement (vol.%)		Theoretical Density (g/cm^3)	Experimental Density (g/cm^3)	Porosity (vol.%)	Grain Size (μm)
	Y_2O_3	Cu				
Mg	-	-	1.740	1.738 ± 0.007	0.13	20 ± 3
Mg/(Y_2O_3+Cu)	0.7	0.3	1.784	1.775 ± 0.001	0.45	9 ± 5
Mg/(Y_2O_3+Cu)	0.7	0.6	1.806	1.792 ± 0.004	0.77	9 ± 4
Mg/(Y_2O_3+Cu)	0.7	1.0	1.835	1.825 ± 0.002	0.62	8 ± 4

9.2.1.2 Microstructure

Results of grain size measurements (Table 9.1) revealed a significant reduction in average grain size of Mg/(Y_2O_3+Cu) hybrid nanocomposites. Among composite samples, the grain size was not reduced with increasing presence of reinforcements. To investigate the formation of twins after compression, the failed surfaces of the samples were polished, etched and analyzed using FESEM.

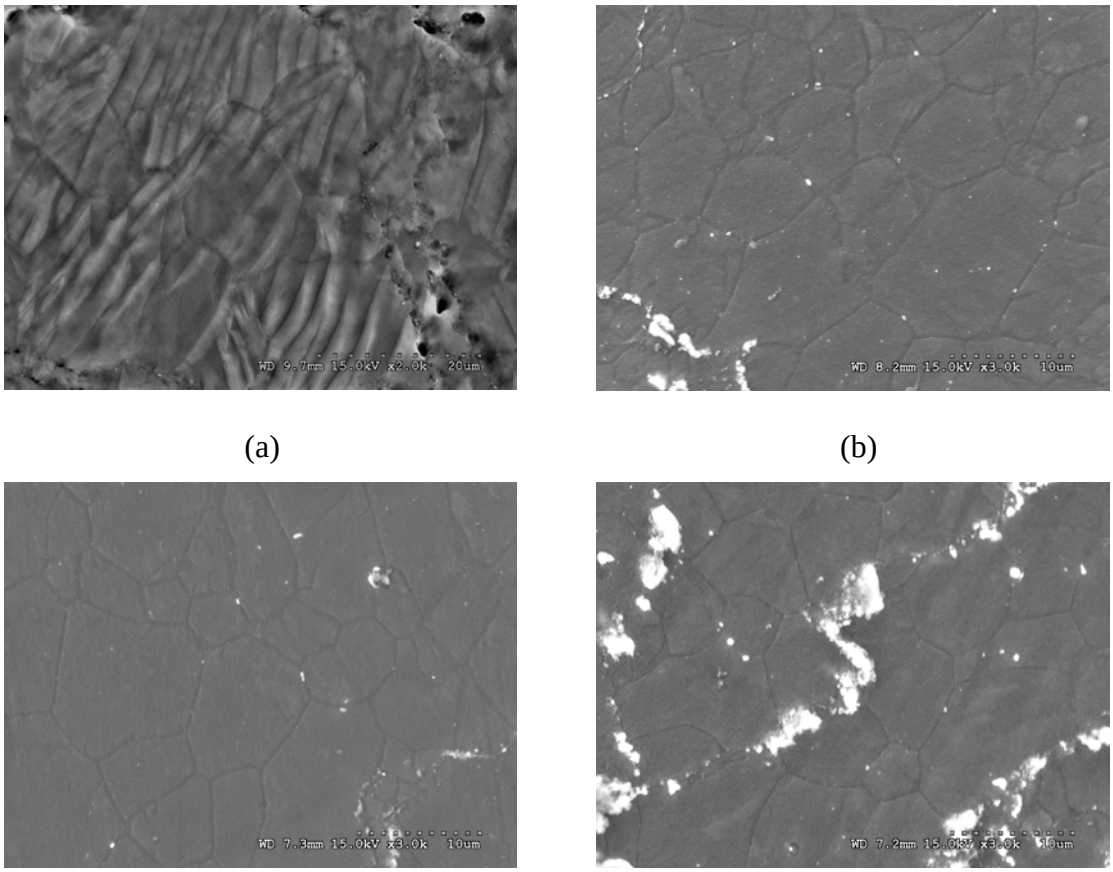

(a) (b)

(c) (d)

Figure 9.1. Representative micrographs showing: (a) twin formation in Mg, and absence of twinning in (b) Mg/(0.7Y_2O_3+0.3Cu), (c) Mg/(0.7Y_2O_3+0.6Cu) and (d) Mg/(0.7Y_2O_3+1.0Cu) hybrid nanocomposites after compression.

Characterization of etched surface of Mg after compression showed the presence of numerous twinned grains (Figure 9.1a). However, no evidence of twin formation in the grains was observed in the case of hybrid nanocomposite samples (Figures 9.1(b-d)). Figure 9.2 shows the distribution of secondary phases in Mg matrix. Secondary phases were reasonably well distributed in all nanocomposite samples. An increasing presence of clustered secondary phases was also observed with increasing addition of copper in Mg/0.7Y_2O_3 composition.

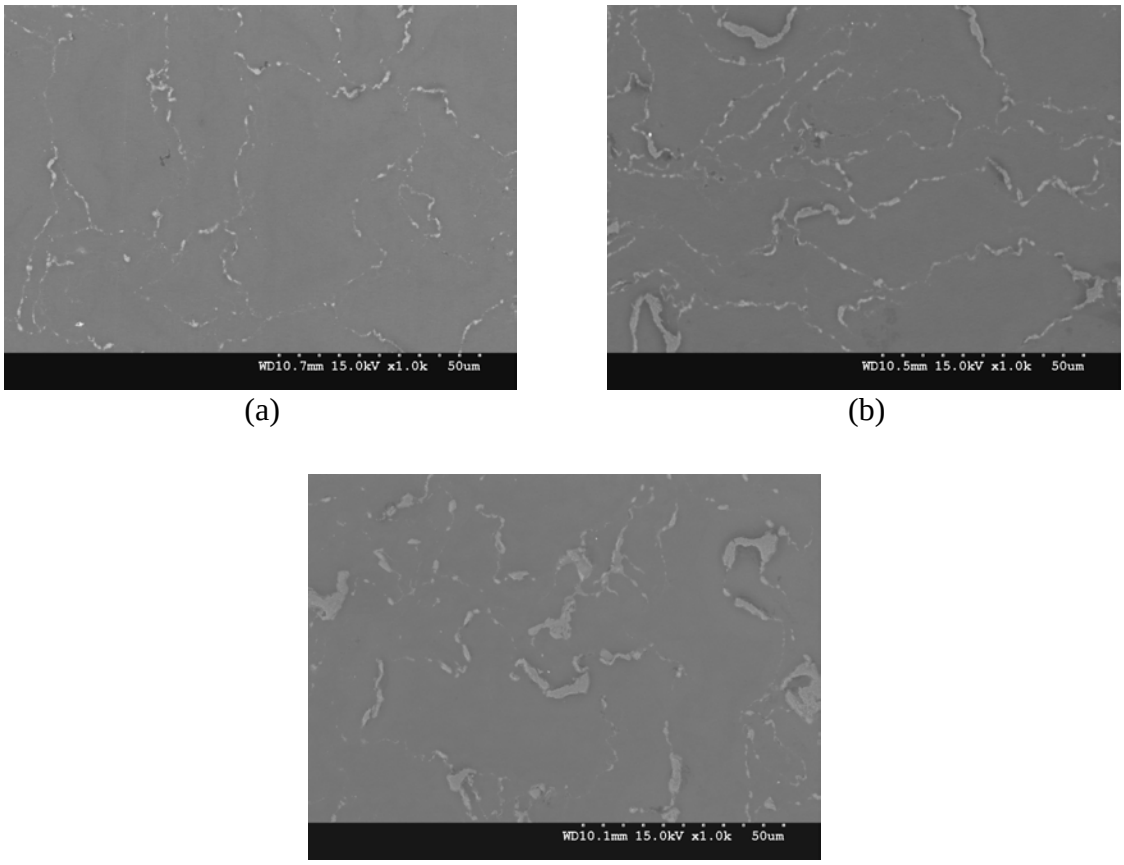

(a) (b)

(c)

Figure 9.2. FESEM micrographs showing distribution of second phases in: (a) Mg/(0.7Y_2O_3+0.3Cu), (b) Mg/(0.7Y_2O_3+0.6Cu) and (c) Mg/(0.7Y_2O_3+1.0Cu) hybrid nanocomposites.

9.2.1.3 X-Ray Diffraction Studies

Figure 9.3 shows the results of X-ray diffraction analyses for Mg and Mg nanocomposite samples. No matching peaks of Y_2O_3 and MgO phases were observed in any samples. Nanocomposite samples showed the peaks corresponding to Cu and Mg_2Cu phases and their intensities increased with increasing presence of copper.

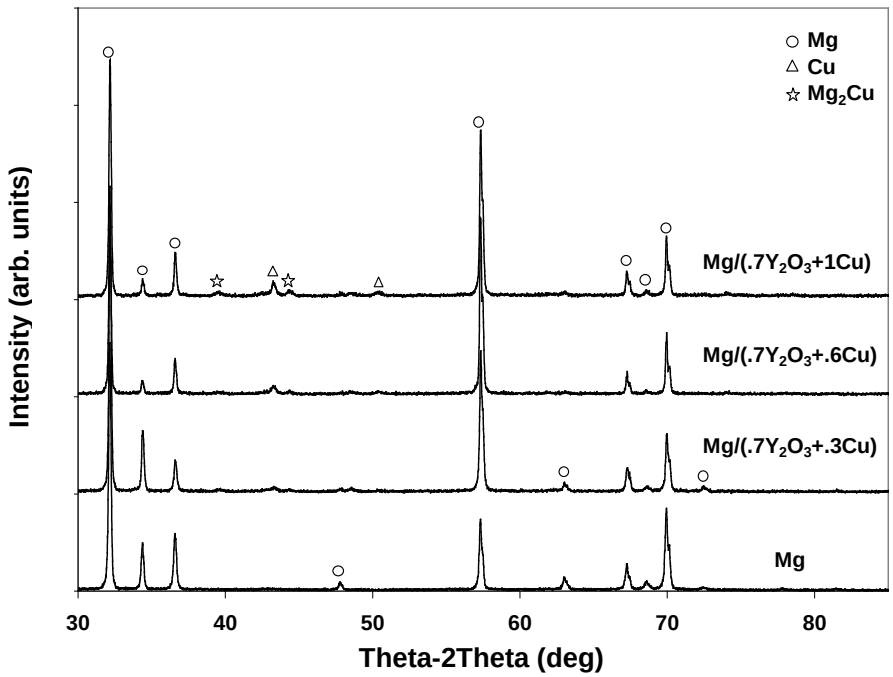

Figure 9.3. X-ray diffractograms of Mg, and Mg/(Y_2O_3+Cu) hybrid nanocomposites.

Figure 9.4 shows the XRD scans of Mg and Mg/(0.7Y_2O_3+l.0Cu) hybrid nanocomposite samples before and after compression in both transverse and longitudinal directions. Three peaks from low angle side to high angle side within 30°-40° angle range correspond to prism (10-10), basal (0002) and pyramidal (10-11) crystallographic planes. Before compression, similar crystallographic orientation was observed in Mg and hybrid nanocomposite samples. No strong extrusion texture where preferred orientation of basal (0002) planes was along the extrusion direction (compression axis) was observed. A strong extrusion texture means the intensity of basal plane peak (0002) should be the highest among three peaks in longitudinal direction.

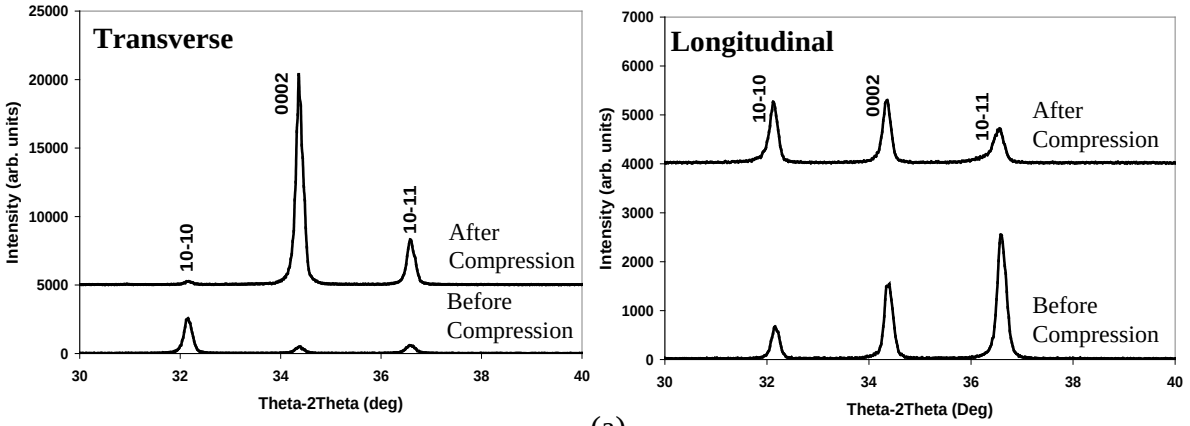

(a)

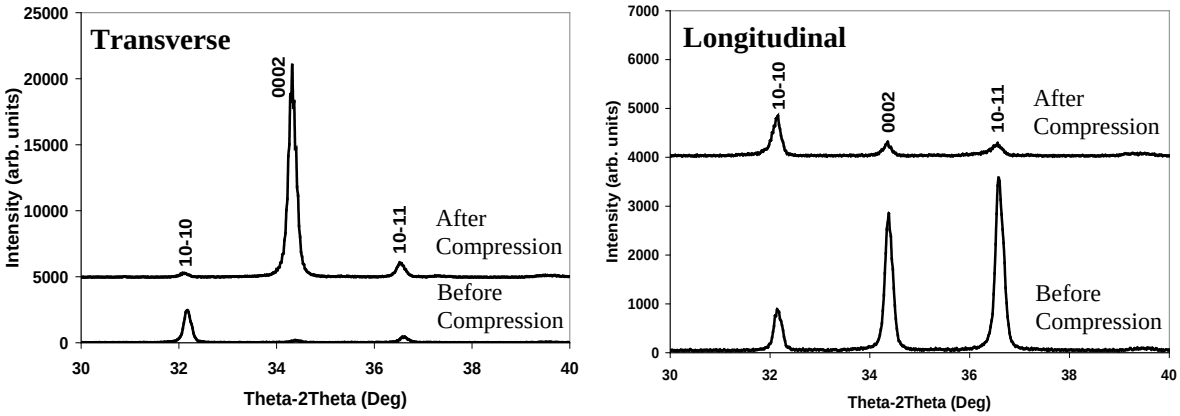

(b)

Figure 9.4. XRD results of: (a) Mg and (b) Mg/(0.7Y_2O_3+1.0Cu) hybrid nanocomposite before and after compressive loading in transverse and longitudinal directions.

As the observed basal peak is the second strongest peak in longitudinal direction, the initial texture can be said as weak extrusion texture in both samples. However, as the prism (10-10) peak is the strongest one in transverse direction suggests that the basal planes are oriented parallel to the compressive axis at the beginning of compressive loading. After compression, crystal planes are reoriented in both samples. In case of Mg, strong basal texture was observed in transverse direction whereas it (basal texture) remained unchanged in longitudinal direction (Figure 9.4a).

In case of composite sample, the same strong basal texture as in Mg sample can be seen in transverse direction whilst it (basal texture) became significantly weak in longitudinal direction (Figure 9.4b).

9.2.1.4 Microhardness

Table 9.2 shows the microhardness measurements taken from the polished surfaces of pure and reinforced magnesium samples. The results revealed a significant increase in microhardness of magnesium due to the addition of hybrid reinforcements (Y_2O_3+Cu) in magnesium matrix. Marginal increase in microhardness was also observed with increasing presence of copper.

Table 9.2 Results of grain size, microhardness and room temperature compressive properties of Mg and Mg nanocomposites.

Materials	Grain Size (μm)	Microhard-ness (HV)	0.2%CYS (MPa)	UCS (MPa)	Failure Strain (%)
Mg	20 ± 3	37 ± 2	70 ± 7	280 ± 9	26.9 ± 3.2
Mg/(0.7Y_2O_3+0.3Cu)	9 ± 5	53 ± 3	114 ± 3	388 ± 7	13.1 ± 1.2
Mg/(0.7Y_2O_3+0.6Cu)	9 ± 4	57 ± 2	117 ± 6	396 ± 10	12.8 ± 1.7
Mg/(0.7Y_2O_3+1.0Cu)	8 ± 4	61 ± 4	156 ± 9	411 ± 8	12.5 ± 0.7

9.2.1.5 Compressive Flow Behavior

The compressive stress-strain curves for pure Mg and hybrid nanocomposites are shown in Figure 9.5. During initial work hardening after yielding, similar characteristics in deformation behavior were observed from the flow curve in unreinforced and reinforced samples. After initial period, work hardening steadily

increased to a peak stress followed by flow softening where stress almost dropped to 20 MPa with increasing strain in case of magnesium. For hybrid nanocomposites, rapid work hardening up to peak stress was followed by a sudden failure without further deformation. Flow softening was not observed in any of the composite samples. These observations indicate that composite flow behavior differed from that of magnesium after the work hardening stage. No difference in flow behavior during hardening was observed among composite samples. Gradual strength improvement was observed for composites with increasing presence of copper.

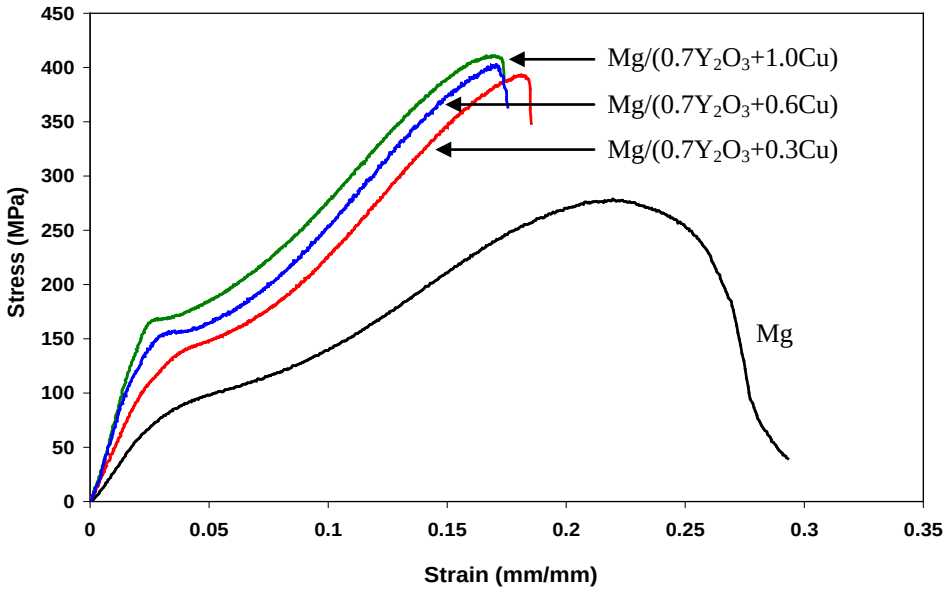

Figure 9.5. Representative stress-strain curves showing different flow behaviors of Mg and Mg hybrid nanocomposites.

9.2.1.6 Compressive Properties

The results from room temperature compressive tests can be seen from Table 9.2. As compared to Mg, 0.2% compressive yield strength and ultimate compressive strength were remarkably improved in hybrid nanocomposites while failure strain was

compromised. Among hybrid nanocomposites, Mg/(0.7Y_2O_3+1.0Cu) revealed best strengths without any degradation in failure strain considering standard deviation.

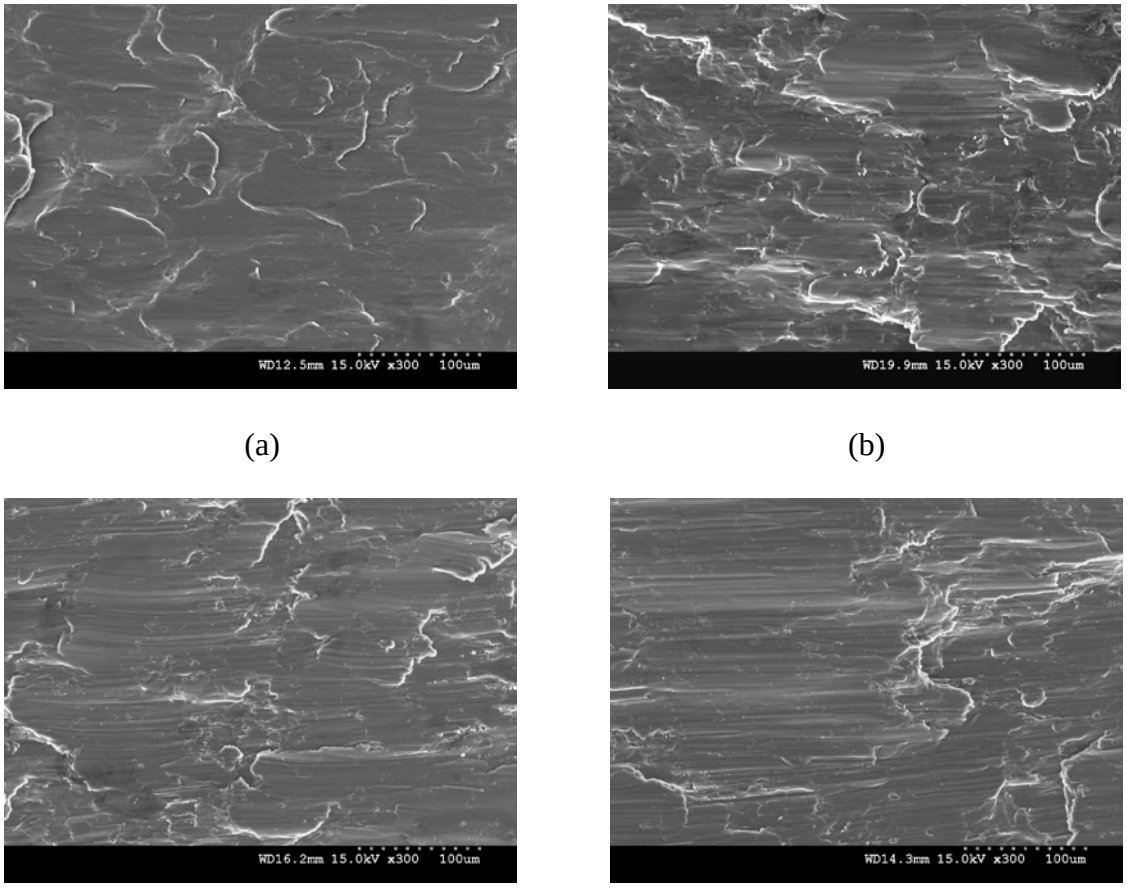

Figure 9.6. Compressive failure surfaces showing:(a) less evidence of shear banding in Mg and intense shear banding in hybrid nanocomposites (b) Mg/(0.7Y_2O_3+0.3Cu), (c) Mg/(0.7Y_2O_3+0.6Cu) and (d) Mg/(0.7Y_2O_3+1.0Cu).

9.2.1.7 Fractography

Figure 9.6 shows the surfaces of samples failed under compressive loading. In case of Mg, less evidence of shear band formation was observed. In case of hybrid nanocomposites, shear band formation was relatively more prominent.

9.2.2 Discussion

9.2.2.1 Orientation of Crystal Planes

As seen from XRD analysis (Figure 9.4), the absence of basal (0002) peak before compression and appearance of strong basal peak after compression in transverse direction indicated that there were changes in crystal orientation in both Mg and its reinforced counterparts. Here, attention will be placed on the orientation changes of basal planes since anisotropic mechanical properties in magnesium follows the changes in basal plane orientation relative to compressive axis. In case of pure Mg, the peak related to basal (0002) plane was observed in both transverse and longitudinal directions after compression. This indicates that some of the basal planes were located perpendicular to the compressive loading axis (c-axis parallel to compressive loading axis) and some were along the compressive loading axis (c-axis perpendicular to compressive loading axis) which means that pure c-axis compression did not occur during compressive loading. In case of hybrid nanocomposites, the strongest peak of basal (0002) plane in transverse direction and extremely weak intensity of that plane in longitudinal direction was observed after compression. This shows that most of the basal (0002) planes were orientated perpendicular to compressive loading axis after compression. This further implies that there was c-axis compression of composite samples during compression. Brown et al. [17] investigated the reorientation of crystal planes during compression using high intensity powder diffractometer (HIPD). They observed that the reorientation of basal plane in Mg alloy begins at relatively low stress level. Once reorientation was set, no further change in basal texture was observed throughout the loading period until compression was competed. The basal orientation was reflected by the appearance of high intensity peak related to basal

plane from the diffraction pattern. In line with their observation, it can be concluded that the basal orientation (texture) obtained after completion of compression was the consequence of the reoriented texture during compression.

9.2.2.2 Microhardness

Results from microhardness measurements revealed that the presence of hybrid (Y_2O_3+Cu) reinforcements in magnesium matrix leads to a noticeable improvement in average microhardness of magnesium. This can commonly be attributed to: (a) presence and fairly good distribution of harder and stronger secondary phases in magnesium matrix, (b) an increase in resistance to localized matrix deformation due to the presence of reinforcements/intermetallics, (c) reduction in matrix grain size and (d) additional hardening due to the formation of Mg_2Cu intermetallics. Results also showed the gradual but marginal improvement in average microhardness with increasing presence of copper nanoparticulates in hybrid nanocomposites. This can be attributed to the presence of more intermetallics due to an increased amount of copper. Results also imply that intermetallics behave like supplementary reinforcements besides yttria and copper, providing effective hardening in hybrid nanocomposites [35].

9.2.2.3 Compressive Deformation

Under compressive loading at room temperature, both 0.2% compressive yield strength and ultimate compressive strength of magnesium hybrid nanocomposites were clearly higher than those of unreinforced magnesium (Table 9.2 and Figure 9.5). Similar observations of yield and compressive strength improvement were made in Mg

and Mg alloy composites [5, 8, 9, 11]. Same trend was also observed in Li and Y containing Mg alloys as compared to pure Mg [15]. Generally, the deformation behavior of composite materials depends mostly on the modification of matrix microstructure due to the incorporation of reinforcing phases to base matrix. For strongly textured metals like magnesium, however, variation in crystallographic orientation (texture) is relatively important and consideration is taken for such effect on their deformation mechanism.

First, from the microstructural aspect, the strength improvement in composites can be primarily ascribed to: (a) less micro-porosity, (b) good distribution of secondary phases, (c) load transfer mechanism (d) strain misfit and (e) difference in Coefficient of Thermal Expansion (CTE) between magnesium matrix and reinforcements, (f) Orowan strengthening and (g) grain refinement. In the present study, yielding in composite samples was observed at higher stress level as compared to pure Mg (Table 9.2 and Figure 9.5). Yield strength can be increased due to the presence of reinforcing phases in composite materials provided porosity is limited [36]. In the present study, minimal presence of micro pores particularly associated with reinforcement clusters was observed in all nanocomposite formulations (Figure 9.2). The difference in porosity amounts between monolithic and reinforced samples was marginal (see Table 9.1). Good distribution of secondary phases is another factor to improve the strength of composites. The secondary phases have the ability to hinder the initiation of dislocation motion to achieve high yield strength and to further resist the plastic flow during plastic deformation to increase material's work hardening. With increasing presence of copper particulates at fixed amount of yttria (0.7vol.%) in composite samples, more intermetallic formation is expected. Again, with increasing

presence of secondary phases, increased tendency of cluster formation inevitably occurred in the composite microstructure (Figure 9.2). Irrespective of increasing number of clusters with increasing presence of Cu, the overall distribution of secondary phases was still reasonably uniform in all composites. This is evident from the hardness and compressive testing results of the composite with highest amount of Cu (Mg/0.7Y_2O_3+1.0Cu)) that exhibited best hardness, 0.2% CYS and UCS without any significant compromise on failure strain when compared to other composites (Table 9.2). Another important mechanism that contributes to strength enhancement is load transfer mechanism. Effective load transfer depends on good matrix-reinforcement/secondary phase bonding and reasonably uniform distribution of these phases in base matrix. Observation of minimal porosity at matrix-secondary phase interface and within clusters of secondary phases (translates to suitable bonding) and good distribution of secondary phases could have favorable effect on delaying the yielding of composite samples. For hybrid nanocomposites, matrix plastic deformation was constrained by the presence of stronger and more rigid secondary phases (Y_2O_3, Cu and Mg_2Cu intermetallics). It has been reported earlier that under compressive loading, relatively large quantity of coarse particles is beneficial for load bearing capability [36, 37]. In the present study, this can be translated to increase in Mg_2Cu phase in the matrix due to increasing presence of Cu. Besides, the increasing amount of secondary phases (Y_2O_3+Cu+intermetallics) reduces the effective interparticle spacing making the motion of dislocation more difficult under applied load leading to progressive increase in strengths. This is consistent with the result of the present study as highest hardness and strengths (0.2%CYS and UCS) are realized in (Mg/0.7Y_2O_3+1.0Cu)) hybrid nanocomposite (Table 9.2).

Strength enhancement in case of composite samples can also be attributed to incompatibility in deformation (strain misfit) between matrix and secondary phases (Y_2O_3, Cu and intermetallics). Under the application of load, geometrically necessary dislocations are generated to accommodate the misfit strains between plastically deforming matrix and elastically deforming secondary phases [38]. The increase in number of dislocations is also further assisted due to the difference in CTE between Mg and secondary phases (metal/ceramic/intermetallic). The common outcome of the increase in dislocation density in the matrix is the increase in strength of material as established before [39, 40]. The progressive increase in strengths with increasing addition of copper at nano length scale can also be attributed to progressive increase in contribution of Orowan strengthening (Figure 9.5). The effect of grain size on strength enhancement can be neglected in the present study as its variation was statistically insignificant in case of composites samples (Table 9.1).

Secondly, variation in yield and ultimate compressive strengths of Mg and hybrid nanocomposites can be discussed based on crystallographic orientation under compressive loading. As seen from the XRD results, weak extrusion texture with some basal planes aligned parallel to the compression axis but less evidence of basal planes perpendicular to compression axis was observed before compression. After compression, reorientation of basal planes perpendicular to compression axis was found in both Mg and nanocomposite samples. It can be attributed to the activation of {10-12} twinning [13, 15, 16] and such twin formation is evident from similar concave nature of flow curves in the case of Mg and nanocomposites during initial work hardening (Figure 9.5). Previous studies [13, 16, 18] on compressive deformation of Mg alloys have shown that concave portion in flow curve is related to the formation of

{10-12} twinning. This type of twinning is the most common deformation mode observed in compressed Mg based materials especially when basal planes are initially parallel to compressive loading. Yielding of the samples is thus believed to be due to initiation of twinning. However, yielding of hybrid nanocomposites occurred at significantly higher stress as compared to Mg. Possible reason for this improvement is the suppression of the activation of twinning due to grain refinement. In an earlier study, it was established that coarse grain structure favors easy activation of twinning leading to lower yield strength [15]. Further, in yet another study [18] conducted on Mg-3Al-1Zn alloy, it was established that stress required for twin activation increases with decreasing grain size. The observed yielding phenomena in Mg and Mg hybrid nanocomposites with respect to grain size are thus consistent with these studies.

As discussed in section 9.2.2.1, some basal planes are still aligned parallel to the compression axis during compressive loading in Mg (Figure 9.4a), indicating twinning is favorable in Mg with continued plastic deformation since {10-12} twinning deformation is operative in such basal orientation. This presumption was supported by the evidence of numerous twinned grains observed from the microstructure of compressively deformed Mg sample. It was also shown in recent study [16] that high fraction of twinned grains after compression was resulted in AZ31 alloy in which basal planes are orientated parallel to compression axis. Twinning could act as obstruction to dislocation motion during plastic deformation and large amount of twinning is advantageous to provide high work hardening [18]. In the present study, an outcome of extensive twinning could translate into a moderately high degree of working hardening in Mg (Figure 9.5). In addition, extensive twinning due to easy twin propagation without obstacles (secondary phases) could clarify the slow

hardening rate in pure magnesium. In case of composite samples, basal planes are almost completely aligned perpendicular to the compression axis during compression after completion of crystal reorientation (see section 9.2.2.1). For magnesium compressed along c-axis, twinning is not likely to occur. Lack of twinning was found in compressively deformed Mg single crystal in which the test sample was specially prepared in such a way that basal planes are initially aligned perpendicular to the compression axis [41]. Above said study also reported the activation of basal slip and {11-22} <-1-123> slip systems (<c+a> pyramidal slip) due to c-axis compression. In the current study, basal planes are not initially aligned perpendicular to compression axis. As explained earlier, reorientation of basal planes perpendicular to compression axis observed after compression was due to the formation of twinning. Only after completed reorientation, deformation in nanocomposites continues with c-axis compression. Studies [15, 25] have reported that deformation by slip takes place after ceasing of twin growth or saturation of twinning. Brown et al. [17] reported that a sharp decrease in basal (0002) peak intensity from diffraction pattern was related to the activation of pyramidal slip in reoriented grain in which diffraction was taken normal to the loading axis and onset of such slip activation with twin saturation gave rise to an increased hardening rate in AZ 31B alloy. In another study [25], activation of basal slip with strong basal texture after twinning saturation and slip-twin interaction leads to fast work hardening increment in compressed AZ31 Mg alloy. The observed rapid work hardening in magnesium hybrid nanocomposites could be accounted for the activation of some possible slip systems, assuming twinning ceases after basal plane reorientation (c-axis compression). Moreover, Barnett et al. [18] showed that slip dominated flow was observed for magnesium alloy with fine grain size and low

amount of twinning was found after compression. From the current study, no evidence of twinning was observed from microstructure of compressed nanocomposites although it could have very few twinned grains. It can therefore be concluded that the flow during later stage of strain hardening could be slip dominated flow. As compared to Mg, ultimate compressive strength is obviously higher in hybrid nanocomposites. This could be primarily attributed to nearly complete basal orientation perpendicular to compression axis which is advantageous for activation of slip in nanocomposite as compared to Mg. Among composite samples, an increase in amount of secondary phases led to increasing trend of work hardening. This could be due to the higher resistance to twin and slip deformation as a consequence of increasing presence of secondary phases.

Although yield and compressive strengths of nanocomposites are higher than that of Mg, ductility was adversely affected. Micro-composites often exhibit reduced ductility when compared to unreinforced Mg and Mg alloy matrix [5, 9]. As seen from the XRD results, magnesium is partly under c-axis compression during compressive loading. From the previous study [41], {10-12} twinning is not likely to occur under c-axis compression in hcp metals. However, if deformation of polycrystals is due to extensive twinning under c-axis compression, ductility improvement can be expected. Another study [42] reported the formation of other twin forms ({10-11), {30-34} and {10-13} habit twins) during c-axis compression of magnesium. In the present study, more than one type of twinning is possible in compressively deformed Mg due to the crystal orientation observed (Figure 9.4) and section 9.2.2.1) in which some basal plane orientation could favor {10-12} twinning and other deforms by habit twins. The observed high ductility of magnesium can therefore be accounted by extensive

twinning deformation. In nanocomposites, twin formation was not apparent and possible slip systems were limited for plastic deformation to continue. This could be the main reason for the comparatively low ductility of nanocomposites. Results also revealed no significant difference in ductility level of nanocomposites with increasing presence of Cu. This indicates that ductility variation within nanocomposites is independent of microstructure changes, such as high amount of secondary phases and clusters in hybrid nanocomposites.

9.2.2.4 Compressive Failure Analysis

Fracture surfaces of magnesium nanocomposites revealed the presence of shear bands (Figures 9.6(b-d)). Presence of shear bands represents intense localized plastic deformation. Ion et al. [43] observed shear banding in single phase Mg alloy. According to their investigation, shear band formation was due to heterogeneous deformation in materials arising from localized deformation at grain boundary leaving cores of the grains undeformed under compressive loading. Relatively fast work hardening rate was also seen in the sample deformed by shear banding. From the studies on Al alloys and composites [44, 45], it was suggested that enhanced work hardening is the important factor that promotes shear banding. The observations made by these studies reflect the shear banding behavior observed in hybrid nanocomposites. Under rapid work hardening, inhomogeneous plastic deformation is expected in nanocomposites due to the presence of secondary phases and comparatively large amount of grain boundaries. Localized plastic deformation in the vicinity of either grain boundary or matrix-secondary phase interface could proceed along the direction of maximum shear stresses as the applied compressive load increases. The increasing

presence of secondary phases in composite samples could thus be the possible cause for increased formation of shear bands in nanocomposites. In pure Mg, the minimal presence of shear band can be attributed to relatively homogenous deformation due to reduced grain boundary area and absence of secondary phases. From the previous investigation [44], the appearance of strong shear banding in cold rolled Al/Mg_2Si alloys with fine precipitates was observed as compared to precipitate free alloy matrix and shear banding increased with increasing volume fraction of precipitates. Study on Al/SiC micro composites under impact compression [45] also revealed shear bands that were formed relatively with more ease when compared to pure Al alloy matrix. The results of the present study thus suggest that higher tendency of shear band formation in Mg based hybrid nanocomposites can be attributed to the presence of secondary phases and this behavior is similar, in principle, with the observations made on Al alloys and composites.

9.3 Mg/(Y_2O_3+Ni) Hybrid Nanocomposites

9.3.1 Results

9.3.1.1 Density and Grain Size Measurements

The density results from Table 9.3 show that there was no significant difference in theoretical and experimental densities for both monolithic and composite samples. This indicates the feasibility of current processing route, PM method involving hybrid microwave sintering route, to synthesize highly dense materials [2, 28, 46]. The densification response was also not affected markedly due to increasing presence of second phases in Mg. The average grain size was reduced significantly in

composite samples when compared to Mg. However, no significant change in grain size was observed with increasing presence of nickel in Mg/0.7Y_2O_3 nanocomposites.

9.3.1.2 Twinning Behavior

Figures 9.7 and 9.8 show the microstructures of Mg and Mg/(0.7Y_2O_3+1.0Ni) hybrid nanocomposite in as-extruded condition and following compression at different strain levels up to failure. In case of Mg, less amount of twinning was observed in the sample compressed to strain of 2.5% and 21%, and to fracture point (Figures 9.7(b, e and f)). The extensive twinned grains were found in the sample compressed at strain of 7.5% and 12% (Figures 9.7(c and d)). In case of Mg/(0.7Y_2O_3+1.0Ni) composite, a few twinned grains was observed in the sample compressed to strain of 2.5 and 12% (Figures 9.8(b and d)), and numerous twinned grains was observed at 7.5% strain (Figure 9.8c). No twinning was present in the grains of the sample compressed to 16% strain and compressively failed composite (Figures 9.8(e and f)).

Table 9.3 Results of density and grain morphology determinations.

Material	Reinforcement (vol.%)		Theoretical Density (g/cm^3)	Experimental Density (g/cm^3)	Grain Size (μm)
	Y_2O_3	Ni			
Mg	-	-	1.740	1.738 ± 0.007	20 ± 3
Mg/(Y_2O_3+Ni)	0.7	0.3	1.785	1.778 ± 0.002	9 ± 3
Mg/(Y_2O_3+Ni)	0.7	0.6	1.806	1.802 ± 0.002	6 ± 2
Mg/(Y_2O_3+Ni)	0.7	1.0	1.835	1.829 ± 0.002	5 ± 2

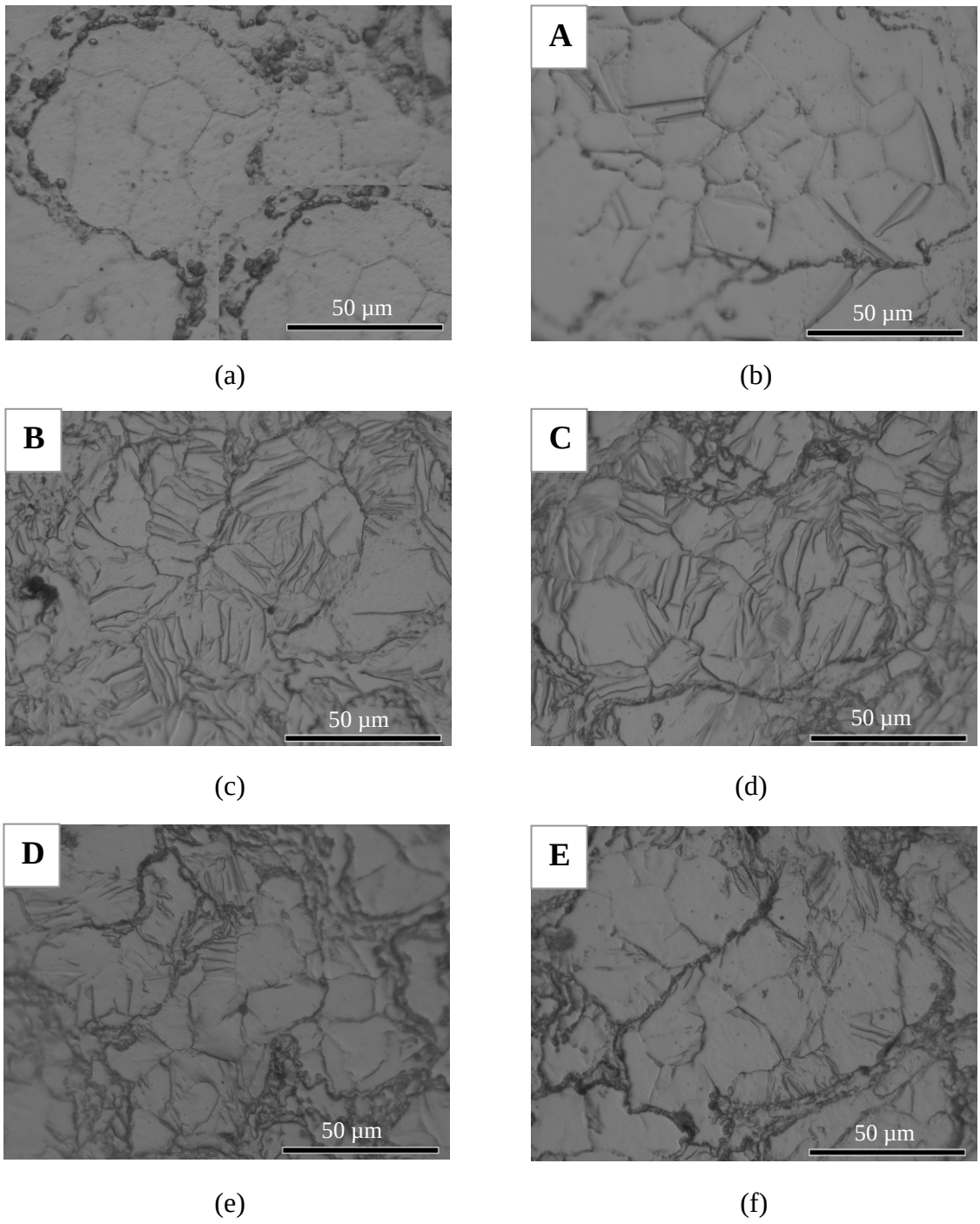

Figure 9.7. Optical micrographs showing microstructural evolution in Mg in: (a) as-extruded condition, and at compressive strain of: (b) 2.5%, (c) 7.5%, (d) 12%, (e) 21% and (f) ~29% (fracture point).

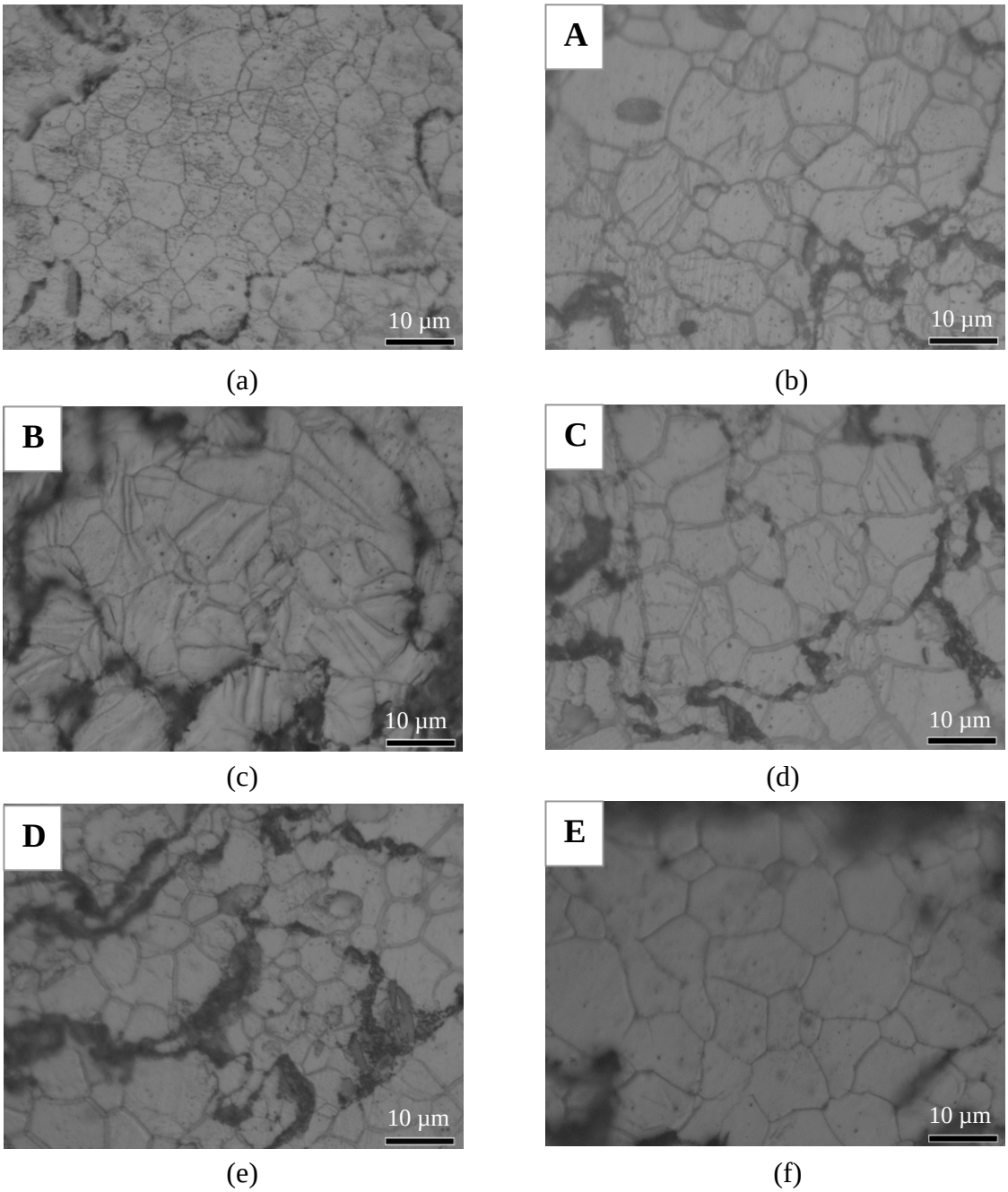

Figure 9.8. Optical micrographs showing microstructural evolution in Mg/(0.7Y_2O_3+1.0Ni) hybrid nanocomposite in: (a) as-extruded condition, and at compressive strain of: (b) 2.5%, (c) 7.5%, (d) 12%, (e) 16% and (f) ~17% (fracture point).

9.3.1.3 XRD analysis and Crystal Orientation

The results of X-ray diffraction analyses are shown in Figure 9.9. From the results, the peaks corresponding to Ni and Mg_2Ni phases were observed in hybrid nanocomposite samples and their intensities increased with increasing presence of nickel. However, no matching peaks for Y_2O_3 and MgO phases were observed in any samples.

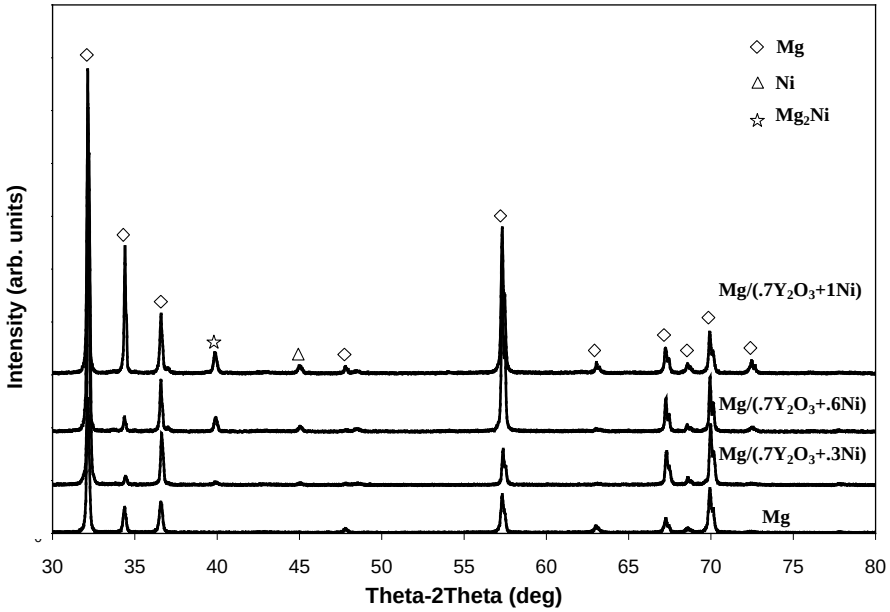

Figure 9.9. XRD analyses for Mg and Mg/(Y_2O_3+Ni) hybrid nanocomposites.

Figure 9.10 shows the variation of crystal orientation in relation to the XRD peak patterns with increasing fracture strains starting from as extruded sample (0% strain) to compressively failed sample in both transverse and longitudinal directions for Mg and Mg nanocomposite. Three peaks from low angle side to high angle side within 30°- 40° angle range correspond to prism (10-10), basal (0002) and pyramidal (10-11) crystallographic planes.

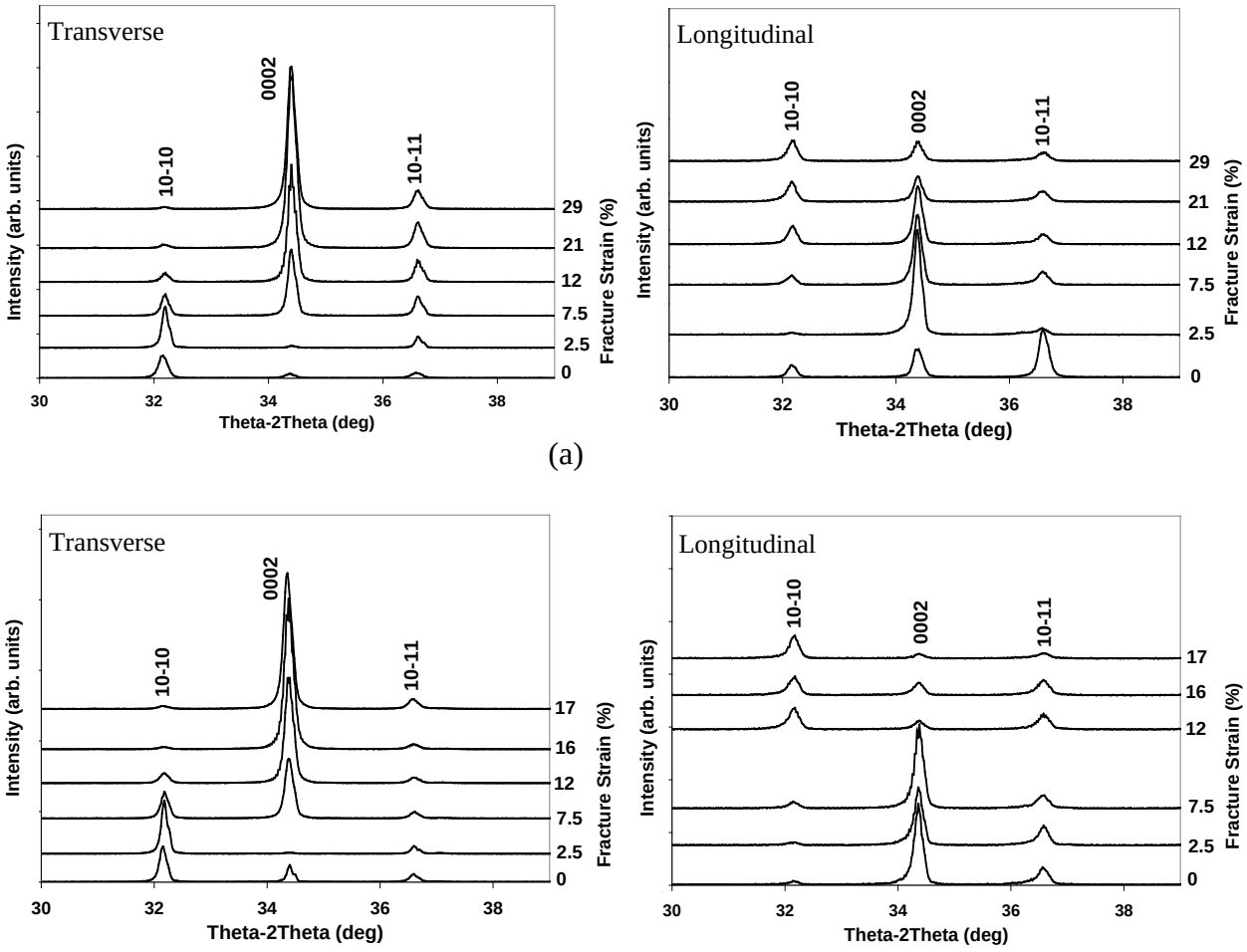

Figure 9.10. XRD results from transverse and longitudinal scans showing crystal orientation changes at different compressive strains for: (a) pure Mg and (b) Mg/(0.7Y_2O_3+1.0Ni) hybrid nanocomposite.

In as extruded condition, the basal peak was not the strongest one in longitudinal scan of Mg sample (Figure 9.10a). In Mg/(0.7Y_2O_3+1.0Ni) nanocomposite, low intensity basal peak was seen in transverse scan although this peak was the strongest in longitudinal scan (Figure 9.10b). For the as-extruded sample to have strong extrusion texture, basal peak should appear only in longitudinal scan as the strongest peak which means that almost all basal (0002) planes aligned parallel to

the extrusion direction (compression axis). In the present study, it can be said that there was weak extrusion texture in as-extruded samples of Mg and Mg nanocomposite. After compression to 2.5% strain, both samples showed a strong extrusion texture where only one strong basal peak was observed in Mg and the peak was the strongest one in nanocomposite from longitudinal scan whereas only high intensity prism peak was appeared with no basal peak formation in both samples from transverse scan. At 7.5% strain, the appearance of strong basal peak and prism peak with reduced intensity was detected in transverse scan whereas the basal peak in longitudinal scan maintained as the strongest peak in both samples. At strain of 12%, the prism peak began to disappear and the appearance of noticeably strong basal peak was observed from transverse scan for both Mg and Mg nanocomposite. From longitudinal scan at 12% strain, the basal peak almost disappeared in nanocomposite sample whilst it (basal peak) was still the strongest peak in Mg sample. From 12% strain until fracture point in both samples, the basal (0002) plane orientation in terms of the appearance of basal peaks remained the same in transverse scan. On the other hand in longitudinal scan, reduced intensity but remaining peak of basal (0002) plane was observed in Mg (Figure 9.10a). However, it was not the case for Mg nanocomposite where the basal (0002) peak intensity was much weaker and almost disappeared at fracture point (Figure 9.10b).

9.3.1.4 Flow Curves

The compressive flow curves for pure Mg and Mg/($0.7Y_2O_3$+1.0Ni) hybrid nanocomposite are shown in Figure 9.11. During initial work hardening after yielding, both flow curves showed similar region with concave nature around point B. At point

C, beyond the concave section, more rapid work hardening rate was observed in nanocomposite when compared to Mg. In case of Mg, work hardening steadily increases up to a peak stress followed by flow softening, where stress almost dropped to 20 MPa with increasing strain. For hybrid nanocomposites, rapid work hardening up to peak stress followed by a sudden failure without further deformation, showing less ductile nature of composite sample when compared to Mg. These observations indicate that composite flow behavior did not follow the matrix flow behavior in the last stage of deformation.

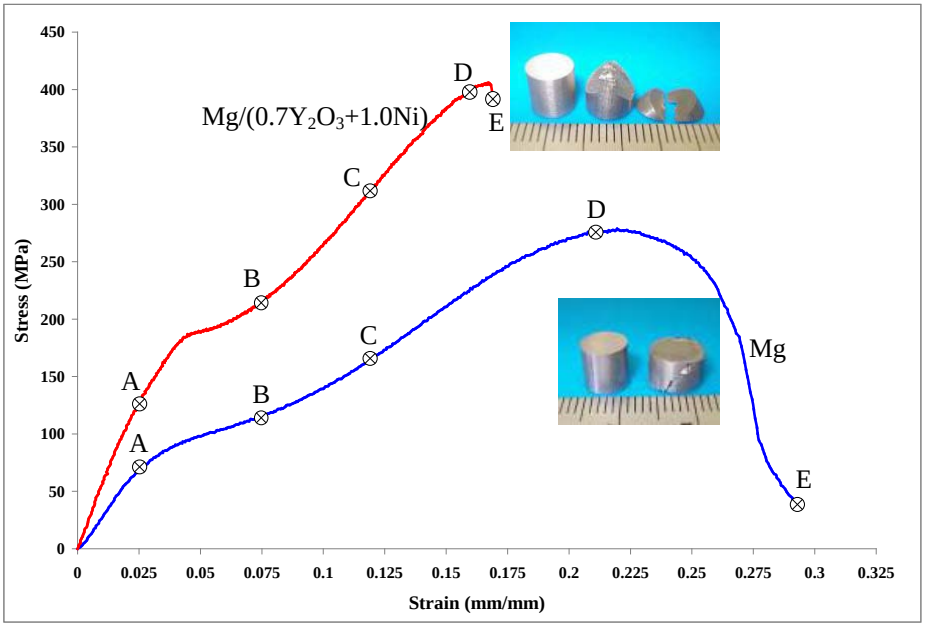

Figure 9.11. Compressive stress-strain curves showing different flow behaviors of Mg and Mg/(Y_2O_3+Ni) hybrid nanocomposite.

9.3.1.5 Compressive Properties

Table 9.4 shows the results from uniaxial compressive tests at room temperature. As compared to Mg, a significant improvement in 0.2% compressive yield strength and ultimate compressive strength in hybrid nanocomposites was

observed. The increasing presence of nickel particulate reinforcements in hybrid nanocomposites had no critical influence on either strengths (0.2%CYS and UCS) or failure strain of the corresponding composites. Regardless of the increasing amount of second phases, similar level of strength and failure strain was observed in hybrid nanocomposite samples considering the standard deviation.

Table 9.4 Results of room temperature compressive properties of Mg and Mg nanocomposites.

Materials	0.2%CYS (MPa)	UCS (MPa)	Failure Strain (%)
Mg	70 ± 7	280 ± 9	26.9 ± 3.2
Mg/(0.7Y_2O_3+0.3Ni)	154 ± 5	402 ± 3	11.0 ± 0.8
Mg/(0.7Y_2O_3+0.6Ni)	154 ± 9	394 ± 4	11.5 ± 1.5
Mg/(0.7Y_2O_3+1.0Ni)	154 ± 3	406 ± 8	10.1 ± 1.0

9.3.1.6 Fractography

Figure 9.12 shows the compressive failure surfaces of Mg/(Y_2O_3+Ni) hybrid nanocomposites. Similar shear band formation from the surfaces was observed as in Mg/(Y_2O_3+Cu) hybrid nanocomposites.

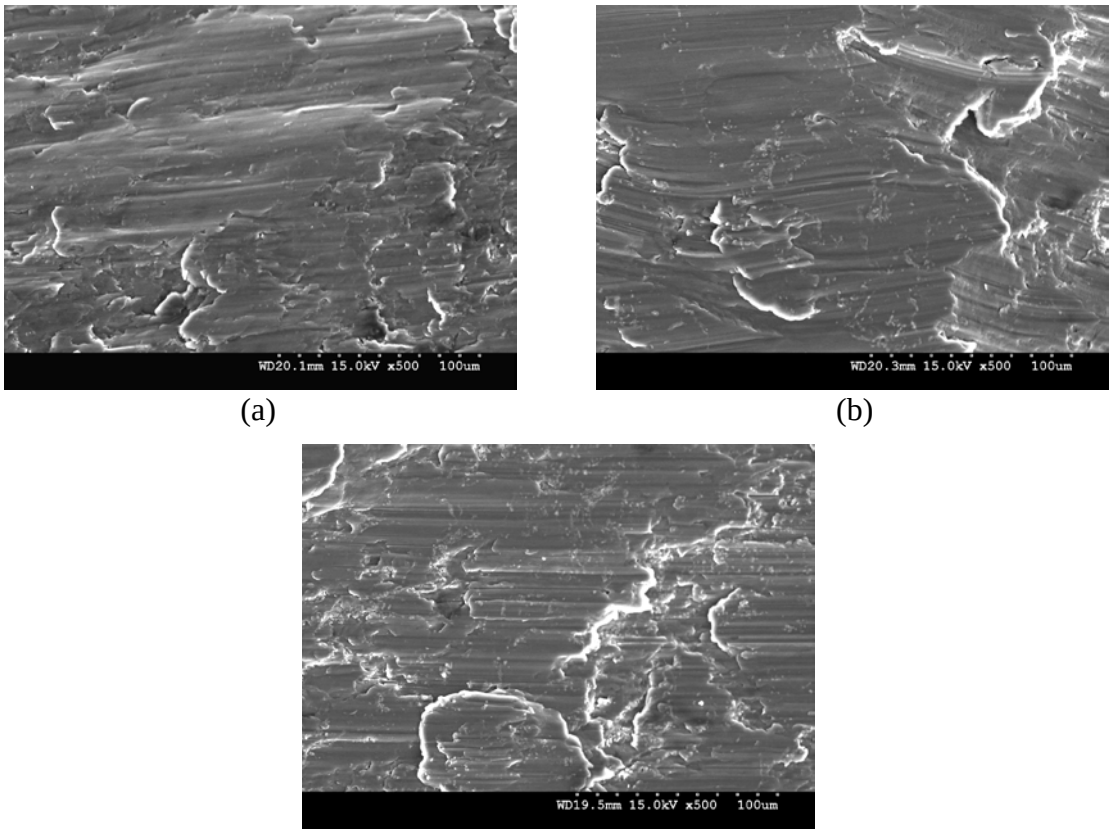

(a) (b)

(c)

Figure 9.12. Compressive failure surfaces of: (a) Mg/(0.7Y_2O_3+0.3Ni), (b) Mg/(0.7Y_2O_3+0.6Ni) and (c) Mg/(0.7Y_2O_3+1.0Ni).

9.3.2 Discussion

9.3.2.1 Orientation of Crystal Planes

The orientation of crystal planes under compressive loading was investigated by analyzing the changes in XRD peaks corresponding to crystal planes in both transverse and longitudinal scans for Mg and Mg nanocomposites (Figure 9.10). Especially under compressive loading, orientation changes in basal (0002) planes of Mg and Mg based materials take an important role in determining the resultant deformation behavior of materials. In the present study, initial crystal orientation showed weak extrusion texture in both as-extruded Mg and Mg nanocomposite.

However, strong extrusion texture with basal (0002) plane aligned parallel to the extrusion direction or compression axis was perceived in both samples at 2.5% compressive strain. In related flow curve in figure 9.11, 2.5% strain represents point A and the samples were still in elastic region at this point. This indicates that almost all basal (0002) planes are located along the compression axis or c-axis was located perpendicular to the compression axis before yielding. At 7.5% strain after yielding, reorientation of basal (0002) planes was observed in both samples with appearance of strong basal peak in transverse scan. This describes that basal (0002) planes began to align perpendicular to the compression axis. At 12% strain, nearly all basal (0002) planes are reoriented perpendicular to the compression axis up to fracture point (Figure 9.10b and see in section 9.3.1.3) in case of composite sample. This means that the composite sample was under c-axis compression starting around 12 % compressive strain till failure point. Unlike composite sample, pure c-axis compression was not totally achieved in pure Mg. Although reorientation of basal (0002) planes began to occur at 7.5% strain (Figure 9.10a), the basal peaks were still detected and stronger when compared to composite sample at all strain levels up to fracture in longitudinal scan of Mg.

9.3.2.2 Strengthening Effect of Second Phases

From the compressive test results (Table 9.4 and Figure 9.11), Mg/(Y_2O_3+Ni) hybrid nanocomposites achieved a noticeably high level of both 0.2% compressive yield strength and ultimate compressive strength over pure magnesium. This strength improvement can be attributed mainly due to the presence of second phases through: (a) grain refinement [6, 9, 11, 47], (b) load transfer mechanism [6, 9, 11, 36, 47] and

(c) increased dislocation density arises primarily from Orowan mechanism [6, 11] and coefficient of thermal expansion (CTE) mismatch between Mg matrix and reinforcement phases [6, 11, 36, 47]. However, the increasing amount of second phases in nanocomposites did not appear to enhance strengthening effect as seen from similar strength level for all composite formulations (Table 9.4).

9.3.2.3 Compressive Deformation Mechanisms

The flow curves of pure Mg and Mg/(0.7Y_2O_3+1.0Ni) nanocomposite (Figure 9.4) showed difference in strength and flow behavior. Magnesium, one of the hexagonal metals, can deform generally by slip and twinning deformation. Particularly at room temperature, Mg and Mg based materials usually exhibit low deformability due to the limited number of slip systems. Previous studies [16, 26, 48] have reported the influence of initial crystal orientation and basal plane orientation of extruded or rolled samples on compressive properties and deformation behavior. In the present study, the initial orientation of both Mg and its composite counterpart showed the same weak extrusion texture. Having the same initial orientation mode, similar deformation response from both samples was observed from the flow curve up to a strain of approximately 7.5%. Although the extrusion texture was weak in both as extruded samples, basal (0002) planes were mostly aligned parallel to the compressive axis (c-axis perpendicular to compressive axis). Under this basal plane orientation, twinning is the most favorable deformation mode in hexagonal materials. And the most common type of twinning in Mg based materials under this orientation is {10-12} twinning. Before yielding at 2.5% strain (point A in flow curve), the evidence of a few twins in some grains was observed in both Mg and composite samples (Figures

9.7(b), 9.8(b) and 9.11). After yielding at 7.5% strain, massive twinned grains were abundantly observed in both Mg and Mg composite. These observations clarify that initial basal plane orientation parallel to the compression axis is the key reason for twinning and yielding of the samples was due to twinning. It is basically in agreement with the reports on Mg alloy systems [16, 17, 18] which observed the strong extrusion texture as the cause of twinning. From the XRD analysis, the appearance of sharp increase in basal peak which was initially absent at 2.5% strain was found in the transverse scan at a strain of 7.5%. From the flow curve, 7.5% strain was at point B and the curve is in concave shape around B point. It was therefore confirmed that twinning cause rotation of basal planes from parallel to perpendicular to the compression axis and the concave portion in the flow curves is the indicative of the onset of extensive twinning. Influence of twinning deformation on the basal reorientation and the related concave nature of flow curve was previously investigated only on Mg alloys [16, 17, 25].

Beyond 7.5% strain, different hardening response was seen from the flow curves between two samples, a steady increment in work hardening followed by work softening in Mg and a rapid increment in hardening without flow softening leading to final failure in Mg nanocomposite. As seen from the flow curves and crystal orientation from XRD analyses (Figures 9.10 and 9.11), hardening response of Mg and Mg/(Y_2O_3+Ni) nanocomposite was mainly influenced by the changes in orientation of basal (0002) planes at the later stage of compression. At a strain of 12%, extensive twinning was seen from the micrograph (Figure 9.7d) in case of Mg whereas comparatively fewer amount of twinned grains was observed in case of nanocomposite (Figure 9.8d). This twinning behavior was explained by the observed basal peak

pattern from XRD analysis. The remaining basal peak was observed in longitudinal scan in case of pure Mg even though same basal reorientation was found from transverse scan in both Mg and composite samples. This showed that there still have basal (0002) planes aligned parallel to the compression axis and this basal orientation has the ability to support twinning to be continued. From 12% to 21% strain (point C and D in Mg flow curve), gradual strain hardening was observed in pure Mg. With evidence of extensive twinning at point C, there can be twin hardening since twin boundaries serve as barrier to dislocation motion like grain boundaries [6, 18, 49]. At 21% strain, twinning was found only in a few grains in Mg sample and most of them are twin free grains (Figure 9.7e). The disappearance of twinning in most grains can be related to the reorientation of most of the basal (0002) planes perpendicular to the compression axis (Figure 9.10a) [41]. On the other hand, twinning can still have a chance to activate due to the fact that some basal (0002) planes are still aligned parallel to the compression axis. From 21% strain to failure point (point D and E in flow curve) in Mg sample, strain softening was also observed from the flow curve and this can be attributed to the less twinning (Figure 9.11). This indicates that hardening in Mg sample vanished due to the lack of enough twinning.

In case of Mg composite, almost all basal (0002) planes are aligned perpendicular to the compression axis (c-axis compression) at a strain of 12% up to failure (Figure 9.10b). For magnesium compressed along c-axis, twinning is not likely to occur. From the previous study [41], lack of twinning was evident in compressively deformed Mg single crystal in which the test sample was specially prepared in such a way that basal planes are initially aligned perpendicular to the compression axis. From 12% strain to fracture point (~17% strain), the observed large amount of twin free

grains (Figure 9.8d) and no twinning in composite samples (Figures 9.8(e and f)) is reflected by the basal orientation perpendicular to the compression axis (c-axis compression). It can again be confirmed from the current study that twinning is not easy to operate under c-axis compression. As explained earlier, reorientation of basal planes perpendicular to compression axis during compression was due to the formation of twinning (at 7.5% strain). Only after completed reorientation (at 12% strain), deformation in nanocomposites continues with c-axis compression. It could thus be true that twinning is not the prime deformation mode for the samples having basal (0002) planes perpendicular to the compression axis not only as the initial orientation but also during compression. Above mentioned study [41] also reported the activation of basal slip and {11-22} <-1-123> slip systems (<c+a> pyramidal slip) due to c-axis compression. Studies [15, 25] have reported that deformation by slip takes place after ceasing of twin growth or saturation of twinning. Brown et al. [17] reported that a sharp decrease in basal (0002) peak intensity from diffraction pattern was related to the activation of pyramidal slip in reoriented grain in which diffraction was taken normal to the loading axis and onset of such slip activation with twin saturation gave rise to an increase hardening rate in AZ 31B alloy. In another study [25], activation of basal slip with strong basal texture after twinning saturation and slip-twin interaction leads to fast work hardening increment in compressed AZ31 Mg alloy. The hardening behavior in Mg composite around 12% (point C in flow curve) could be due to the deformation by slip and interaction between slip and remaining twins which can be seen in the micrographs (Figure 9.8d). The rapid work hardening after 12% strain could be accounted by the activation of some possible slip systems with no further twinning in composite samples (Figures 9.8(e and f)). Barnett et al. [18] showed that slip

dominated flow was observed for magnesium alloy with fine grain size and low amount of twinning was found after compression. From the current study, no evidence of twinning was observed from microstructure of nanocomposite around peak strength region (around 16% strain). It can therefore be concluded that the flow at last stage of strain hardening region (between 12% and 16%) could be slip dominated flow. Since the active slip systems in the composite sample are limited together with no twinning for the deformation to be sustained, composite sample failed suddely after peak stress (Figure 9.11).

9.4 Conclusions

1. Monolithic Mg and Mg composites containing hybrid (Y_2O_3+Cu) and (Y_2O_3+Ni) nanoparticulates can be fabricated using powder metallurgy route involving energy efficient microwave sintering followed by hot extrusion.
2. Synthesized nanocomposites showed relatively homogeneous microstructural evolution through grain size reduction and good secondary phase distribution regardless of increasing amount of metal particulates, Cu and Ni.
3. Extrusion texture with basal plane aligned parallel to the compression axis was responsible for the activation of twinning and yielding in both Mg and its composite.
4. Significant improvement in compressive yield strength and ultimate compressive strength was attained in hybrid Mg nanocomposites as compared to Mg. Microstructural homogenization as well as preferred orientation of basal

(0002) planes normal to loading axis under compression are seen as the main contributing factors.

5. An increase in Cu addition led to the increasing trend of 0.2%CYS and UCS in case of Mg/(Y_2O_3+Cu) nanocomposite system whilst increasing presence of Ni had no prominent effect on both 0.2%CYS and UCS in case of Mg/(Y_2O_3+Ni) nanocomposite system.
6. High ductility of Mg under compression can be primarily attributed to the continuous formation of twins. Lack of twinning coupled with limited slip systems can be attributed to be the main cause for reduced ductility of hybrid nanocomposites.
7. Unlike pure magnesium, the evidence of prominent shear banding from the compressive failure surfaces of hybrid nanocomposites can be attributed to the heterogeneity in deformation due to the presence of secondary phases in Mg matrix under compressive loading.

9.5 References

[1] S.J. Tjong, Adv. Eng. Mater., 9 (2007) 639-652.

[2] K.S. Tun and M. Gupta, Comp. Sci. Tech., 67 (2007) 2657-2664.

[3] K.S. Tun, M. Gupta and T.S. Srivatsan, Mater. Sci. Tech., available online at 24 April 2009.

[4] Q.B. Nguyen, M. Gupta and T.S. Srivatsan, Mater. Sci. Eng. A, 500 (2009) 233-237.

[5] D.J. Towle and C.M. Friend, Mater. Sci. Tech., 9 (1993) 35-41.

[6] G. Garces, M. Rodrıguez, P. Perez and P. Adeva, Mater. Sci. Eng. A, 419 (2006) 357-364.

[7] M. Guden, O. Akil, A. Tasdemirci, M. Ciftcioglu and I.W. Hall, Mater. Sci. Eng. A, 425 (2006) 145-155.

[8] B.Q. Han and D.C. Dunand, Mater. Sci. Eng. A, 277 (2000) 297-304.

[9] J.Q. Li, L. Wang, H.W. Cheng, H.F. Zhang, Z.Q. Hu and H.N. Cai, Mater. Sci. Eng. A, 474 (2008) 24-29.

[10] Z. Szaraz, Z. Trojanova, M. Cabbibo and E. Evangelista, Mater. Sci. Eng. A, 462 (2007) 225–229.

[11] Q.B. Nguyen and M. Gupta, Comp. Sci. Tech., 68 (2008) 2185-2192.

[12] M.M. Avedesian, H. Baker (Editors), *ASM Specialty Handbook: Magnesium and Magnesium Alloys*, Ohio, ASM International, 1999.

[13] L. Jiang, J.J. Jonas, A.A. Luo, A.K. Sachdev and S. Godet, Mater. Sci. Eng. A, 445–446 (2007) 302-309.

[14] M.R. Barnett, J. Light Metals, 1 (2001) 167-177.

[15] S.R. Agnew, M.H. Yoo and C.N. Tome, Acta Mater., 49 (2001) 4277-4289.

[16] J. Jiang, A. Godfrey, W. Liu and Q. Liu, Mater. Sci. Eng. A, 483-484 (2008) 576-579.

[17] D.W. Brown, S.R. Agnew, M.A.M. Bourke, T.M. Holden, S.C. Vogel and C.N. Tome, Mater. Sci. Eng. A, 399 (2005) 1–12.

[18] M.R. Barnett, Z. Keshavarz, A.G. Beer and D. Atwell, Acta Mater., 52 (2004) 5093-5103.

[19] J. Jiang, A. Godfrey and Q. Liu, Mater. Sci. Tech., 21 (2005) 1417-1422.

[20] G. Garces, F. Domınguez, P. Perez, G. Caruana and P. Adeva, J. Alloys Compd., 422 (2006) 293-298.

[21] J. Bohlen, P. Dobron, J. Swiostek, D. Letzig, F. Chmelik, P. Luka and K.U. Kainer, Mater. Sci. Eng. A, 462 (2007) 302-306.

[22] S.B. Yi, C.H.J. Davies, H.G. Brokmeier, R.E. Bolmaro, K.U. Kainer and J. Homeyer, Acta Mater., 54 (2006) 549-562**.**

[23] P. Yang, Y. Yu, L. Chen and W. Mao, Scripta Mater., 50 (2004) 1163-1168

[24] M.A. Gharghouri, G.C. Weatherly, J.D. Embury and J. Root, Philos. Mag. A, 79 (1999) 1671-1695.

[25] Y.N. Wang and J.C. Huang, Acta Mater., 55 (2007) 897-905.

[26] R. Gehrmann, M.M. Frommert and G. Gottstein, Mater. Sci. Eng. A, 395 (2005) 338-349.

[27] M. Shahzad and L. Wagner, Mater. Sci. Eng. A, 506 (2009) 141-147.

[28] M. Gupta and W.L.E. Wong, Scripta Mater., 52 (2005) 479-483.

[29] W.L.E. Wong and M. Gupta, Adv. Eng. Mater., 9 (2007) 902-909.

[30] ASM Handbook, *Binary Phase Diagram, in Alloy Phase Diagrams,* Vol. 3, Materials Park, OH, ASM International, 1992, p.172.

[31] Y.C. Kang and S.L. Chan, Mater. Chem. Phys., 85 (2004) 438-443.

[32] S.K. Thakur, K. Balasubramanian and M. Gupta, Trans. ASME, 129 (2007) 194-199.

[33] D.J. Lloyd, Int. Mater. Rev., 39 (1994) 1-23.

[34] D.L. McDanels, Metall. Trans. A, 16A (1985) 1105-1115.

[35] J.H. Westbrook, *Intermetallic Compounds*, New York, John Wiley & Sons, 1967, p. 471.

[36] D.P. Mondala, N.V. Ganesh, V.S. Muneshwar, S. Dasa and N. Ramakrishnan, Mater. Sci. Eng. A, 433 (2006) 18-31.

[37] Z.H. Tan, B.J. Pang, D.T. Qin, J.Y. Shi and B.Z. Gai, Mater. Sci. Eng. A, 489 (2008) 302-309.

[38] M. Kouzeli and A. Mortensen, Acta Mater., 50 (2002) 39-51.

[39] D.C. Dunand and A. Mortensen, Mater. Sci. Eng. A, 144 (1991) 179-188.

[40] Z. Zhang and D.L. Chen, Scripta Mater., 54 (2006) 1321-1326.

[41] T. Obara, H. Yoshinga and S. Morozumi, Acta Metall., 21 (1973) 845-853.

[42] H. Yoshinaga, T. obara and S. Morozumi, Mater. Sci. Eng., 12 (1973) 255-264.

[43] S.E. Ion, F.J. Humphreys and S.H. White, Acta Metall., 30 (1982) 1909-1919.

[44] J. Liu, Scripta Metall., 23 (1989) 1811-1816.

[45] Z. Ling, L. Luo and B. Dodd, J. De Phys. IV, 4 (1994) 453-458.

[46] K.S. Tun and M. Gupta, J. Alloys Compd., 466 (2008) 140-145.

[47] Z. Gnjidic, D. Bozic and M. Mitkov, Mater. Character., 47 (2001) 129-138.

[48] S. Kleiner, P.J. Uggowitzer, Mater. Sci. Eng. A, 379 (2004) 258-263.

[49] I. Karaman, H. Sehitoglu, A.J. Beaudoin, Y.I. Chumlyakov, H.J. Maier and C.N. Tome, Acta Mater., 48 (2000) 2031-2047.

CHAPTER 10

GENERAL CONCLUSIONS

CHAPTER 10

GENERAL CONCLUSIONS

I. Development of Mg/Y_2O_3 Nanocomposites

1. Conventional solid state powder metallurgy technique incorporating rapid microwave sintering and hot extrusion can be successfully used to synthesize near dense Mg composites containing nano Y_2O_3 particulates.

2. Distribution of reinforcement was dependent on amount of Y_2O_3 particulates. Porosity was minimal and nanopores were observed.

3. The increasing presence of nanosize Y_2O_3 particulates leads to an increase in 0.2%YS, UTS, ductility and work of fracture. Coefficient of thermal expansion showed reverse trend indicating an increase in thermal stability.

II. Optimization of Primary and Secondary Processing Parameters

1. Near dense Mg and Mg/Y_2O_3 nanocomposite can be synthesized using hybrid microwave sintering approach and with sintering heat rates of 49˚C/min and 20˚C/min.

2. Microstructural coarsening such as larger grain size and less uniformity of reinforcement distributions observed in the samples sintered at low heating rate led to a decrease in yield and tensile strengths when compared to the samples sintered at high heating rate.

3. For synthesis of Mg/Y_2O_3 nanocomposite, high heating rate is recommended for realizing superior combination of tensile properties.

4. For both pure Mg and Mg/Y_2O_3 nanocomposite, an increase in extrusion ratio led to an increase in density and reduction in porosity. An increase in extrusion ratio also led to an improvement in homogeneity of microstructure in terms of grain morphology and reinforcement distribution.

5. An increasing trend of microhardness and strengths for both pure and nanocomposite samples was observed with increasing extrusion ratio.

III. Development of Magnesium Hybrid Nanocomposites

1. Magnesium hybrid nanocomposites, $Mg/(Y_2O_3+Cu)$ and $Mg/(Y_2O_3+Ni)$, were successfully synthesized using the hybrid microwave sintering approach, which enables lower production cost for powder metallurgy processed materials.

2. Hybrid nanocomposites showed relatively homogeneous microstructure. Grain size was comparatively lower compared to $Mg/0.7Y_2O_3$ and distribution of

secondary phases was uniform regardless of increasing amount of metal particulates (Cu and Ni).

3. An increase in amount of metal particulates as hybrid reinforcements led to a progressive increase in microhardness of Mg matrix.

4. The addition of hybrid (yttria+metal) reinforcements in pure magnesium led to a remarkable improvement in both 0.2% yield strength and ultimate tensile strength at an optimum hybrid nanocomposite composition depending on the type of metal particulates used.

5. A considerable improvement in ductility was observed in hybrid nanocomposites as compared to that of pure magnesium except for one composition ($Mg/(0.7Y_2O_3+1.0Ni)$). The ability of retaining high ductility of Mg/Y_2O_3 suggests the efficiency of hybrid reinforcement methodology.

6. Significant improvement in 0.2% compressive yield strength and ultimate compressive strength was attained in hybrid Mg nanocomposites when compared to Mg. Microstructural homogenization as well as preferred orientation of basal (0002) planes normal to loading axis under compression are seen as the main contributing factors.

7. An increase in Cu addition led to the increasing trend of 0.2% CYS and UCS in case of $Mg/(Y_2O_3+Cu)$ nanocomposite system whilst increasing presence of Ni

had no prominent effect on both 0.2%CYS and UCS in case of Mg/(Y_2O_3+Ni) nanocomposite system.

8. High ductility of Mg under compression can be primarily attributed to the continuous formation of twinning. Lack of twinning coupled with limited slip systems can be attributed to be the main cause for reduced ductility of nanocomposites.

9. Unlike pure magnesium, the evidence of prominent shear banding from the compressive failure surfaces of hybrid nanocomposites can be attributed to the heterogeneity in deformation due to the presence of secondary phases in Mg matrix under compressive loading.

CHAPTER 11

RECOMMENDATIONS

CHAPTER 11

RECOMMENDATIONS

In the current research work, new magnesium based nanocomposites are developed using cost/energy efficient hybrid microwave sintering technique as part of the blend-press-sinter powder metallurgy route. To further investigate the magnesium based nanocomposites and to assess the feasibility of the current processing route, future work may be explored as follows:

1. Corrosion and oxidation studies can be conducted on the developed nanocomposite materials to assess the reliability of materials in different environments.
2. Wear, damping, fatigue and high temperature mechanical properties should be conducted to evaluate the performance of developed nanocomposites to be used in various structural applications.
3. To understand more on the microstructure and deformation behavior of nanocomposites, TEM study should be conducted.
4. Further development of magnesium/metal nanocomposites with selected metal reinforcements and magnesium/(ceramic+metal) hybrid nanocomposites with different combinations of ceramic+metal hybrid reinforcements can be explored.
5. Other than mixing or blending of matrix and reinforcement powders, mechanical milling using balls can be used to achieve more homogeneous

dispersion of reinforcements, especially for Mg nanocomposites with high volume percentage of reinforcements.

6. To investigate the effectiveness of microwave sintering, conventional sintering using resistant heating can be conducted on the Mg nanocomposites and comparison with microwave sintered materials should be studied.
7. Study on pore morphology can be conducted on microwave sintered samples and conventionally sintered samples to investigate the effect of pore morphology on mechanical properties of synthesized materials.
8. The effect of green density on microwave sinterability of Mg nanocomposite can be studied.

Development and Characterization of New Magnesium Based Nanocomposites

APPENDIX

APPENDIX A

Information for Microwave Sintering Set-up

Model : Sharp (Multimode microwave oven)

Power : 0.9 kW (Maximum output power for microwave)

Frequency : 2.45 GHz

Outside Dimensions : 520 mm x 309 mm x 502 mm (W x H x D)

Inner ceramic crucible : Zirconia

Outer ceramic crucible : Alumina

Microwave susceptor : SiC powder

Insulation material : Microwave transparent Fiberfrax boards

Microwave Sintering

- Before sintering of the samples, temperature calibration of set-up was made.
- K-type thermocouple was used for temperature measurement.
- Timing for sintering duration was taken when the temperature was reached near to the melting point of the material.
- Samples were not soaked before sintering and no holding time was provided after reaching to the desired temperature.
- Sintered sample was kept in the microwave set-up until it was cooled down to near room temperature before taking out.